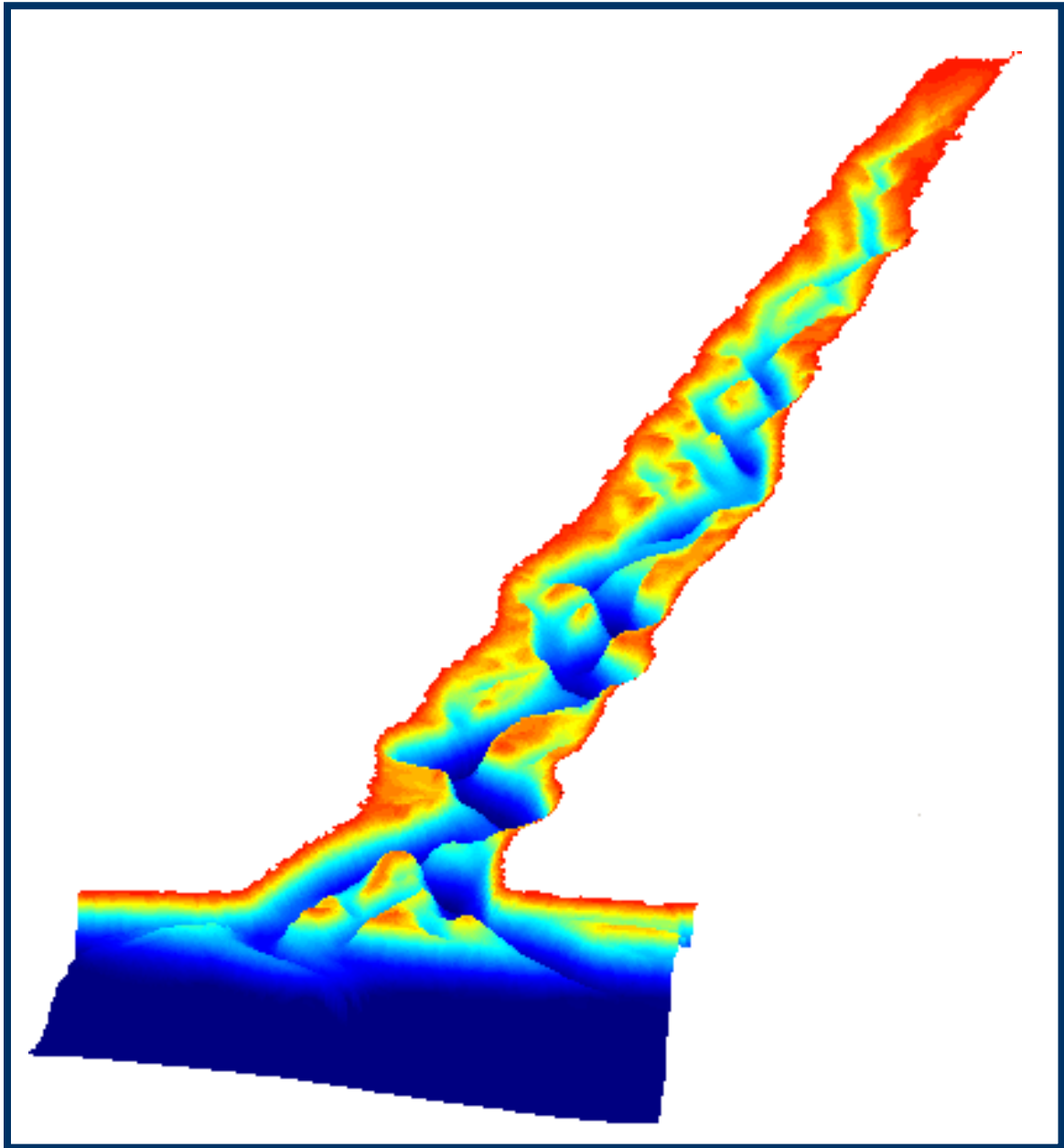


**UNESCO-IHE  
INSTITUTE FOR WATER EDUCATION**



**Bank Erosion and Long-Term Morphodynamic  
Equilibrium in Alluvial Estuaries**

Dang Quang Thanh

MSc Thesis WSE-CEPD-06.07

March 2006

UNESCO-IHE  
Institute for Water Education







# **Bank Erosion and Long-Term Morphodynamic Equilibrium in Alluvial Estuaries**

Master of Science Thesis  
by  
**Dang Quang Thanh**

Supervisor  
**Mick van der Wegen, MSc.,(UNESCO-IHE)**

Examination committee

**Prof. J.A. Roelvink, PhD, MSc. (UNESCO-IHE)**  
**Prof. H.H.G Savenije, PhD, MSc. (UNESCO-IHE, TU Delft)**  
**Zheng Bing Wang PhD, MSc. (TU Delft, WL|Delft Hydraulics)**

This research is done for the partial fulfilment of requirements for the Master of Science degree at the  
UNESCO-IHE Institute for Water Education, Delft, the Netherlands

**Delft**  
**March 2006**

The findings, interpretations and conclusions expressed in this study do neither necessarily reflect the views of the UNESCO-IHE Institute for Water Education, nor of the individual members of the MSc committee, nor of their respective employers.

---

## Abstract

Estuarine areas are related to many human activities of increasing social and economic importance such as navigation, recreation, fishing and aquaculture, sand mining, land reclamation and in some cases hydrocarbon mining. On the other hand, many estuaries and lagoons form the basis of highly valuable and sometimes unique ecosystems. The understanding of the morphology of an estuary system is required for present day and future management. However, understanding and predicting the morphodynamic evolution of estuaries is still limited, because of its complexity and because it involves a wide range of time and spatial scales.

The main objective of this thesis is to investigate the morphodynamic evolution of an alluvial estuary using a process-based model (Delft3D) with special emphasis on bank erosion effects. Special emphasis is also put on an adequate description of the seaward boundary.

The model configuration initially consisted of a rectangular embayment of 500 m wide and 80 km long, with a bed linearly sloping from -15 MSL to 0 at the landward end. Results show that the first 10's of years the banks of the embayment erode rapidly resulting in a filling of the embayment. Additionally, pattern formation takes place at the bed. On a larger timescale the width averaged longitudinal profile develops from linear towards a more concave profile. No equilibrium is reached in terms of the embayment width. This parameter develops towards a landward more linearly than exponentially varying profile. After 800 years the width at the mouth is almost 5 km. Also the width averaged longitudinal profile shows an ongoing development in a continuously sediment exporting embayment.

It is recommended to prolong calculation time and to investigate the effect of the transverse bed slope on the sediment transport more closely.



---

## **Acknowledgements**

The work herein presented is the result of a study done for the partial fulfilment of the Master of Science degree at the UNESCO-IHE Institute for Water Education, Delft, the Netherlands.

I here by express my gratitude to the Government of Netherlands and the Department of Hydraulic Engineering of UNESCO-IHE (Port development and Coastal Engineering) for having sponsored this study.

I am also grateful to the Department of Dike Management and Flood control, Ministry of Agriculture and Rural Development in Vietnam for releasing me to pursue this course in such favorable environment.

I would like to express my special sincere gratitude to Mick van der Wegen, lecturer in Hydraulic Engineering Department, UNESCO-IHE, Delft, for his guidance valuable suggestions and insightful comments on my work.

I would like to thank all the staff members of UNESCO-IHE for the help and encouragement they have given me during my stay and study in Delft.



---

## Table of Contents

Abstract.....	iv
Acknowledgements .....	vi
Table of Contents .....	vii
List of symbols .....	ix
List of figures .....	x
<b>1. Introduction .....</b>	<b>1</b>
1.1. Estuarine morphodynamics .....	1
1.2. Objectives and research questions.....	2
<b>2. Literature review .....</b>	<b>3</b>
2.1. Tidal propagation.....	3
2.2. Tidal asymmetry analysis .....	4
2.3. Tidal damping in ideal estuaries.....	8
2.4. Channel-shoal patterns .....	9
2.5. Bed level equilibrium in longitudinal direction.....	12
2.6. Approaches to numerical morphological modelling .....	13
2.6.1. Tide-averaging approach .....	13
2.6.2. RAM approach .....	14
2.6.3. Online approach with morphology factor.....	16
2.6.4. Parallel online approach .....	17
<b>3. Description of the idealized estuary and modelling setup .....</b>	<b>18</b>
3.1. Numerical model description .....	18
3.1.1. Flow .....	18
3.1.2. Drying and flooding .....	19
3.1.3. Erosion of dry cell .....	19
3.1.4. Morphological time scale factor .....	20
3.1.5. Sediment transport.....	20
3.1.6. Effect of bed-slope .....	21
3.2. Base model schematisation and boundary setup .....	23
3.2.1. Base model schematisation.....	23
3.2.2. Boundary setup.....	24
<b>4. Sensitivity analysis.....</b>	<b>26</b>
4.1. Effect of transverse bed slope.....	26
4.1.1. Effect of $\alpha_{bn}$ to cross-section of embayment.....	26
4.1.2. Effect of $\alpha_{bn}$ to longitudinal profile.....	30
4.1.3. Effect of $\alpha_{bn}$ to shoal pattern .....	33
4.1.4. Discussion for the selection of $\alpha_{bn}$ value.....	33
4.2. Effect of boundary condition.....	35
4.2.1. Effect of boundary condition to cross-section and shoal pattern of embayment .....	35
4.2.2. Effect of boundary condition to longitudinal profile.....	38
4.2.3. Discussion.....	38
4.3. Effect of grain size diameter.....	41

---

<b>5. Result from long term model running.....</b>	<b>43</b>
5.1. Shoal pattern.....	43
5.2. Longitudinal profile.....	52
5.3. Cross-section .....	53
5.4. Cross-section and prism relationship.....	55
5.5. Hydrodynamic equilibrium .....	56
<b>6. Conclusion and recommendation .....</b>	<b>65</b>
6.1. Conclusion.....	65
6.2. Recommendations .....	66
<b>7. References .....</b>	<b>68</b>

---

## List of symbols

Symbol	Description	SI-Unit
$\gamma$	Dronkers asymmetry ratio	
$\varepsilon$	Phase difference between the occurrence of HWS and HW	
$\beta$	Exponent with default value	
$\eta$	Water level	[m]
$\nu$	Diffusion coefficient (eddy viscosity)	[m <sup>2</sup> /s]
$\alpha_{bn}$	Transverse bed gradient factor for bed load transport	
C	Chezy's coefficient	
$c_c$	Emperical coefficient	
D	Water depth w.r.t. MSL	[m]
f	Friction factor ( $f > 1$ )	
F	Tidal froude number = $v/c$ ; $c^2 = gh$	
$F_{x,y}$	x- and y-component of external forces due to wind and waves	[N/m <sup>2</sup> ]
g	Gravitational acceleration ()	[m <sup>2</sup> /s]
H or a	Tidal amplitude	[m]
MORFAC	Morphological scale factor	
THETSD	Global / maximum dry cell erosion factor	
U	Magnitude of total velocity, $U = (u^2 + v^2)^{1/2}$	[m/s]
u	Depth-averaged velocity in u direction	
v	Depth-averaged velocity in v direction	[m/s]
$\rho_w$	mass density of water (kg/m <sup>3</sup> )	



---

## List of figures

Figure 1.1 Scheme of a morphodynamic system.....	1
Figure 1.2 A relationship between the various time and length scales, De Vriend (1996) .....	2
Figure 2.1 Stages of Estuary Development (Pethick, 1994).....	5
Figure 2.2 Branching channel pattern. The smallest channels are assigned to the first order. Two first order channels merge into a second order channel and so on (from Cleveringa and Oost, 1999).....	10
Figure 2.3 Braided channel pattern in the Western Scheldt estuary.....	10
Figure 2.4 Sketch of meandering tidal channel system by Ahnert (1960).....	11
Figure 2.5 Sketch of ebb (E) and flood (F) channel system by Van Veen (1936-1950).....	11
Figure 2.6 Flow diagram of tide-averaging morphodynamic model setup .....	14
Figure 2.7 Flow diagram of RAM approach .....	15
Figure 2.8 Flow diagram of RAM approach .....	16
Figure 2.9 Flow diagram of ‘Parallel online’ approach.....	17
Figure 3.1 model schematisation.....	24
Figure 4.1 Width of embayment with $\alpha_{bn} = 5$ and $\alpha_{bn} = 10$ after 200 years .....	28
Figure 4.2 Cross-section A-A of embayment after 15 years and 200 years.....	28
Figure 4.3 Fitting the length of the cross-section with exponential function in log scale with $\alpha_{bn}=5$ .....	29
Figure 4.4 Fitting the length of the cross-section with exponential function in log scale with $\alpha_{bn}=10$ .....	29
Figure 4.5 Longitudinal profile for first 15 years with different $\alpha_{bn}$ .....	31
Figure 4.6 longitudinal profiles after 200 years with different $\alpha_{bn}$ .....	31
Figure 4.7 Longitudinal different profile for different points in time with coefficient $\alpha_{bn}$ = 5 .....	32
Figure 4.8 Longitudinal different profile for different points in time with $\alpha_{bn} = 10$ .....	32
Figure 4.9 Illustrate of bed-load sediment transport.....	33
Figure 4.10 (a) shoal pattern with $\alpha_{bn} = 5$ ; (b) shoal pattern with $\alpha_{bn} = 10$ .....	34
Figure 4.11 Length of sand bar with (a) $\alpha_{bn} = 5$ ; (b) $\alpha_{bn} = 10$ .....	34
Figure 4.12 Cross section of for different boundary conditions.....	35
Figure 4.13 Shoal pattern of estuary for different tidal propagation direction;.....	36
Figure 4.14 The schematic current patterns at mid-flood and mid-ebb show the effect of interruption of shore-parallel currents by the tidal currents through the inlet by Sha (1989) .....	37
Figure 4.15 Current pattern at mid-ebb (above) and mid-flood (below) at initially of the model resembled with the description of Sha (1989) (Tidal propagation is parallel to the coast).....	37
Figure 4.16 Longitudinal profile of the width-averaged depth for different tidal propagation direction.....	38
Figure 4.17 Tidal current roses for a tidal cycle in the ebb-tidal delta of Texel inlet....	39
Figure 4.18 Current pattern at mid-ebb (above) and mid-flood (below) after 200 years model. Tidal propagation is parallel to the coast.....	40
Figure 4.19 Longitudinal profile of the width-averaged depth for difference in grain size .....	41
Figure 4.20 Width of embayment with for difference in grain size .....	42
Figure 4.21 Shoal pattern of estuary for different grain size; (a) $D_{50} = 240\mu\text{m}$ , (b) $D_{50} =$ $180\mu\text{m}$ , perpendicular tide .....	42

Figure 5.1 Shoal pattern; (a) initial, (b) after 200 years, (c) after 400 years, (d) after 600 years, (e) after 800 years.....	46
Figure 5.2 Fomation of channel and shoal at the first part of estuary .....	47
Figure 5.3 (a) The result from model at 35km from mouth after 600 years, the arrows show the residual sediment transport direction ; (b) Sketch of ebb (E) and flood (F) channel system by Van Veen (1936-1950). (c) Sketch of "circulating sand currents" by Van Veen (1950).....	48
Figure 5.4 The result of model at 50km from mouth after 600 years; the arrows show the residual sediment transport direction. (b) Section of the Western Scheldt estuary, the Netherlands, 1996. The trajectories indicate the direction of the residual velocity. (c) Sketch of meandering tidal channel system by Ahnert (1960). .....	50
Figure 5.5 Water level (dashed) and velocity (line) at the mouth of the estuary (left panel) and halfway up the estuary (right panel). Ebb velocities have a negative sign, flood velocities are positive .....	51
Figure 5.6 Longitudinal profile for different points in time .....	52
Figure 5.7 Width of embayment after 200, 400, 600 and 800 years .....	53
Figure 5.8 Fitting the length of the cross-section with a linear function.....	54
Figure 5.9 Fitting the length of the cross-section with a exponential function .....	54
Figure 5.10 Relation between tidal prism ( $m^3$ ) and the cross-section below MSL ( $m^2$ ) for different points in time plotted on a logarithmic scale. The line represents the relation by Jarret (1976) for a basin with no jetty or single jetty. ....	55
Figure 5.11 Relation between Channel volume below MSL and tidal prism. In relationship with Eysink equation. ....	56
Figure 5.12 $H_{hw}/H_{lw}$ versus $S_{hw}/S_{lw}$ including relation of Dronkers (1998).....	57
Figure 5.13 Ratio of channel depth at High Water (Hhw) and Low Water (Hlw) and the ratio of wet surface at these water levels (Shw and Slw) for all Dutch tidal waters. The curve represents the condition for approximately equal ebb and flood duration and indicates a morphological equilibrium (from Dronkers, 1998). ....	57
Figure 5.14 Diagram of Friedrichs and Aubrey (1988). $V_s$ = Volume of intertidal storage, $V_c$ = Channel volume, $a$ = tidal amplitude at mouth, $h$ is average waterdepth at MSL. Shaded area represents ebb dominant model configurations and clear area flood dominant conditions.....	58
Figure 5.15 $V_s/V_c$ versus $A/h$ of the model .....	58
Figure 5.16 Mean total sediment transport at the mouth after 800 year model.....	59
Figure 5.17 Overview in water level and velocity.....	60
Figure 5.18 Overview in water amplitude and velocity amplitude .....	61
Figure 5.19 Overview in flood duration and ebb duration .....	62
Figure 5.20 over view in time lags .....	63

---

# 1. Introduction

## 1.1. Estuarine morphodynamics

An estuary is an inland river valley or section of the coastal plan, drowned as the sea invaded the lower course of a river during the Holocene sea-level rise. Estuaries are affected by tides, and usually shallower than 20 m. Estuaries attract a variety of human activities, such as navigation, recreation, fishing and aquaculture, sand mining, and land reclamation. On the other hand, many estuaries form the basis of highly valuable and sometimes unique ecosystems. They function as nursery grounds for many species and as resting and feeding grounds for many others. For the proper management of these systems, it is important to be able to predict the impacts of human activities and natural forces, such as sea level rise, changing properties of the tide and changes in the storm climate.

The systematic study of features (landforms) of alluvial sediment which are shaped by the action of water in estuaries is known as estuarine morphology. Morphodynamics concerns the ongoing evolution of morphological features due to the, generally nonlinear, interaction between these features and the forcing hydrodynamic conditions, together with climatic, geological, biological and anthropogenic conditions (see Figure 1.1)

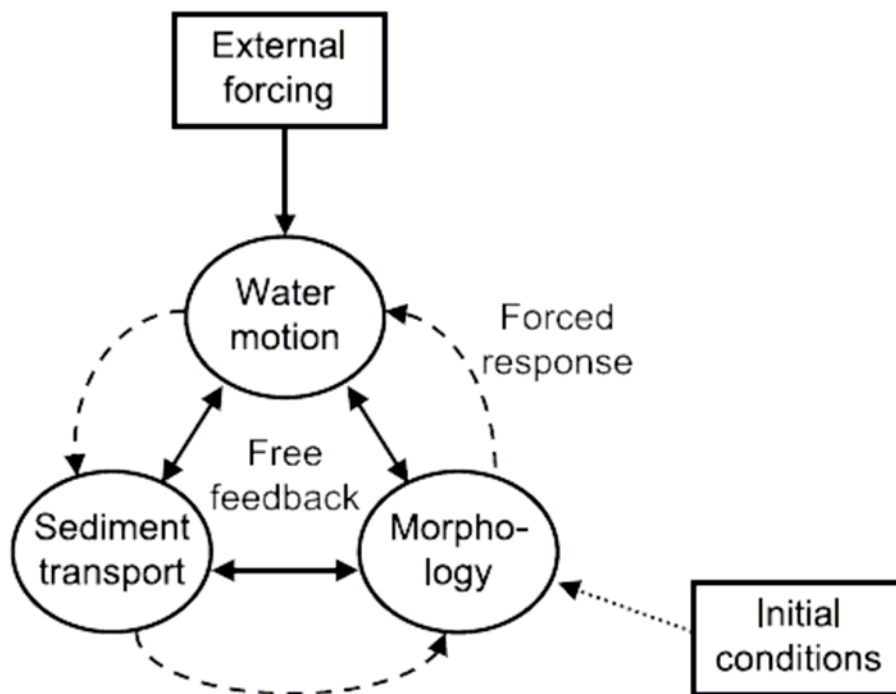


**Figure 1.1** Scheme of a morphodynamic system

---

Characteristic morphological time scales range from hours to several decades or even hundreds of years. Typical length scales may vary from ripples and dunes to sandbanks and complete estuaries. A relationship between the various time and length scales was given by De Vriend (1996) (Figure 1.2)

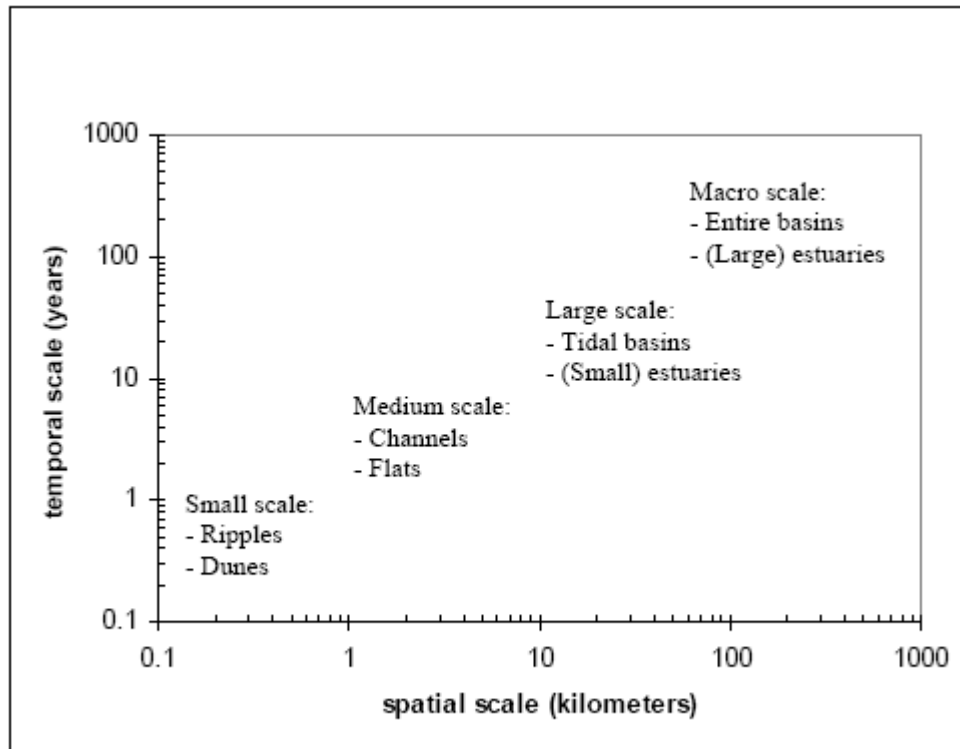


**Figure 1.2** A relationship between the various time and length scales, De Vriend (1996)

## 1.2. Objectives and research questions

The general objective of this research is to investigate the morphodynamic equilibrium of an alluvial estuary with special emphasis on bank erosion effects.

In order to reach the objective a process-based model (D3D) is used. This model describes hydrodynamic process by the shallow water equation and includes different formula to describe the associated sediment transport processes.

---

## 2. Literature review

### 2.1. Tidal propagation

Tides are generated by mutual attraction force between earth, moon and sun. In deep water tide can be described as long harmonic waves with the horizontal tide and the vertical tide having the same phase. The character of tidal wave can be described by tidal amplitude (the height difference between high water level and low water level), celerity (the propagation speed of tidal wave) and tidal period (the period between high water and low water). In estuaries due to the influence of the geometry, the character of the tidal wave will change. This is so called tidal distortion. Some factor causing the tidal distortion:

- The advection and friction terms.
- The propagation speed of tide at the mouth is represented by the celerity ( $c=\sqrt{gh}$ ). So that at high water tide propagates faster than at low water. The period between high water and low water (for a progressive tidal wave this is the ebb period) will thus increase and the flood period will decrease in landward direction. This means that flood velocities will increase and ebb velocities will decrease.
- Friction will result in loss of energy and damp the tidal wave. Additionally, the influence of friction will be larger for smaller water depths. This means that ebb velocities are most subject to friction and, thus, duration of ebb will be larger.
- Low velocities in inertial tidal marshes and flats causing high tide to propagate slower than low tide;
- Depending on the situation, the inlet cross sectional area is smaller during ebb than during flood, forcing higher ebb velocities;

Friedrich and Aubrey (1988) investigated dominated estuaries along the US Atlantic coast and compared the tidal behaviour with the results of a numerical, one-dimensional model based on trapezoidal channel geometry and more gentle sloping tidal flats. They conclude that non-linear tidal distortion is caused by the generation of over tides in an estuary (with  $M_4$  as the main constituent) and is a composite of two principal effects;

- 1) Friction reflected by the ratio of tidal amplitude and the channel depth ( $a/h$ ) and causing relatively shorter floods. This follows from the fact that shallow channels slow the propagation of low water through the estuary, shortening the flood;
- 2) The inertial storage calculated by the ratio of the volume of inertial storage and the volume of the channels at mean sea level. The smaller this ratio is, the shorter

---

ebb will be. This follows from the fact that extensive inertial storage slows the propagation of high water, which shortens the ebb duration;

Furthermore, they conclude that, for small values of  $a/h$  ( $<0.2$ ), estuaries are ebb-dominant and larger values of  $a/h$  ( $>0.3$ ) estuaries are flood-dominant. With surface distortion growing with distance into the estuary, the longer the system, the greater the likelihood of flood dominance.

Later, Friedrichs et al (1990) investigated the impact of relative sea level rise on tidal propagation in shallow, well-mixed estuaries using roughly the same model. This included coarse bed material. Flood dominant estuaries appeared to be more sensitive to changes in the ratio of tidal difference over depth ( $a/h$ ). Ebb dominant estuaries are more sensitive to changes in the ratio of inter-tidal storage over channel volume. Sea level rise results in more pronounced ebb dominance in ebb dominant estuaries and a possible shift from flood dominance to ebb dominance in case of flood dominated estuaries. Morphological developments were not taken into account.

## 2.2. Tidal asymmetry analysis

To define stages of estuary development (Pethick, 1994) referred to the work of (Dronkers, 1986) who recognised two quite distinct estuarine channel types, (Figure 2.1).

The first, termed Type I by (Dronkers, 1986), is a wide deep, rectangular shaped channel cross section whose inter-tidal flats are low, generally below mean seal level. The mean depth of such a channel will increase as the flood tide enters the estuary so that the crest of the flood wave travels more rapidly in deeper water than the trough of the ebb tide:

$$C_{crest} = \sqrt{g(D + 0.5)}$$
$$C_{trough} = \sqrt{g(D - 0.5)}$$

and  $C_{crest} > C_{trough}$

This gives flood tide dominance to these Type I estuaries which will result in a net accumulation of sediment so that deposition takes place in the estuary. Since most of this deposition will take place on the inter-tidal flats of the estuary channel these will rise relatively rapidly in the tidal frame so that the channel cross section changes from its initial wide deep rectangular configuration to a central ‘slot’ channel within high bounding mudflats.

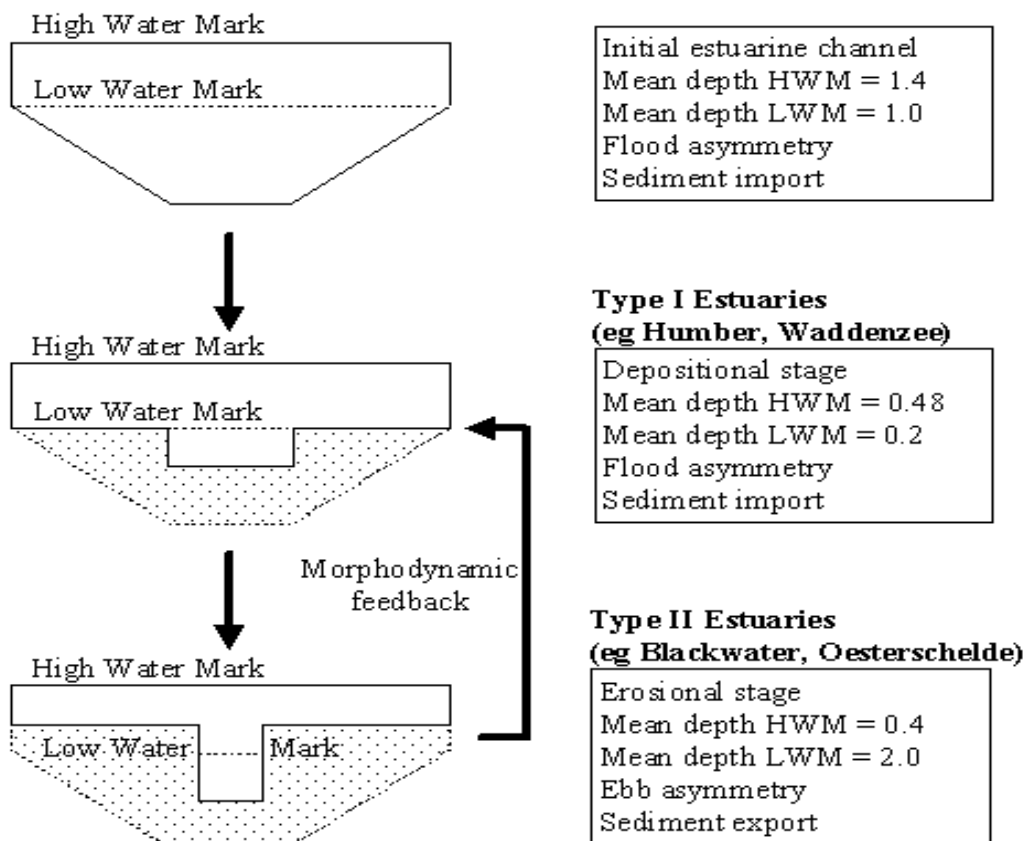


**Figure 2.1** Stages of Estuary Development (Pethick, 1994)

These Type II channels will exhibit a decrease in mean depth as the flood tide enters the estuary due to the large area of high elevation mudflats. The crest of the flood tide therefore moves less rapidly than the trough of the ebb and an ebb tide dominance is set up. Consequently, these Type II estuaries tend to become net exporters of sediment.

If these two channel types are considered as temporal stages in the development of an estuary then it can be seen that Type I estuaries represent the early stages immediately after the Holocene transgression in which wide deep estuaries rapidly infill with sediment. As the inter-tidal flats of the estuary develop however, so sediment supply on the flood is reduced and new morphology is attained - the Type II estuary. If the inter-tidal flats continue to accrete then a net export of sediment will take place and the estuary reverts to Type I. This morphological feedback mechanism then holds the estuary in a dynamic equilibrium oscillating between Type I and Type II characteristics.

The flood or ebb dominance does not necessarily lead to deposition or erosion, instead the asymmetry of the flood and ebb limbs of the tidal velocity curve, and in particular the length of high water slack period as compared to the low water slack,

---

appear to control the net sediment budget of the inter-tidal areas. (Dronkers, 1986) showed that if the high water slack period is more protracted than that at low water then more suspended sediment will be deposited on the upper mudflats at high water than on the lower mudflats at low water. This means that a net landward movement of sediment will take place in the estuary while a longer low water slack will lead to seaward movement.

Moreover, the progression from a Type I to a Type II estuary does not necessarily result in the net export of sediment from an estuary but does imply the movement of sediment from the inter-tidal to the sub-tidal channels

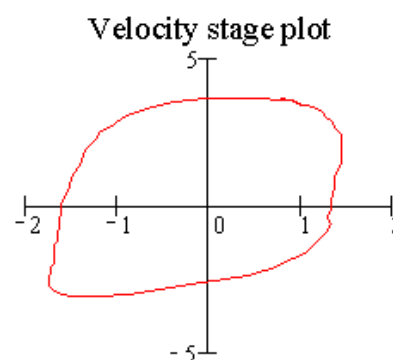
In order to examine along estuary variations in the hydraulics and the potential consequences for sediment transport and estuary form, a number of tidal asymmetry measures can be useful. The simplest representation of asymmetry is to note the difference between the duration of the flood and ebb. This begins to describe the skew in the surface elevation over time as can be seen in the plot below based on tidal conditions just upstream of Hull on the Humber estuary. A number of alternative ways of examining asymmetry are described below, which take fuller account of the variation in flows and periods of slack water as well as their duration.

#### (a) Plots

To gain a visual impression of the degree of asymmetry the plot of velocity and elevation against time illustrates relative duration, rates of change and the phase relationship between elevation and flow.

Examining this type of plot at intervals along the estuary can provide a good

description of the estuary hydraulics. An alternative is the velocity stage plot (shown left), which provides an indication of flood/ebb dominance and highlights the magnitude of velocities at different elevations. A circle or oval represents a symmetric tide and increasing asymmetry produces distorted balloon shapes, where the area of the shape, relative to the axes, indicates flood or ebb dominance. By adding markers on the curve at equal time intervals, or plotting in 3D, one can also take account of the duration at a given stage.



---

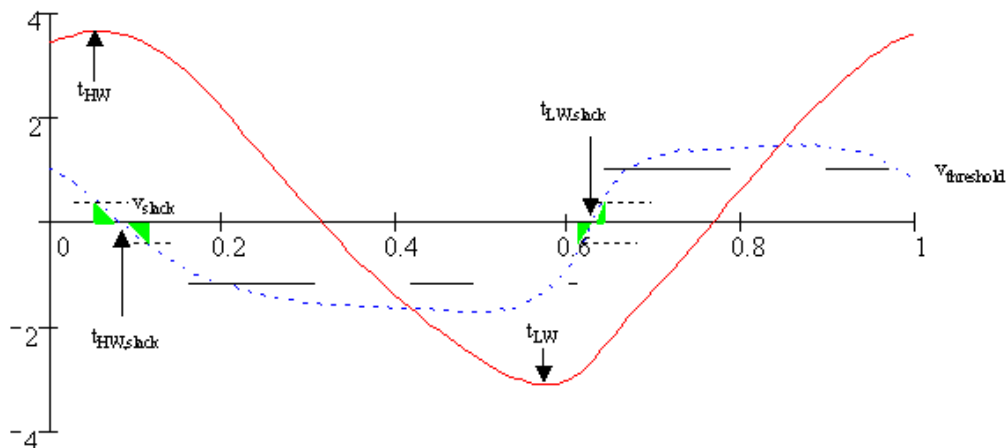
### (b) Dronkers tidal asymmetry ratio

Using the hypothesis that morphological equilibrium equates to a uniform tide, Dronkers derived an asymmetry ratio based on certain estuary form parameters (Dronkers, 1998):

$$\gamma = \left( \frac{h + a}{h - a} \right)^2 \cdot \frac{S_{lw}}{S_{hw}}$$

where  $h$  is the mean hydraulic depth of the estuary given approximately by  $h = a + V_{lw}/S_{lw}$ , although Roberts et al (1998) found that it was more reliable to use  $h_{hw} = V_{hw}/S_{hw}$  and  $h_{lw} = V_{lw}/S_{lw}$ . The other variables are,  $a$ , the tidal amplitude,  $S_{lw}$ , the surface area at low water,  $S_{hw}$ , the surface area at high water, and  $V_{hw}$  and  $V_{lw}$ , the volumes at high and low water. A value of  $\gamma$  equal to one suggests a uniform tide, with values greater than one indicating flood dominance and less than one indicating ebb dominance. This form ratio is proportional to the ratio of the time between high water and the high water slack ( $t_{hw,slack} - t_{hw}$ ) and the time between low water and the low water slack ( $t_{lw,slack} - t_{lw}$ ). Measuring this ratio directly from the tidal curves at various locations in the estuary provides a means of assessing how the asymmetry varies along estuary and the value at the mouth can be compared with the value,  $\gamma$ , derived from the form version, as given above.

### (c) Slack gradient



In an earlier paper, (Dronkers, 1986) noted the importance of maximum velocities, for the movement of the coarse sediment fraction, and the duration of periods of slack water for the movement of fines. This was defined as the rate of change of tidal velocity (i.e. flow gradient) at the time when the velocity is zero. If the rate of change is slower at the high water slack (flatter slope in time series plot above) this provides greater opportunity for fine sediment to settle out than during the more rapid flow reversal at low water. In this case import of sediment is favoured. When the rate of change is slower around low water slack then export of sediment is favoured. For this study the gradients have been calculated and the difference

presented (i.e. SBF-SBE), where a positive value indicates flood dominance and a negative value ebb dominance.

**(d) Slack duration**

Actual tidal curves can be quite complex particularly around the time of slack water. As a consequence the gradient at slack water is not always representative of the slack duration. An alternative approach is therefore to determine the duration of time when the flow is below some threshold,  $v_{\text{slack}}$ . Again taking the difference between high and low water values ( $t_{\text{hw,slack}} - t_{\text{lw,slack}}$ ) provides a measure of the asymmetry for the movement of fine sediments, with positive values indicating flood dominance and negative values ebb dominance.

**(e) Tidal excursion**

Peak velocities on flood and ebb are used as a first indicator to the preferred direction of movement for the coarse sediment fraction. However, this measure takes no account of the duration of such peak velocities. It is quite common for a slightly lower velocity on one stage to prevail for much longer than the higher peak value on the opposing stage. One way to get over this is to calculate the net tidal excursion, which is simply the difference between the areas under the curve for the flood and ebb velocity. Again this may not give a wholly representative indication of movement if there are long periods at relatively low velocities. To overcome this a threshold is introduced,  $v_{\text{threshold}}$ , and the area above the threshold used to calculate the respective flood and ebb excursions. Taking the difference between flood and ebb values gives the net excursion, with positive values indicating flood dominance and negative values ebb dominance.

**2.3. Tidal damping in ideal estuaries**

Tidal damping or amplification occurs depends on the balance between a friction term and amplification term (Savenije 1998).

The tidal damping can be expressed in equation (Savenije 1998, 2001)(for constant bed level and exponential width in longitudinal direction)

$$\frac{dH}{dx} = \frac{H}{h} \left( \frac{\frac{h}{b} - f \frac{g}{C^2} F \sin \varepsilon}{1 + \frac{H}{h} \frac{1}{2F \sin \varepsilon}} \right) \quad (1)$$

in which :

F: Tidal froude number =  $v/c$  ;  $c^2 = gh$

C: Chezy's coefficient

H : tidal amplitude

$\varepsilon$  : phase difference between the occurrence of HWS and HW( or LWS and LW)

$$\varepsilon = \arctan \left[ \frac{\omega b}{(1 - \alpha b)c} \right] \quad (2)$$

where:

$\omega$ : harmonic constant ( $2\pi/T$ )

$b$ : convergence length

$c$ : wave celerity

$\alpha \approx \frac{1}{H} \frac{dH}{dx}$  damping constant

$\sin(\varepsilon)$  is dimensionless number that defines the character of the wave. If  $\sin(\varepsilon) = 1$ , the tidal wave is purely progressive wave (maximum velocity at HW and LW), if  $\sin(\varepsilon) = 0$  the tidal wave is a standing wave (the velocity at HW and LW is zero). In alluvial estuaries the tidal wave is of a mixed character and  $0 < \sin(\varepsilon) < 1$  (Savenije 1992a).

$f$ : friction factor ( $f > 1$ )

$$f = \left[ \frac{1}{1 - \left( \frac{H}{2h} \right)^2} \right] \quad (3)$$

Equation (1) shows us that tidal damping depends on a set of dimensionless numbers, the tidal range to depth ratio  $H/h$ , the estuary shape number  $h/b$ , the friction number  $g/C^2$ , the friction factor  $f$ , the Froude number  $F$ , and the wave-type number  $\sin(\varepsilon)$ .

Look into expression  $\frac{h}{b} - f \frac{g}{C^2} F \sin \varepsilon$  in equation (1) it appears that the longitudinal tidal damping appears to depend primarily on the shape number and friction term. If the shape number is larger than the friction term, there is amplification otherwise there is tidal damping. From equation (1) it can be seen that in an ideal estuary  $\frac{h}{b} = f \frac{g}{C^2} F \sin \varepsilon$  where all parameters are constant along the estuary. Ideal estuary is described by Pillsbury (1956) as no tidal damping or amplification. The increase of energy per unit width of the incoming tidal wave as the banks converge is exactly compensated by friction loss. Consequently width varies exponentially, and depth, roughness and wave celerity are constant along the estuary.

## 2.4. Channel-shoal patterns

Two different types of multiple channel systems can be distinguished, braided patterns and fractal patterns. In fractal or tree-like structures the large inlet channel branches into smaller channels, which branch on their turn and so on. Figure 2.2 shows the tidal-channel system in the Dutch Wadden Sea, which can be

characterized as three- to four-times branching networks (Cleveringa and Oost, 1999). The branch lengths of the channels decrease logarithmically and are related to the tidal prism and the drainage area. Each channel has a certain drainage area, which limits the amount of channels that can be maintained in (a part of) the drainage basin. In the Wadden Sea branching does not continue below the 500-m scale (Cleveringa and Oost, 1999). The upper limit is usually of geological nature (Rinaldo et al., 2001). Between these scale limits, fractal channel systems are similar and without a scale bar it is not possible to devise the scale. Contrary to by tree-like patterns are braided patterns (Rinaldo et al., 2001).



**Figure 2.2** Branching channel pattern. The smallest channels are assigned to the first order. Two first order channels merge into a second order channel and so on (from Cleveringa and Oost, 1999).

Braided patterns are observed by Ahnert (1960) in the estuaries around the Chesapeake Bay, Maryland, USA, and in the Western Scheldt estuary (Figure 2.3) in the Netherlands by Van Veen (1950).

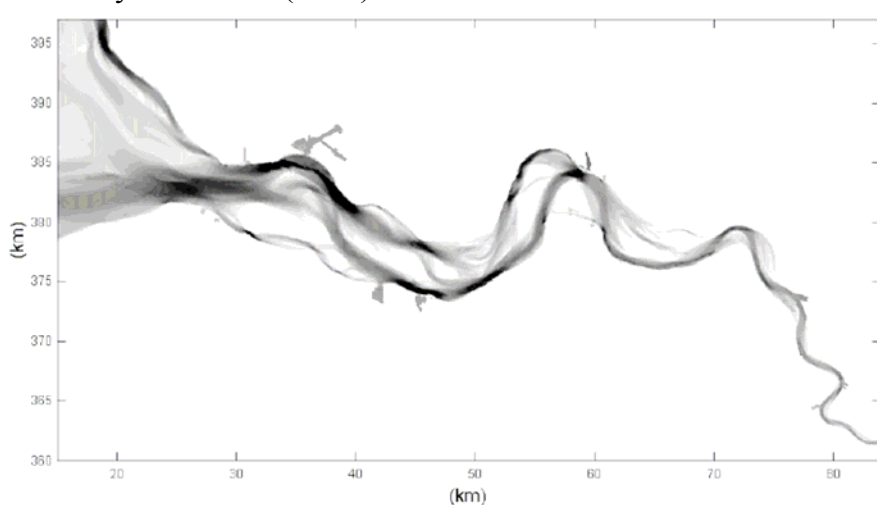


**Figure 2.3** Braided channel pattern in the Western Scheldt estuary.

Ahnert's cartoon of the channel pattern in the Patuxent River estuary shows a sequence of braided ebb- and flood-dominated meanders with a shoal in between (Figure 2.4). He observed that this pattern only occurs at certain stretches in the middle part of the estuaries, and attributes this to the modification of the tidal wave. As the tidal wave enters the estuary it has the character of a progressive wave, where maximum flood currents occur around maximum water levels and maximum ebb-currents around minimum water levels. When the tidal wave proceeds in the estuary, an increasing phase shift between maximum currents and water level develops. At the stretch where this pattern is found, the water levels around high ebb- and flood currents are comparable, thus causing comparable lateral erosion, which result in similar pattern development of ebb- and flood channels.

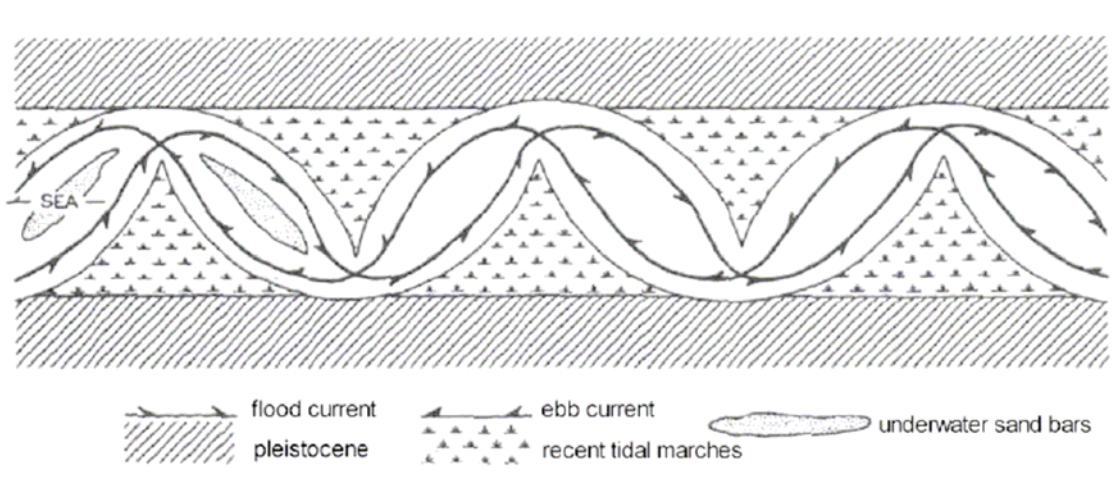


**Figure 2.4** Sketch of meandering tidal channel system by Ahnert (1960).

The Western Scheldt estuary shows a similar braided pattern in the middle stretch of the estuary. Where ebb- and flood-dominated channels meet a threshold develops. In his characterization of ebb- and flood channel systems in the Dutch estuaries, Van Veen (1950) sketches the pattern as an ongoing meandering ebb-channel and flood-dominated side channels, separated by shoals and thresholds (Figure 2.5). Van Veen already made the distinction between the fractal pattern (apple tree) in the Wadden Sea and braided pattern (poplar tree) in the Western Scheldt estuary as two characteristic different types of channel systems in estuaries.

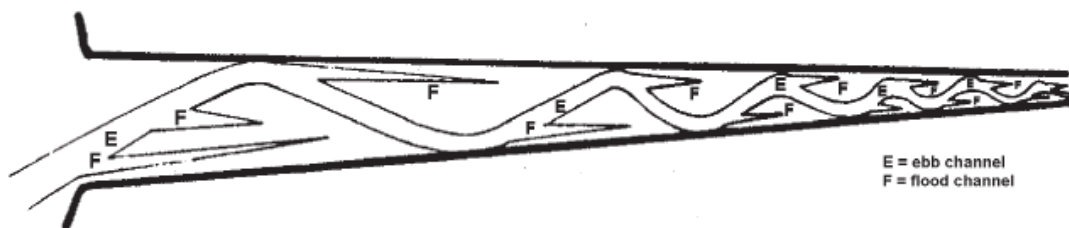


**Figure 2.5** Sketch of ebb (E) and flood (F) channel system by Van Veen (1936-1950).

---

## 2.5. Bed level equilibrium in longitudinal direction

Friedrichs and Aubrey (1996) developed a model for short tidal basins that correlates these forcings with the hypsometry of basins, i.e. the distribution of horizontal surface area with respect to elevation. Convex profiles (from a bottom point-of-view) are associated with tide dominance, thus large tidal amplitudes and minor wave activity, and concave profiles are correlated with wave-dominated basins. The physical background forms the assumption that tidal flats are in equilibrium if the maximum bottom shear stress, resulting from tidal currents and wind waves, is spatially uniform.

Schuttelaars and De Swart (1996) developed a model describing the interaction between tidal currents, sediment transport and bed form changes in a one-dimensional short (compared to the tidal wavelength) embayment with a constant width. The hydrodynamic forcing consisted of a prescribed tidal elevation ( $M_2$  and  $M_4$ ) and zero flux at the closed end. The hydrodynamics were described by the depth integrated shallow water equations. Both a bed load and a suspended load model were considered. They show that equilibrium profiles exist without a prescribed overtide (constantly sloping for the suspended load model and flat bed for the bed load model) and with a prescribed overtide (concave or convex for the suspended load model (depending on the ratio of advective and diffusive transports) and a constant slope for the bed load model).

Schuttelaars and De Swart (2000) extended their earlier model to longer embayments. In case of an externally prescribed  $M_2$  tide unique morphodynamic equilibria are obtained for embayment lengths smaller than the frictional length scale of the tide. In case of an additionally prescribed overtide ( $M_4$ ) the equilibrium is strongly concave for embayment lengths smaller than the  $M_4$  resonance length scale (with the water motion resembling a standing tidal wave). For longer embayments, the equilibrium bottom profiles are weakly concave with a traveling tidal wave. For sufficiently strong  $M_4$  amplitudes multiple morphodynamic equilibria are found. The maximum embayment length, beyond which morphodynamic equilibria cease to exist, decreases with increasing influence of external overtide and bottom friction. Additionally, they showed that bottom friction causes tidal resonance to occur for a shorter length than a quarter of the frictionless tidal wavelength.

Hibma (2003a) compared the results from Schuttelaars and De Swart (1996 and 2000) based on an idealized model to the process-based model described in Lesser et al (2004). She found good resemblance of the results assuming some adaptation of the process-based model at the estuarine mouth (fixed bed level). The results hold both  $M_2$  and  $M_4$  tide constituents at the boundary at the mouth as well as the  $M_4$  constituent generated in the model domain.

---

Lanzoni and Seminara (2002) investigated the morphodynamic equilibrium of a funnel shaped embayment, based on the one dimensional Saint Venant equations. The embayment was frictionally dominated (relatively shallow), consisting of non-cohesive sediment with insignificant inter-tidal storage of water on tidal flats. Due to flood dominance, sediments were trapped leading to a concavity of the longitudinal bed increasing with increasing estuary convergence and leading to a uniquely determined bed level at the mouth. The maximum tidal velocities along the estuary were found to be nearly constant apart from the shallow part at the closed landward end.

## **2.6. Approaches to numerical morphological modelling**

### **2.6.1. Tide-averaging approach**

This approach is based on the fact that morphological changes take place on a far larger time-scale than the hydrodynamics. Thus, morphological changes within a single tidal cycle are usually very small compared to the trends over a longer period and such small changes do not affect the hydrodynamics or sediment transport patterns much. It is then acceptable to consider the bottom fixed during the computation of hydrodynamics and sediment transport over a tidal cycle. The rate of change of the bed level is computed from the gradients in the tidally averaged transport.

In the Figure 2.6 the flow scheme of the tide-averaging approach is shown. Starting from a given bathymetry, the resulting from flow and wave field are fed into a transport model. This model computes bed load and suspended load transport over tidal cycle. The averaged result is applied to compute the bed changes. The update of the bathymetry is looped back to the transport model through the ‘continuity correction’ or to the full hydrodynamic module.

The limitation of this model is time step limited by the accuracy of the time integration, which is a simple Euler method, since higher-order would involve costly iteration over the whole system. Because of this it necessary to update the transport regularly and the continuity correction method is use. But the main limitation of continuity correction is the assumption that the flow rate and pattern remain constant in time. In case of a shallow area becoming shallower, the flow velocity will keep increasing under continuity correction, whereas in reality the flow will increasingly go around the shallow area.

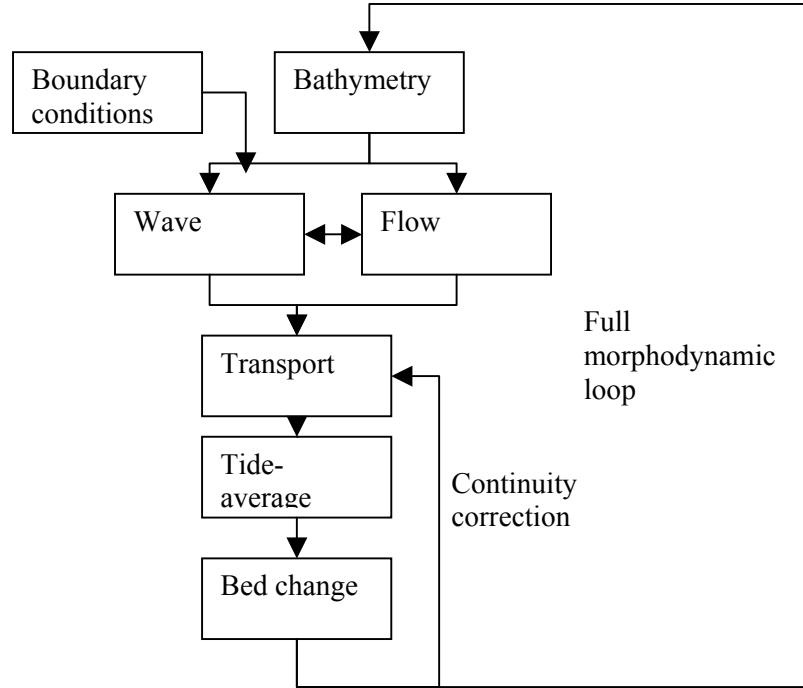


**Figure 2.6** Flow diagram of tide-averaging morphodynamic model setup

### 2.6.2. RAM approach

RAM (Rapid assessment of morphology) is a simple method that gives result of initial transport computations. For a given set of currents and waves, the transport at a given location is assumed to be only a function of the water depth.

$$\frac{\partial z_b}{\partial t} + \frac{\partial S_x}{\partial x} + \frac{\partial S_y}{\partial y} = 0 \quad (4)$$

Where  $z_b$  is the bed level and  $S_x$ ,  $S_y$ , are the sediment transport components. And the equation describing the response of the sediment transport to bottom changes

$$\vec{S} = \frac{\vec{S}_{t=0}}{|\vec{S}_{t=0}|} f(z_b) \quad (5)$$

The form of the function  $f(z)$  can be estimated by considering that the transport usually is proportional to the velocity to a power  $b$

$$|\vec{S}| \sim |u|^b \sim \left( \frac{|\vec{q}|}{h} \right)^b \sim |\vec{q}|^b h^{-b} \quad (6)$$

Where  $\vec{q}$  is the discharge per unit width. Since a similar relationship with the orbital velocity can be assumed, a suitable function is:

$$\left| \vec{S} \right| = A(x, y)h^{-b(x, y)} \quad (7)$$

Where the water depth  $h$  is taken as  $h = HW - z_b$  and  $HW$  is the high water level, which ensure that water depth is always positive.

As a further simplification  $b$  is assumed constant throughout the field. In this case, the value of  $A$  in each point can be derived directly from the local water depth and the initial transport rate.

The combination of equation (4) and (7) can be solved using the same bottom update scheme as in full morphodynamic model and requires very little computation effort. The figure show how RAM model work. As soon as bottom changes become too large, a full simulation of the hydro dynamic and sediment transport is carried out for a number of input conditions. A weight averaged sediment transport field is then determined and the next is RAM computation. The updated bathymetry is then fed back into the detail hydrodynamic transport model. An importance point is that the computation of wave, flow and transport field can be carried out in parallel.

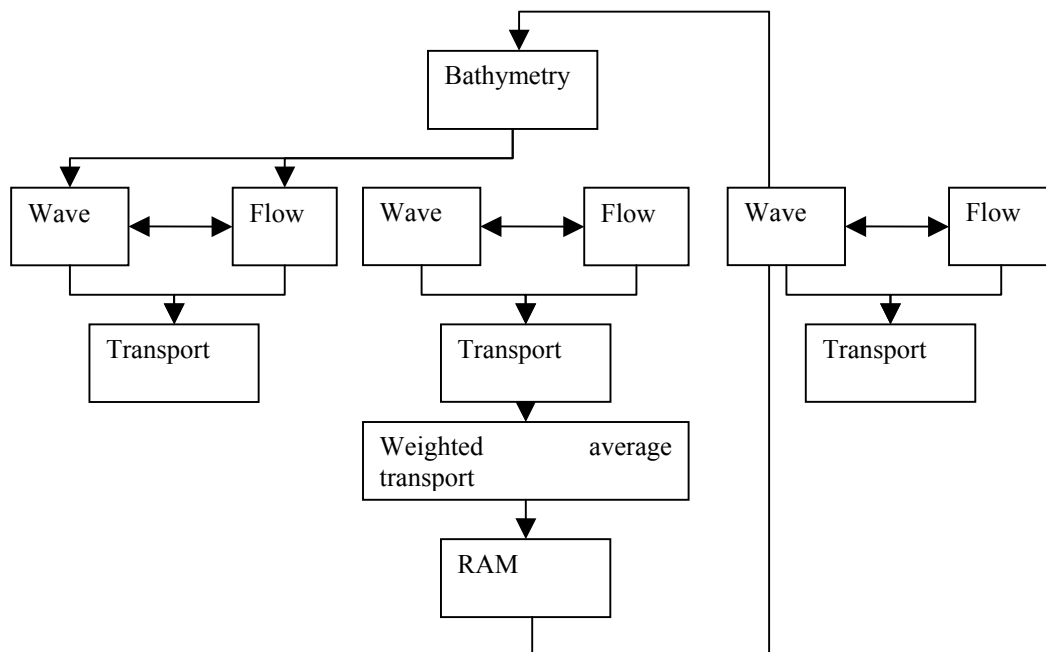


**Figure 2.7** Flow diagram of RAM approach

---

### 2.6.3. Online approach with morphology factor

The two methods above have the common point that the morphology is updated relatively infrequently compare to the number of flow time steps per tidal cycle and the number of transport time steps per cycle.

A different approach is to run flow, sediment transport and bottom updating at the same time steps. However, this method does not take into consideration the different time scales between the flow and morphology. Therefore, a simple device can be used, call the ‘morphological factor’. This factor  $n$  simply increase the depth changes rates by a constant factor, so after a simulation over one tidal cycle we have in fact modelled the morphological changes over  $n$  cycles. The figure below show how the model work

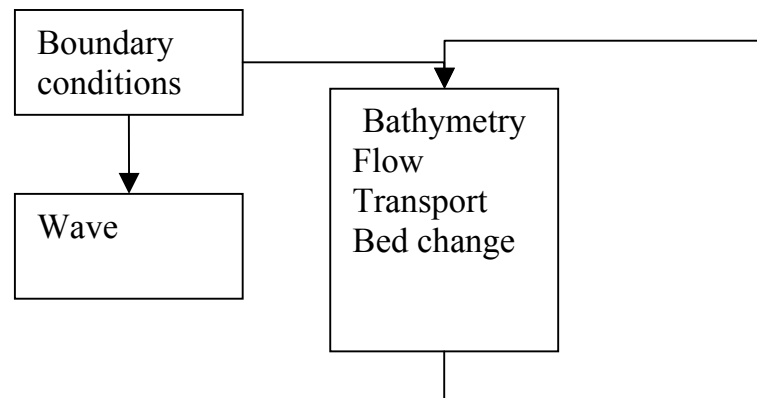


**Figure 2.8** Flow diagram of RAM approach

An importance difference with the two previous methods is that the bottom evolution is computed in much smaller time steps, even when relatively large values of  $n$  are use.

An advantage of the ‘online’ method is that the short-term processes are coupled at flow time-step level, which makes it easy to include various interactions between flow, sediment and morphology, and also removes the need to store large amounts of data between processes.

#### 2.6.4. Parallel online approach

The time interval between conditions (ebb, flood, slack, spring tide, neap etc) is small relative to the morphological time-scale. This lead to the ideal that we can let simulation for different condition run in parallel, as long as they share the same bathymetry which is updated according to the weighted average of the bottom changes due to each condition. The flow scheme of this approach is given in figure 2.9

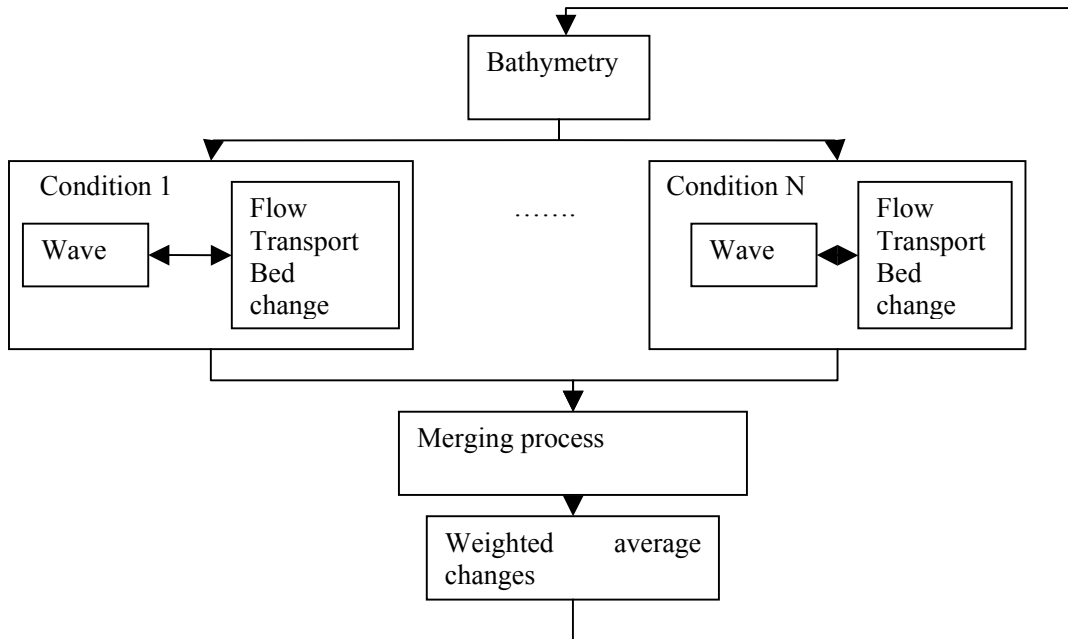


**Figure 2.9** Flow diagram of ‘Parallel online’ approach



---

## 3. Description of the idealized estuary and modelling setup

### 3.1. Numerical model description

The Delft3D modelling system is designed to simulate wave propagation, currents, sediment transport, morphological developments and water quality in coastal, river and estuarine areas (Roelvink and van Banning, 1994; Verbeek et al., 1999). Delft3D is a finite-difference system in which the processes are simulated on a curvilinear grid allowing for an efficient and accurate representation of complex domains. The computational grid is staggered, with the water level, the water depth and the velocity components all defined at different locations within a grid cell (Stelling, 1984). The principal constituents of an estuarine morphodynamic model are the flow, sediment transport and bottom change modules. These will be described below.

#### 3.1.1. Flow

The flow module computes unsteady flow resulting from tidal and meteorological forcings. It is based on the shallow water equations. In this study, the 2DH (2–D depth-averaged) mode is applied and density differences are neglected, thereby constraining the model to well-mixed situations. The depth-averaged equations for conservation of momentum in x- and y-direction are given by:

$$\frac{\partial u}{\partial t} + u \frac{\partial u}{\partial x} + v \frac{\partial u}{\partial y} + g \frac{\partial \eta}{\partial x} - fv + \frac{gu|U|}{C^2(d+\eta)} - \frac{F_x}{\rho_w(d+\eta)} - \nu \left( \frac{\partial^2 u}{\partial x^2} + \frac{\partial^2 u}{\partial y^2} \right) = 0$$

and

$$\frac{\partial v}{\partial t} + u \frac{\partial v}{\partial x} + v \frac{\partial v}{\partial y} + g \frac{\partial \eta}{\partial x} - fu + \frac{gv|U|}{C^2(d+\eta)} - \frac{F_y}{\rho_w(d+\eta)} - \nu \left( \frac{\partial^2 v}{\partial x^2} + \frac{\partial^2 v}{\partial y^2} \right) = 0$$

The depth averaged continuity equation is given by:

$$\frac{\partial \eta}{\partial t} + \frac{\partial u(d+\eta)}{\partial x} + \frac{\partial v(d+\eta)}{\partial y} = 0$$

in which:

C : Chézy coefficient (m<sup>1/2</sup>/s)

d : water depth w.r.t. MSL (m)

---

$g$  : gravitational acceleration ( $m^2/s$ )  
 $f$  : Coriolis parameter ( $s^{-1}$ )  
 $F_{x,y}$  : x- and y-component of external forces due to wind and waves ( $N/m^2$ )  
 $u, v$  : depth-averaged velocity components ( $m/s$ )  
 $U$  : magnitude of total velocity,  $U = (u^2 + v^2)^{1/2}$  ( $m/s$ )  
 $\rho_w$  : mass density of water ( $kg/m^3$ )  
 $\nu$  : diffusion coefficient (eddy viscosity) ( $m^2/s$ )  
 $\eta$  : water level ( $m$ )

### 3.1.2. Drying and flooding

In tidal areas, the shallow parts become dry during low tide. In the FLOW-module, flooding and drying is represented by removing grid cells that become dry when the tide falls, and reactivating cells that become wet when the tide rises. If the total water depth in a velocity point is below a certain threshold (0.1 m in this study), this point is set dry, which means that the velocity is set equal to zero. The computational cell is closed at the side normal to the velocity. If the water level rises and the total water depth is greater than twice the threshold, the velocity point is reactivated. When all four velocity points of a computational cell surrounding a water level point are dry, this cell is excluded from the computation.

### 3.1.3. Erosion of dry cell

In the case of erosion near a dry beach or bank, the standard scheme will not allow erosion of the adjacent cells, even when a steep scour hole would develop right next to the beach. Therefore, a scheme has been implemented, where for each wet cell (if there are dry points adjacent to it) the erosion volume is distributed over the wet cell and the adjacent dry cell. The distribution is governed by a user-specified factor THETSD, which determines the fraction of the erosion to be assigned (evenly) to the adjacent dry cells if THETSD equals zero, the standard scheme is used; if THETSD equals 1, all erosion that would occur in the wet cell is assigned to the adjacent dry cell.

A modification to this method may be done by specifying a parameter HMAXTH larger than the threshold depth for computing sediment transport, SEDTHR. In this case, the factor THETSD is replaced by a factor THET which is computed as:

$$\begin{aligned}
 thet &= (h1 - sedthr) / (hmaxth - sedthr) * thetsd \\
 thet &= \min (thet, thetsd)
 \end{aligned}$$

Here,  $h1$  is the local water depth. The purpose of this formulation is to allow erosion of parts that are inactive in terms of transport but still wet, while limiting the erosion

---

of the dry cell. If erosion of the dry cell is desired, this option is not recommended, so HMAXTH should be set less than SEDTHR. In order to ensure that HMAXTH always less than SEDTHR we assigned HMAXTH = -999 in the model. It means that 100% erosion volume is always assigned to a dry cell.

#### **3.1.4. Morphological time scale factor**

One of the complications inherent in carrying out morphological projections on the basis of hydrodynamic flows is that morphological developments take place on a time scale several times longer than typical flow changes (for example, tidal flows change significantly in a period of hours, whereas the morphology of a coastline will usually take weeks, months, or years to change significantly). One technique for approaching this problem is to use a “morphological time scale factor” whereby the speed of the changes in the morphology is scaled up to a rate that it begins to have a significant impact on the hydrodynamic flows. This can be achieved by specifying a non-unity value for the variable MORFAC in the morphology input file.

The implementation of the morphological time scale factor is achieved by simply multiplying the erosion and deposition fluxes from the bed to the flow and vice-versa by the MORFAC-factor, at each computational time-step. This allows accelerated bed-level changes to be incorporated dynamically into the hydrodynamic flow calculations.

While the maximum morphological time scale factor that can be included in a morphodynamic model without affecting the accuracy of the model will depend on the particular situation being modelled, and will remain a matter of judgement, tests have shown that the computations remain stable in moderately morphologically active situations even with MORFAC-factors in excess of 1000. We also note that setting MORFAC = 0 is often a convenient method of preventing both the flow depth and the quantity of sediment available at the bottom from updating, if an investigation of a steady state solution is required.

#### **3.1.5. Sediment transport**

The sediment transport is determined, with access to a variety of semi-empirical formulae and a depth integrated advection-diffusion solver for suspended sediment. The transport computations are based on the time-dependent current fields. Two different sediment transport options for non-cohesive sediment were tested in this study. First, a total-load transport formula, where the total sediment transport is the sum of bed load and equilibrium suspended load transport. In this study the transport relation of Engelund and Hansen (1967) is used:

$$S = S_b + S_{se} = \frac{0.05\alpha U^2}{g^{0.5} C^3 \delta^2 d_{50}}$$

where:

- U magnitude of flow velocity (m/s)
- $\Delta$  relative density =  $(\rho_s - \rho_w) / \rho_w$
- C friction coefficient
- $D_{50}$  median grain size (m)
- $\alpha$  calibration coefficient

### 3.1.6. Effect of bed-slope

The adjustment of bed-load transport for bed-slope effects is executed in two steps. Firstly, the effect is computed for a bed slope in the same direction as the flow velocity in the bottom layer. Secondly, the effect is computed for a bed slope normal to the flow velocity in the bottom layer longitudinal. The two contributions are added to one bed-load sediment transport vector.

#### a) Longitudinal bed slope

The magnitude of the bed-load transport vector is adjusted if a bed slope exists in the direction of the bed-load transport vector. This bed slope is calculated as:

$$\frac{\partial z_b}{\partial s} = \frac{\partial z_{(u)}}{\partial x} \frac{S_{b,x}''}{|S_b''|} + \frac{\partial z_{(v)}}{\partial y} \frac{S_{b,y}''}{|S_b''|}$$

$$\left( \frac{\partial z_b}{\partial s} \right)_{\max} = 0.9 \tan^{-1}(\phi)$$

Where:

- $\frac{\partial z_b}{\partial s}$  bed slope in the direction of bed-load transport.
- $\frac{\partial z_{(u)}}{\partial x}$  bed slope in the positive x direction evaluated at the U point.
- $\frac{\partial z_{(v)}}{\partial y}$  bed slope in the positive y direction evaluated at the V point.
- $\phi$  internal angle of friction of bed material (assumed to be 30°).

Remarks:

$z_b$  is the depth down to the bed from a reference height (positive down), a downward bed slope returns a positive value).

The bed slope is calculated at the U and V points as these are the locations at which the bed-load transport vector components will finally be applied.

The size of the adjustment is calculated following a modified form of the expression suggested by Bagnold (1966):

$$\bar{S}'_b = \alpha_s \bar{S}''$$

or, in vector component form:

$$S'_{b,x} = \alpha_s S''_{b,x}$$

$$S'_{b,y} = \alpha_s S''_{b,y}$$

Where:

$$\alpha_s = 1 + \alpha_{bs} \left[ \frac{\tan(\phi)}{\cos\left(\tan^{-1}\left(\frac{\partial z}{\partial s}\right)\right)\left(\tan(\phi) - \frac{\partial z}{\partial s}\right)} - 1 \right]$$

and  $\alpha_{bs}$  is a user specified tuning parameter, ALFABS (default = 1.0).

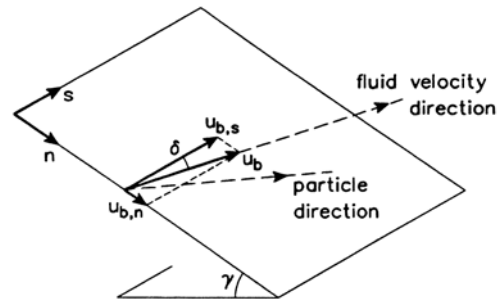
### ***b) Transverse bed slope***

The direction of the bed-load transport vector is adjusted if a bed slope exists in the direction normal to the bed-load transport vector. This bed slope is calculated as:

$$\frac{\partial z_b}{\partial n} = \frac{\partial z_{(u)}}{\partial x} \frac{S''_{b,x}}{|S''_b|} + \frac{\partial z_{(v)}}{\partial y} \frac{S''_{b,y}}{|S''_b|}$$

An additional bed-load transport vector is then calculated, perpendicular to the main bed load transport vector. The magnitude of this vector is calculated using a formulation based on the work of Ikeda (1982, 1988) as presented by van Rijn (1993) by setting the reference coordinates  $s$  and  $n$  aligned with and perpendicular to the local flow direction respectively. This implies that there is no flow in the  $n$  direction: i.e.

$$u_{b,n} = 0 :$$



$$S_{b,n} = |S'_b| \alpha_{bn} \frac{u_{b,cr}}{|\bar{u}_b|} \frac{\partial z_b}{\partial n}$$

where:

$S_{b,n}$  additional bed-load transport vector. The direction of this vector is normal to the unadjusted bed-load transport vector, in the down slope direction.

$|S'_b|$  magnitude of the unadjusted bed-load transport vector (adjusted for longitudinal bed slope only):

$$|S'_b| = \sqrt{(S'_{b,x})^2 + (S'_{b,y})^2}$$

$\alpha_{bn}$  user specified coefficient,  $ALFA_{bn}$  (default = 1.5 ).

$u_{b,cr}$  critical (threshold) near-bed fluid velocity.

$|\bar{u}_b|$  near-bed fluid velocity vector.

$\frac{\partial z_b}{\partial n}$  bed slope in the direction normal to the unadjusted bed-load transport vector.

## 3.2. Base model schematisation and boundary setup

### 3.2.1. Base model schematisation

The idealised estuary on which this research focuses is 80 km long and has a constant width of 400 m, the open sea is rectangular 10km length and 7km width (Fig. 3.1). The underlying grid has a mesh size of 200 m x 100 m in longitudinal and transverse direction, respectively. The initial bottom level is 20 m below MSL at the mouth, linearly decreasing to zero at the landward boundary, linearly increasing to 40m seaward with slope 1:100. The landward boundary is fixed and impermeable. The lateral boundary in the channel is +2m above MSL and erodable.

The bed material consists of uniform sand with  $d_{50} = 240\mu\text{m}$ . The initial bed-level in the channel is given randomly with maximum 5% of the water depth at MSL. For the bottom roughness, a constant Manning coefficient of  $0.026 \text{ s.m}^{-1/3}$  is used

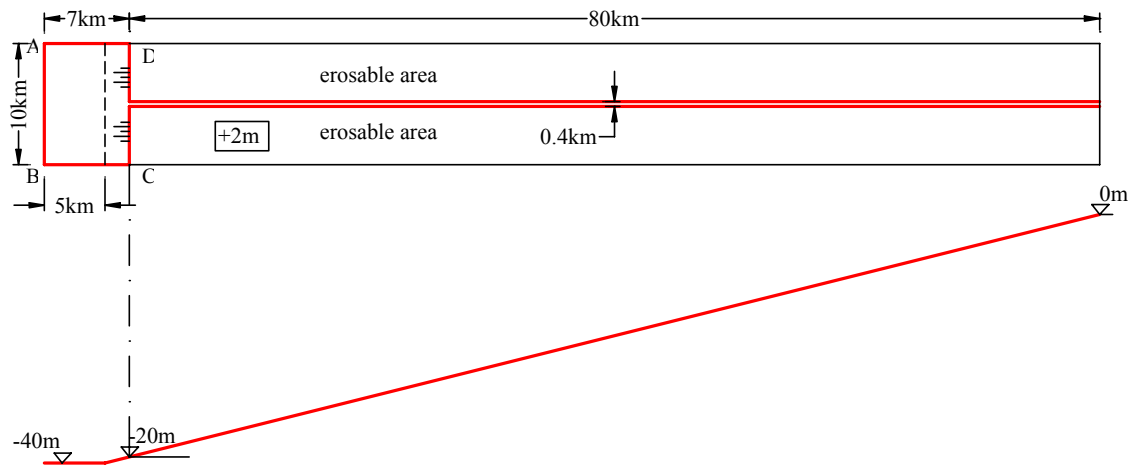


**Figure 3.1** model schematisation

### 3.2.2. Boundary setup

In this thesis we focus on two kinds of tides. One is tidal propagation parallel to the coast meaning that the model is located in the northern sphere and another one is tidal propagation perpendicular to the coast. This means that the model is located at the equator, or that the foreshore is relatively deep.

#### a) *Tidal propagation perpendicular to the coast*

Western boundary (AB): Water level amplitude 1.75m, phase is constant and equal to zero.

Southern and northern boundary (BC and AD): Neumann boundary with gradient amplitude and with constant phase equal to zero.

- All boundaries have frequency 30 degree/hour meaning that the tidal period is 12 hours

#### b) *Tidal propagation parallel to the coast*

With tidal propagation parallel to the coast from A to B. The boundary condition is calculated according to Roelvink and Walstra (?).

The tidal wave length :

$$L = c.T = \sqrt{gh}.T = \sqrt{9.81 * 40}.12 * 60 * 60 = 855km$$

The tidal alongshore wave number:

$$k = 2\pi/L = 7.34 * 10^{-6} \text{ rad/m}$$

Phase difference between the southern and northern is:

$$10000 * 7.34 * 10^{-6} = 0.0734 \text{ rad} = 4.2 \text{ deg}$$

The boundary conditions are then:

*Western boundary (AB):* Water level amplitude 1.75m, phase linearly varying from 0 deg at southern end to 4.2 deg at northern end.

*Southern boundary (AD):* Neumann boundary with water level gradient amplitude  $1.75 * 7.34 * 10^{-6} = 1.28 * 10^{-5}$  and phase 90 deg.

*Northern boundary (BC):* Neumann boundary with water gradient amplitude  $1.28 * 10^{-5}$  and phase 94.2 deg.

---

All boundaries have frequency 30 degree/hour meaning that the tidal period is 12 hours.

---

## 4. Sensitivity analysis

### 4.1. Effect of transverse bed slope

The effect of the transverse bed slope can be adjusted by the user specified coefficient  $\alpha_{bn}$ .

The default value of  $\alpha_{bn}$  is 1.5. When using this value the results are unrealistic probably because of the large morphological factor used. Therefore, we consider increasing this value. Two values of  $\alpha_{bn}$  were tested with  $\alpha_{bn}$  equal to 5 and  $\alpha_{bn}$  equal to 10 for a boundary condition with the tidal propagation perpendicular to the coast. The results are considered in terms of longitudinal profile, cross-section and shoal pattern aspects.

#### 4.1.1. Effect of $\alpha_{bn}$ to cross-section of embayment

Figure 4.1 and Figure 4.2 show the widths of the embayment in longitudinal direction of the two models with  $\alpha_{bn} = 5$  and  $\alpha_{bn} = 10$  for 15 years and 200 years. These widths were determined at mean water level. The initial width of channel is 400m. After 200 year the width of the mouth is about 2.5km with  $\alpha_{bn}$  equal to 5 and about 3.0km with  $\alpha_{bn}$  equal to 10.

According to Savenije (1992), the width of embayment can be described as an exponential function:

$$B = B_o \exp\left(-\frac{x}{b}\right)$$

Where:

$B_o$ : the width at the mouth of estuary

$b$ : Convergence length at MSL

Figure 4.3 and Figure 4.4 show the widths of on a log scale and fitted with an exponential function. The results show that the variation of the width over distance after 200 years slightly fit with exponential function.

With  $\alpha_{bn} = 5$  the fitting exponential function is:

$$B = 2152e^{-2E-5x}$$

$$\text{or } B = 2152 \exp\left(-\frac{x}{50}\right)$$

And R-square value:  $R^2 = 0.919$

---

With  $\alpha_{bn} = 10$  the fitting exponential function is:

$$B = 2662e^{-3E-5x}$$

$$\text{or } B = 2152 \exp\left(-\frac{x}{33}\right)$$

And R-square value:  $R^2 = 0.937$

With  $\alpha_{bn}$  equal to 5 the convergence length is 50km and with  $\alpha_{bn}$  equal to 10 the convergence length is 33km. So, it is clear that with higher values for  $\alpha_{bn}$  the width of the embayment is wider, more converging and also a better fit to the exponential function. And with higher  $\alpha_{bn}$  the change of cross-section in longitudinal direction is more irregular.

So, obviously with higher value of  $\alpha_{bn}$  more dry-cells are eroded. Let consider the mechanism of dry-cell erosion. A dry-cell is eroded when a wet-cell next to it is eroded. Then the amount of sand to be eroded will be assigned to this dry-cell until this dry-cell become wet. With higher value of  $\alpha_{bn}$  the transverse bed-load transport will be higher and so that the amount of sand was taken from the adjacent dry-cell is higher. Consequently, the adjacent dry-cell will be become lower. This is the explanation for with higher value of  $\alpha_{bn}$  the bank slope is milder and the speed of slope development is faster (Figure 4.2)

When the slope is milder the speed of slope develop is slower with time or seem stop developing; particular in this case is after 15 years for  $\alpha_{bn}$  equal to 10 and absolutely more than 15 years for  $\alpha_{bn}$  equal to 5. And at a fix value of  $\alpha_{bn}$  we have a fix value of bank slope at balance condition.

Consequent of the developing of the bank slope is that sediment transported originates from the bank to fill up the main channel. So we could say that, at initial stage (about 15 years) the channel develops due to the bank erosion, and after that time the channel develops mainly in longitudinal direction.

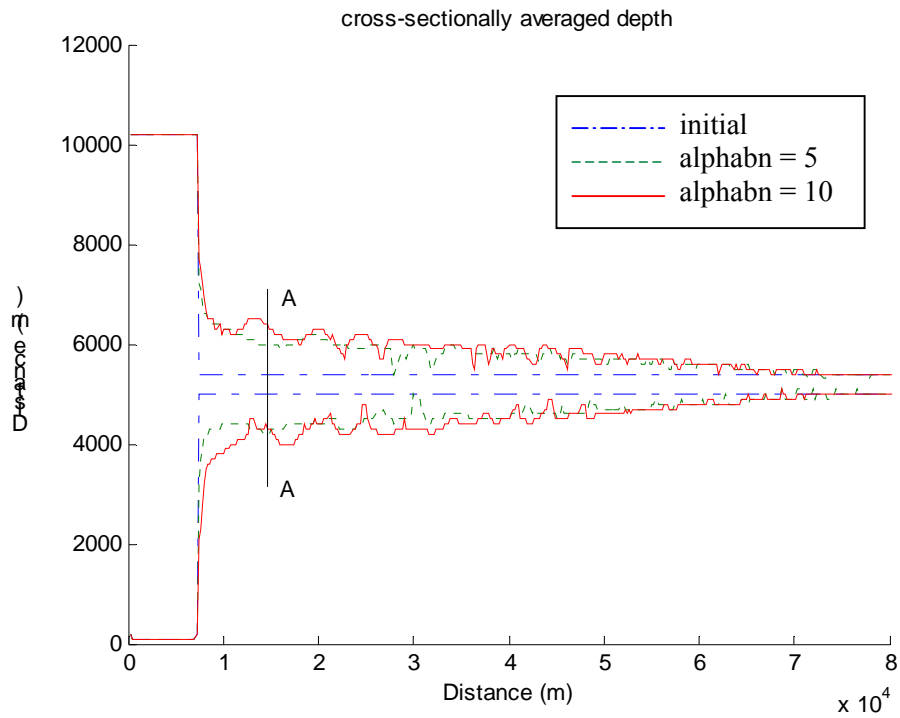


**Figure 4.1** Width of embayment with  $\alpha_{bn} = 5$  and  $\alpha_{bn} = 10$  after 200 years

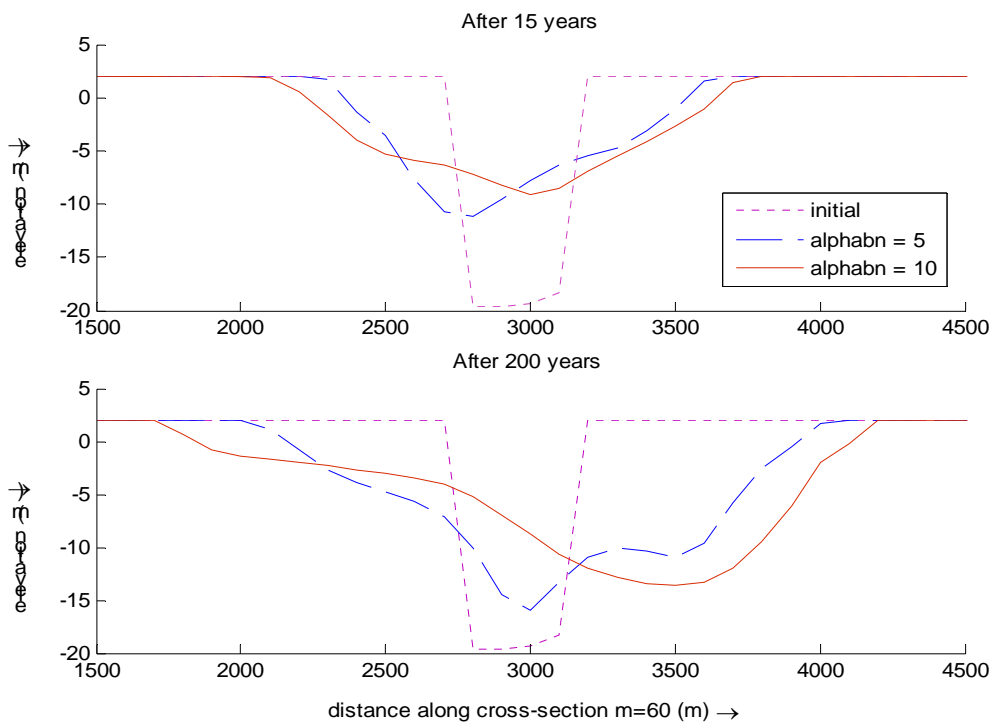


**Figure 4.2** Cross-section A-A of embayment after 15 years and 200 years

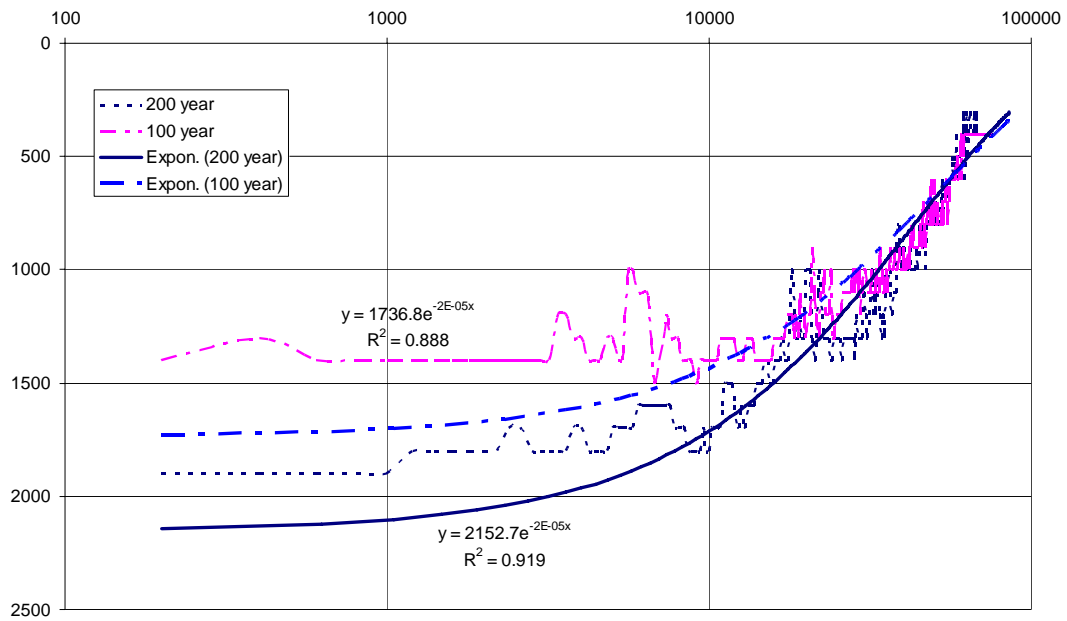


**Figure 4.3** Fitting the length of the cross-section with exponential function in log scale with  $\alpha_{bn}=5$

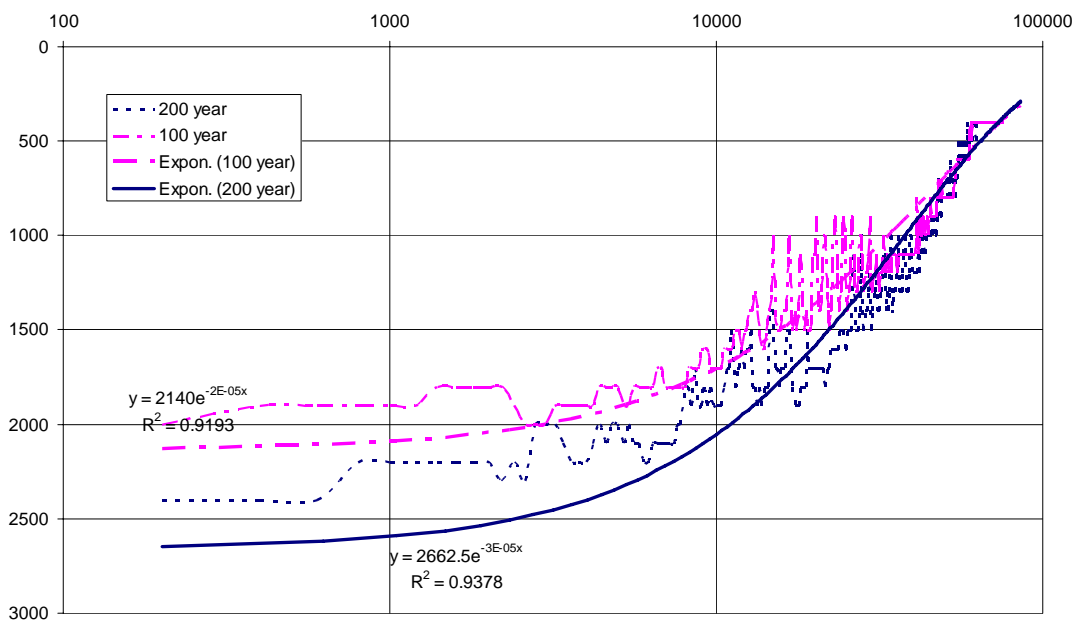


**Figure 4.4** Fitting the length of the cross-section with exponential function in log scale with  $\alpha_{bn}=10$

---

#### 4.1.2. Effect of $\alpha_{bn}$ to longitudinal profile

Figure 4.5 shows the longitudinal profile of the two models with  $\alpha_{bn}$  equal to 5 and  $\alpha_{bn}$  equal to 10 in first 3 years and 15 years. The longitudinal profile was determined by taking the average depths that are greater than zero of the cross-section of the embayment. (This should be : the longitudinal profile was determined by taking the average depth over the crosssection of the embayment)

Initially, the longitudinal profile decreases linearly from 20m depth at the mouth to 0m depth at the close end. After 15 years and 200 years, the longitudinal profile is shallower. With  $\alpha_{bn}$  equal to 10 it is shallower than with  $\alpha_{bn}$  equal to 5. The reason of this can be explained by two phenomena. One is because of the widening of the embayment and so that more cell is below MSL lead to more cell with shallow depth is taken into average (with  $\alpha_{bn}$  equal to 10 the cross-section is wider than  $\alpha_{bn}$  equal to 5). Another one is because of sediment material from the bank erosion filling up the channel (with  $\alpha_{bn}$  equal to 10 more sediment transport eroded than  $\alpha_{bn}$  equal to 5). The combination of this two phenomena causes the longitudinal profile to get shallower (Figure 4.6).

Figure 4.7 and Figure 4.8 show the longitudinal profile of the two models with  $\alpha_{bn}$  equal to 5 and  $\alpha_{bn}$  equal to 10 in 100 years and 200 years. We see a common point of these two figures that the mean depth of longitudinal profile after 100 year and 200 year almost equal and the shape is more or less the same. After 200 years the shape is more concave at the mouth and more convex at the end than after 100 years. This means that the sediment is distributed differently in longitudinal direction. Lanzoni and Seminara (2002) describe this equilibrium as the result of asymmetries in surface elevation and tidal currents leading to net sediment flux within a tidal cycle in landward direction. Consequently, sediment is trapped within the estuary and the bottom profile evolves asymptotically towards an equilibrium configuration.

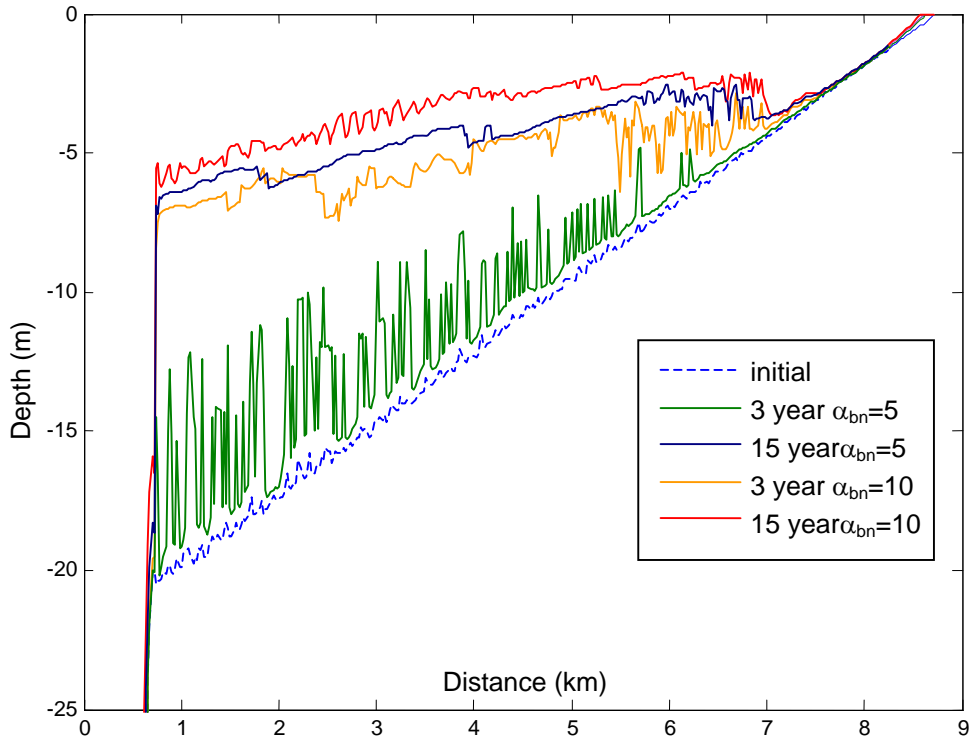


**Figure 4.5** Longitudinal profile for first 15 years with different  $\alpha_{bn}$

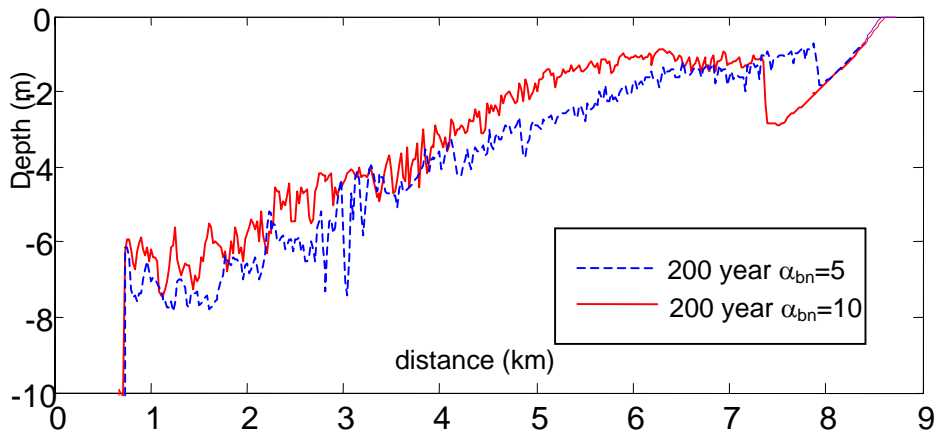


**Figure 4.6** longitudinal profiles after 200 years with different  $\alpha_{bn}$

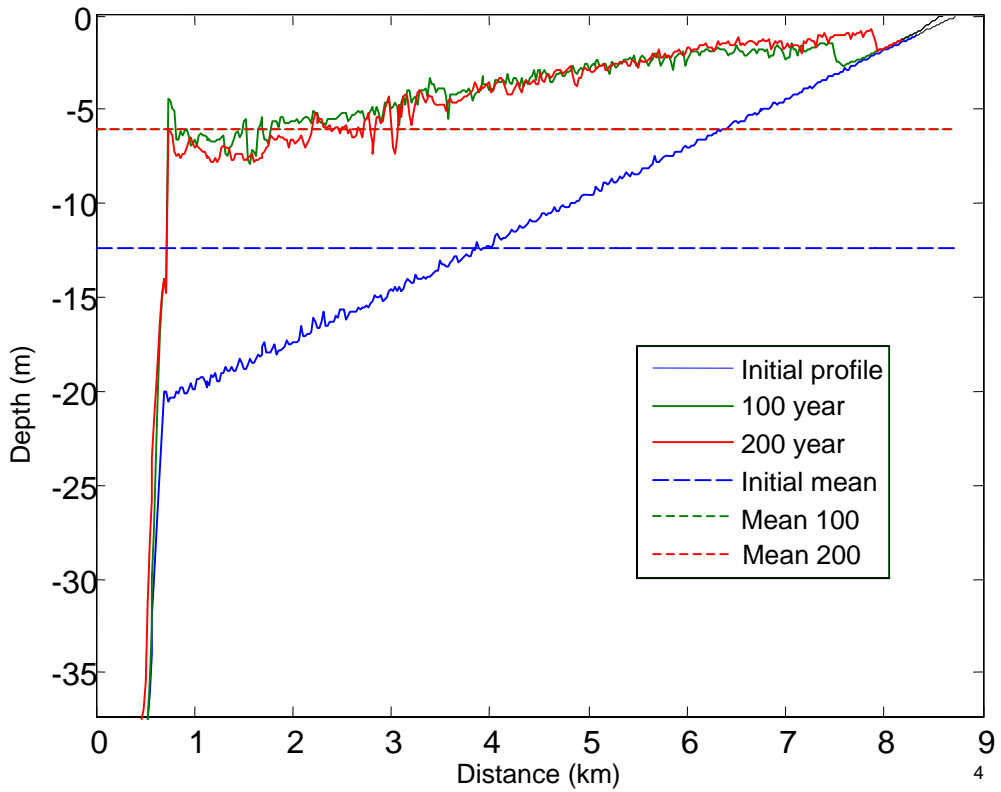


**Figure 4.7** Longitudinal different profile for different points in time with coefficient  $\alpha_{bn} = 5$

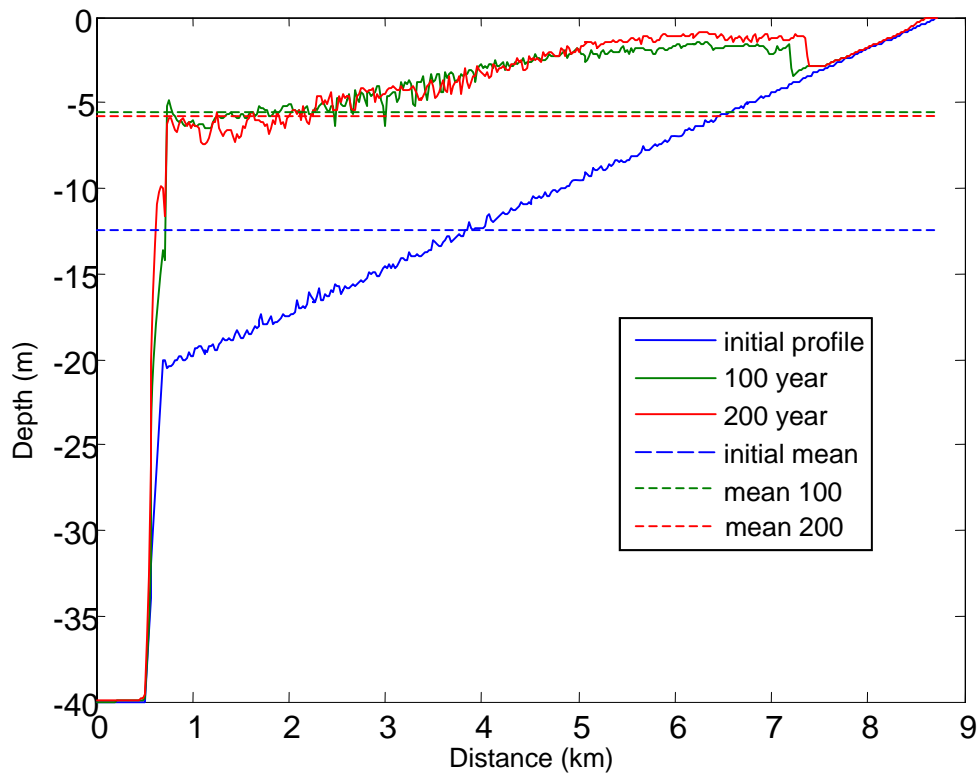


**Figure 4.8** Longitudinal different profile for different points in time with  $\alpha_{bn} = 10$

### 4.1.3. Effect of $\alpha_{bn}$ to shoal pattern

Figure 4.10 shows the shoal pattern of two models. It clear that with  $\alpha_{bn}$  equal to 10 the main channel is more bended than  $\alpha_{bn}$  equal to 5 therefore the length of sand bar is shorter (Figure 4.11).

The explanation of these differences is that with higher value of  $\alpha_{bn}$  the vector of transverse bed-load transport is bigger (as illustrate in Figure 4.9) This leads to sediment being transported further, faster with a direction of movement more perpendicular to the bank.

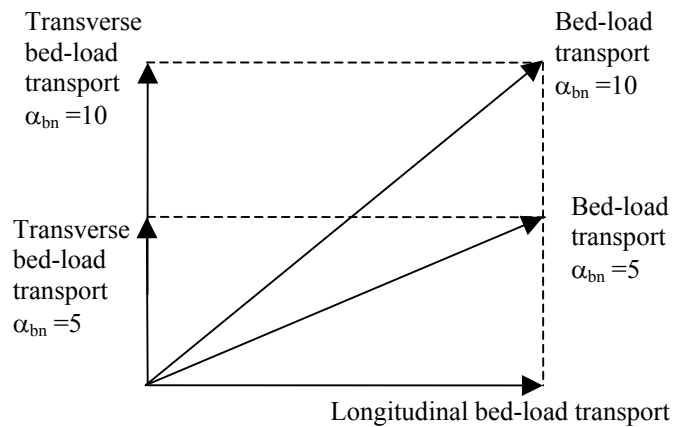


**Figure 4.9** Illustrate of bed-load sediment transport

### 4.1.4. Discussion for the selection of $\alpha_{bn}$ value

The default value of coefficient  $\alpha_{bn}$  was suggested by Ikeda(1982) is 1.5 based on measured value for bed load transport in transverse slope along a straight channel in a wind-tunnel. But when using this value in Delft3D model it seems that this value is not leading to realistic results. Because of the erosion mechanism for dry cells in Delft3D model, when a wet-cell is eroded the amount of sand will be taken from the dry-cell if there is a dry-cell adjacent to that wet-cell. But when this dry-cell becomes wet it will not distribute the amount of sand to the wet-cell although this wet-cell is still eroded. This mechanism causes a very steep slope next to a very shallow wet-cell. Thus, in order to promote the erosion of the wet-cell we suggest using higher value of  $\alpha_{bn}$ . In this thesis the value of  $\alpha_{bn}$  equal to 5  $\alpha_{bn}$  equal to 10 were examined. Also with  $\alpha_{bn}$  equal to 1.5 lead to unstable morphodynamic behavior with high value for morphology factor. However  $\alpha_{bn}$  equal to 10 is to high if considering the suggested value by Ikeda(1982). So, we recommend that the value of  $\alpha_{bn}$  should be equal to 5.

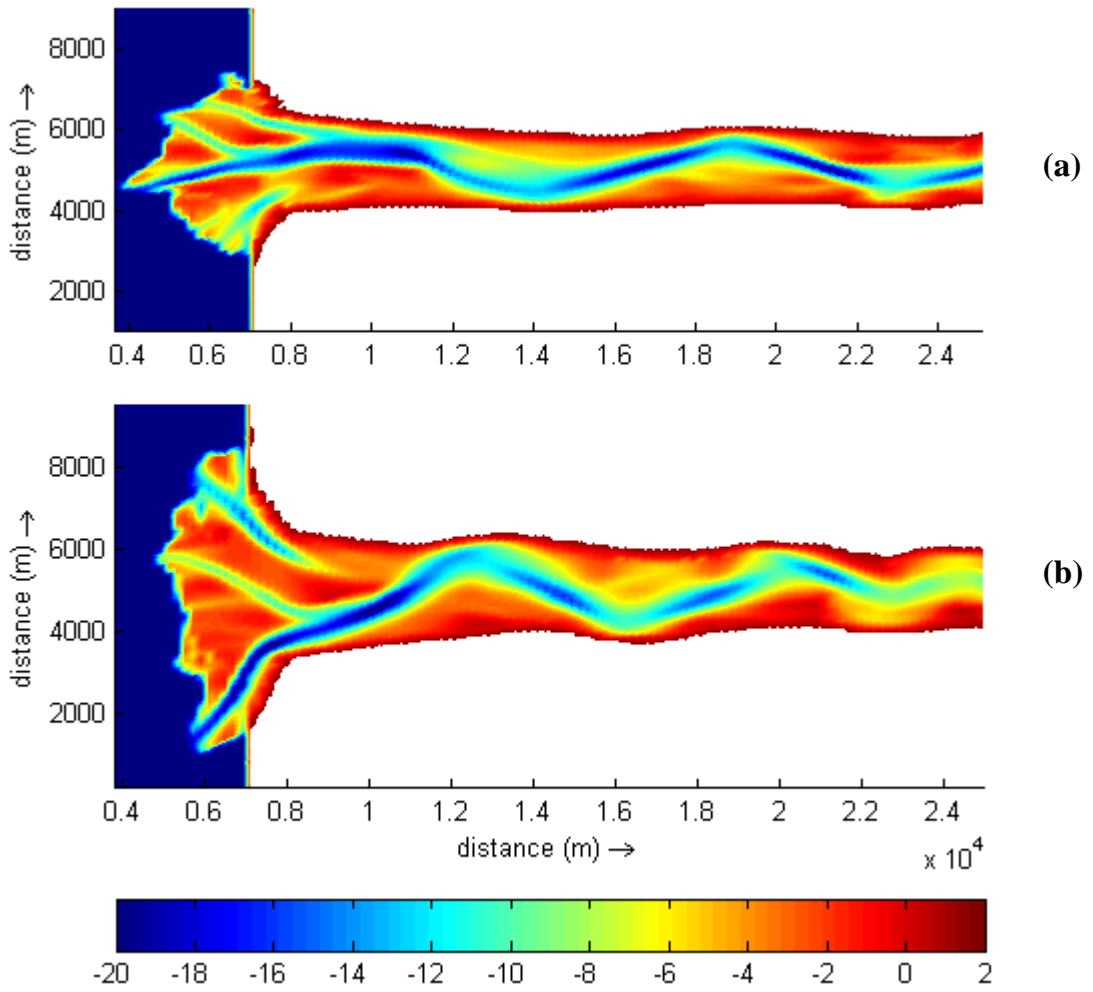


**Figure 4.10** (a) shoal pattern with  $\alpha_{bn} = 5$ ; (b) shoal pattern with  $\alpha_{bn} = 10$

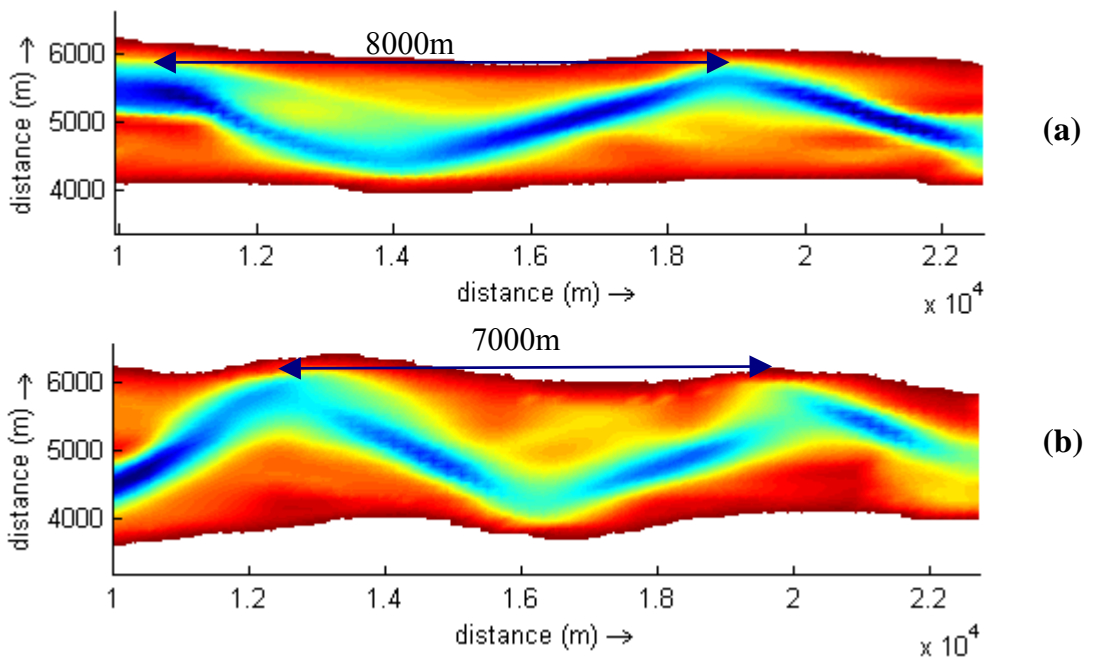


**Figure 4.11** Length of sand bar with (a)  $\alpha_{bn} = 5$ ; (b)  $\alpha_{bn} = 10$

---

## 4.2. Effect of boundary condition

Two models were run with different boundary conditions. The boundary is considered to simulate tidal propagation perpendicular to the coast and parallel to the coast. The setup of the boundary condition was described in section 3.2.2

### 4.2.1. Effect of boundary condition to cross-section and shoal pattern of embayment

Figure 4.12 shows the cross-section of the two models, which have a different boundary condition. Comparing the width of the channel in longitudinal direction, it shows that there is no big difference. Only at the mouth, in case of a tidal propagation parallel to the coast, the left bank is more eroding than the right bank.

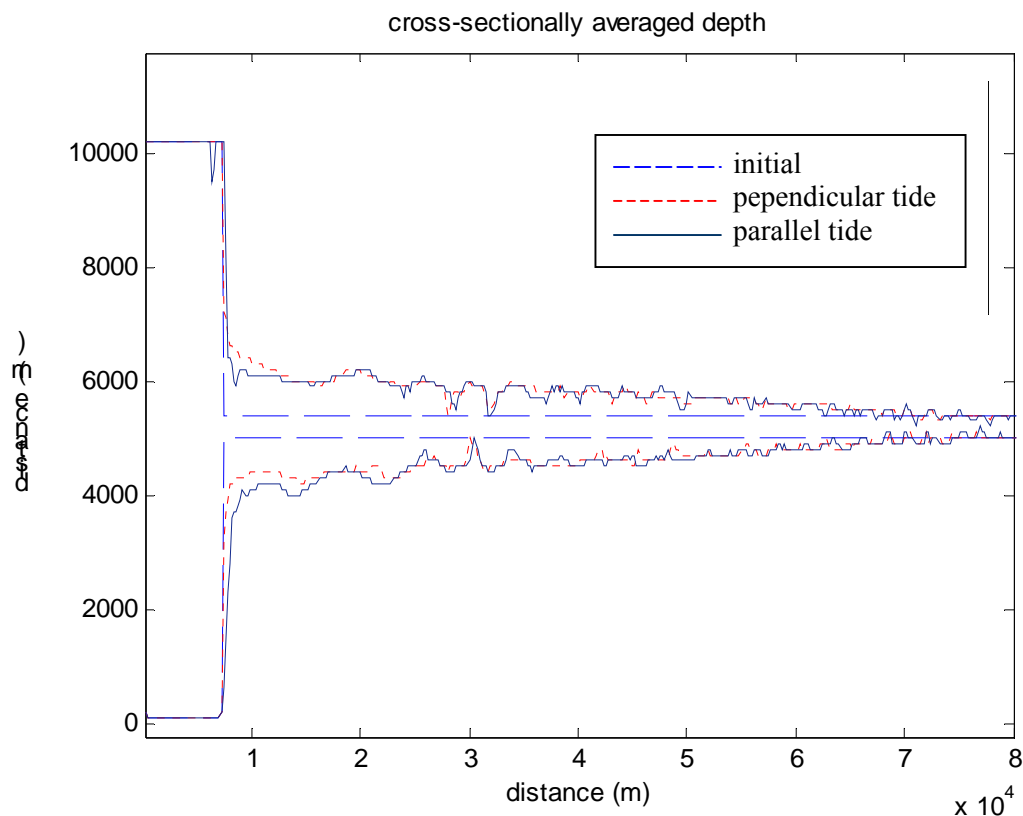


**Figure 4.12** Cross section of for different boundary conditions

Figure 4.13 shows the shoal pattern. It is easy to see that, with parallel tide, the channel is more aligned to the left and more bended. At the mouth of the estuary the shoal pattern shows a big in difference. With perpendicular tide the shoal pattern is symmetric and tends to develop toward the sea. But with parallel tide the shoal pattern is not symmetric and tends to develop aligned with the coast. This is due to the main direction of sediment transport in the direction of tide propagation. With

parallel tide the sediment transport fluctuates parallel to the coast and with perpendicular tide the sediment fluctuate perpendicular to the coast.

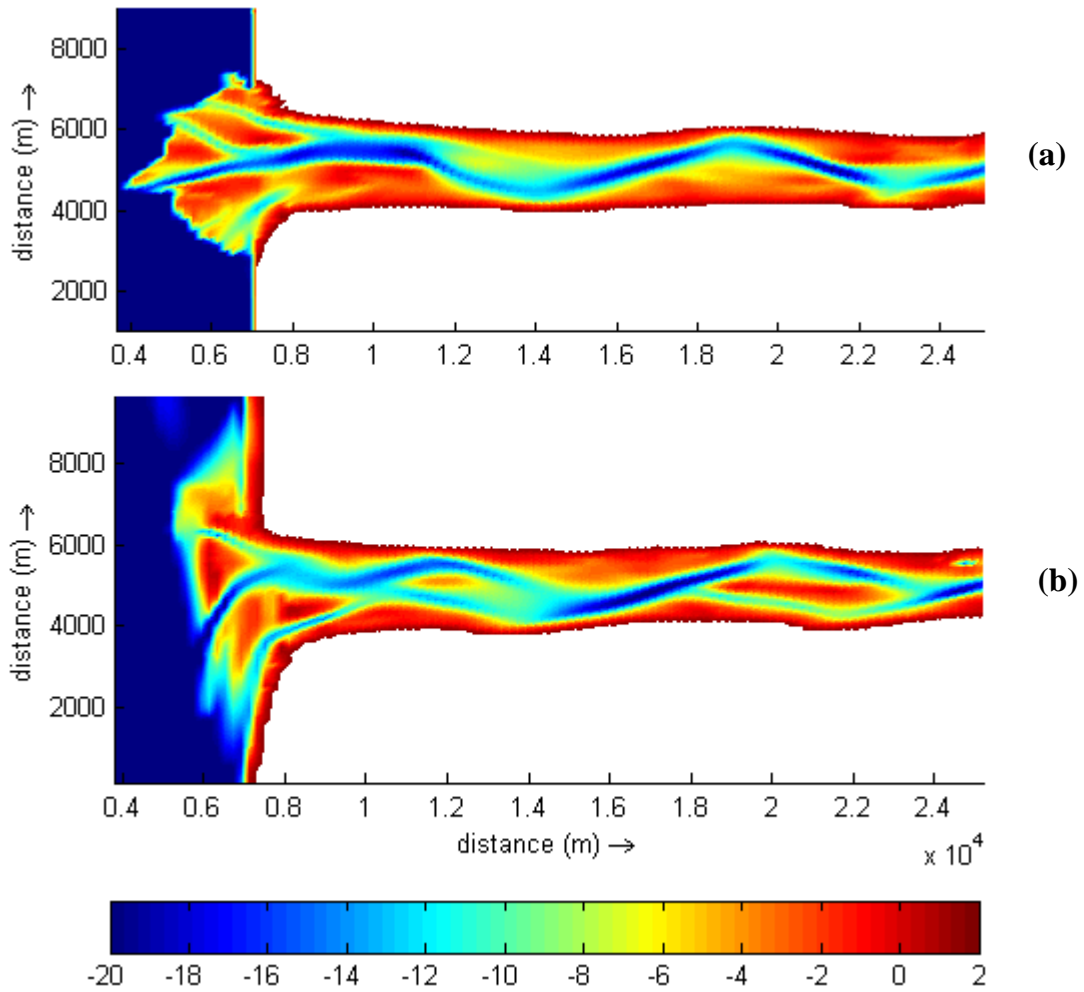


**Figure 4.13** Shoal pattern of estuary for different tidal propagation direction;  
(a) perpendicular tide, (b) parallel tide

Look closer to the pattern when tidal propagation is parallel to the coast, we see that shoals develop more in the right bank. The reasons for this is described by Sha (1989). Near the mouth, the shore-parallel tidal currents are interrupted by the tidal current through the inlet normal to the shoreline (Figure 4.14). South of the mouth, the shoreline tidal currents are enhanced by the current through the channel. North of the mouth, the shoreline tidal currents are deflected and refracted during the ebb and flood tides respectively. This interaction between shore-parallel and shore-normal tidal currents produces a circular current ellipse north of the mouth. Consequently, the current velocity in this direction is low. This tidal current pattern near the mouth favours shoal development north of the inlet and channel development to the south. The main channel is indeed aligned asymmetrically to the south of the estuary.

Figure 4.15 shows the current pattern of the model at mid-flood and mid-ebb after 200 years which tide parallel to the coast is validation with described by Sha (1989)

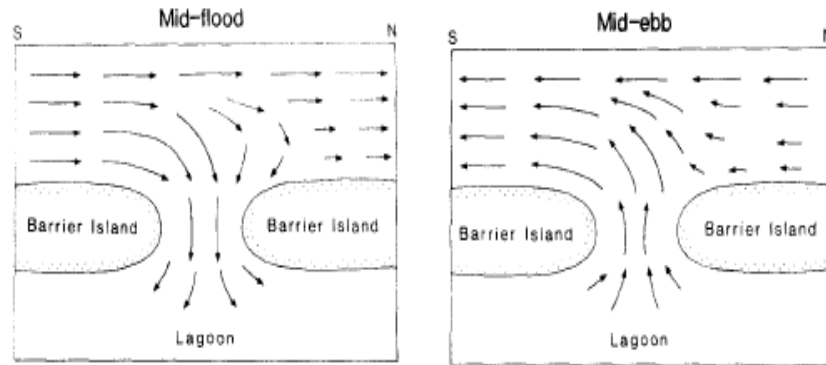


**Figure 4.14** The schematic current patterns at mid-flood and mid-ebb show the effect of interruption of shore-parallel currents by the tidal currents through the inlet by Sha (1989)

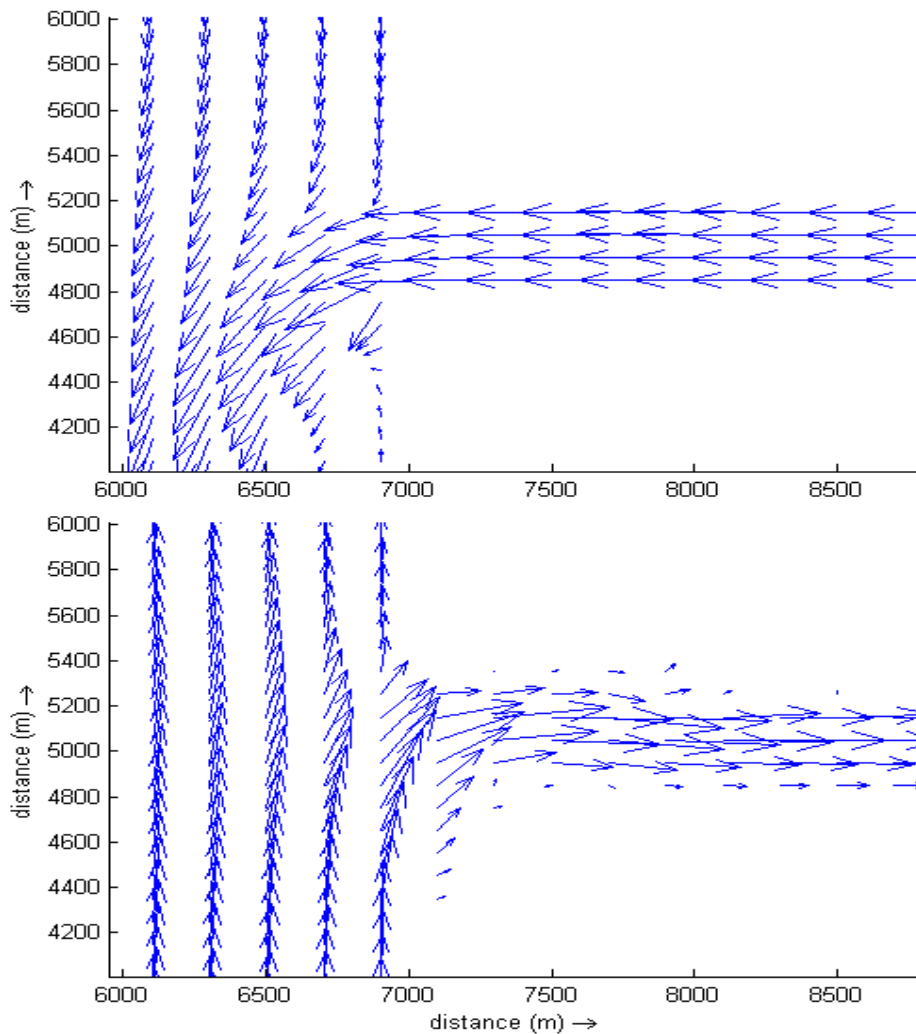


**Figure 4.15** Current pattern at mid-ebb (above) and mid-flood (below) at initially of the model resembled with the description of Sha (1989) (Tidal propagation is parallel to the coast)

### 4.2.2. Effect of boundary condition to longitudinal profile

Figure 4.16 shows the longitudinal profile of the two models, which have a different boundary condition. It is clear that there is not so big difference between them. Some points to consider are that the mean value of the longitudinal profile in case of the parallel tide is lower than perpendicular tide (maybe with parallel tide the basin export more sediment to the sea) and that the sill at the mouth of the estuary is lower.

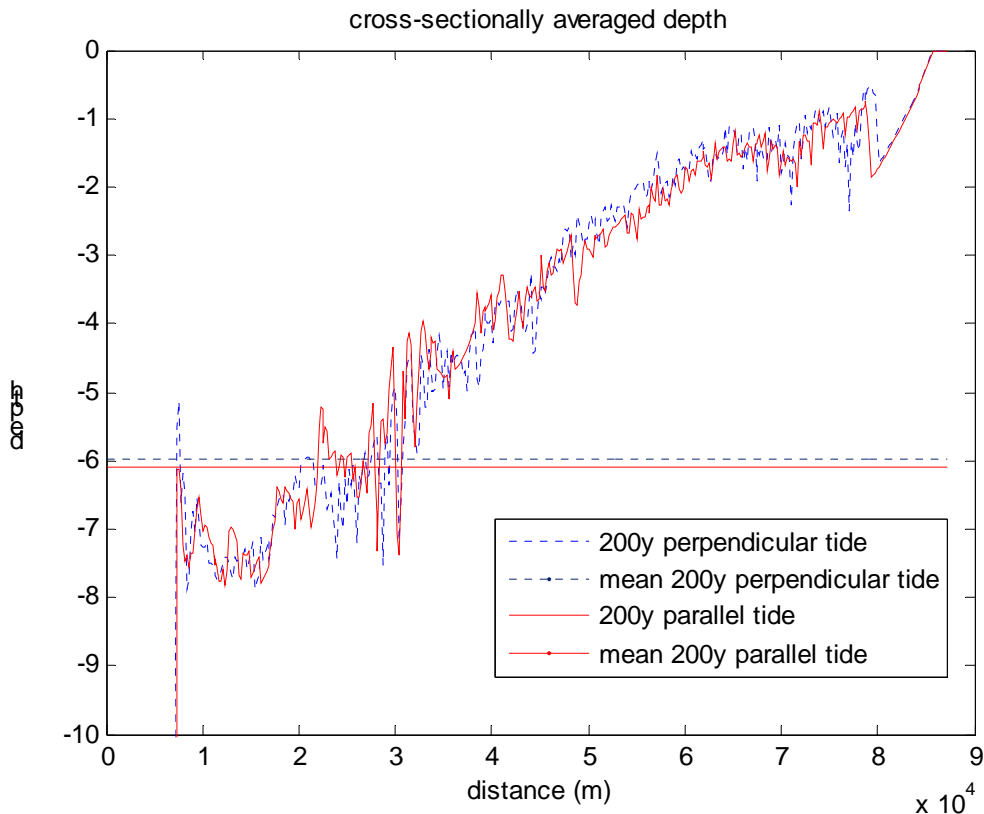


**Figure 4.16** Longitudinal profile of the width-averaged depth for different tidal propagation direction

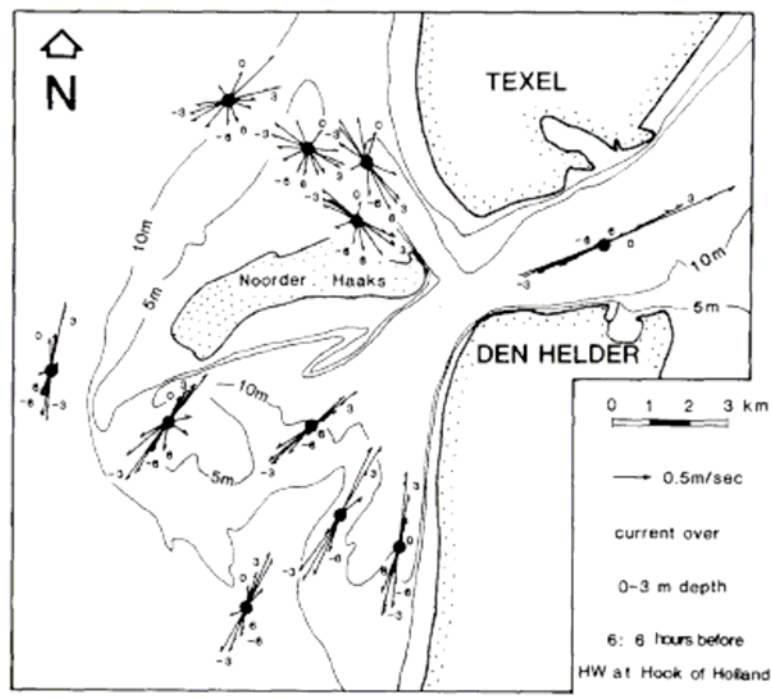
### 4.2.3. Discussion

With different boundary conditions, the model shows different results. The boundary influences the shoal pattern in the basin but the difference is not too big. Most difference is at the mouth of the estuary. In reality, due to the effect of Coriolis' force the tide has a tendency to propagate parallel to the coast depending on the local geometry. In the northern hemisphere, the tide propagates from left to right and with reverse direction in the southern hemisphere. Obviously, at the equator the tide propagates perpendicular to the coast. However, tides propagating perpendicular to

the coast are hardly found in the world. When using the parallel tide in this research we located the model at 51° latitude north (same latitude with Netherlands).

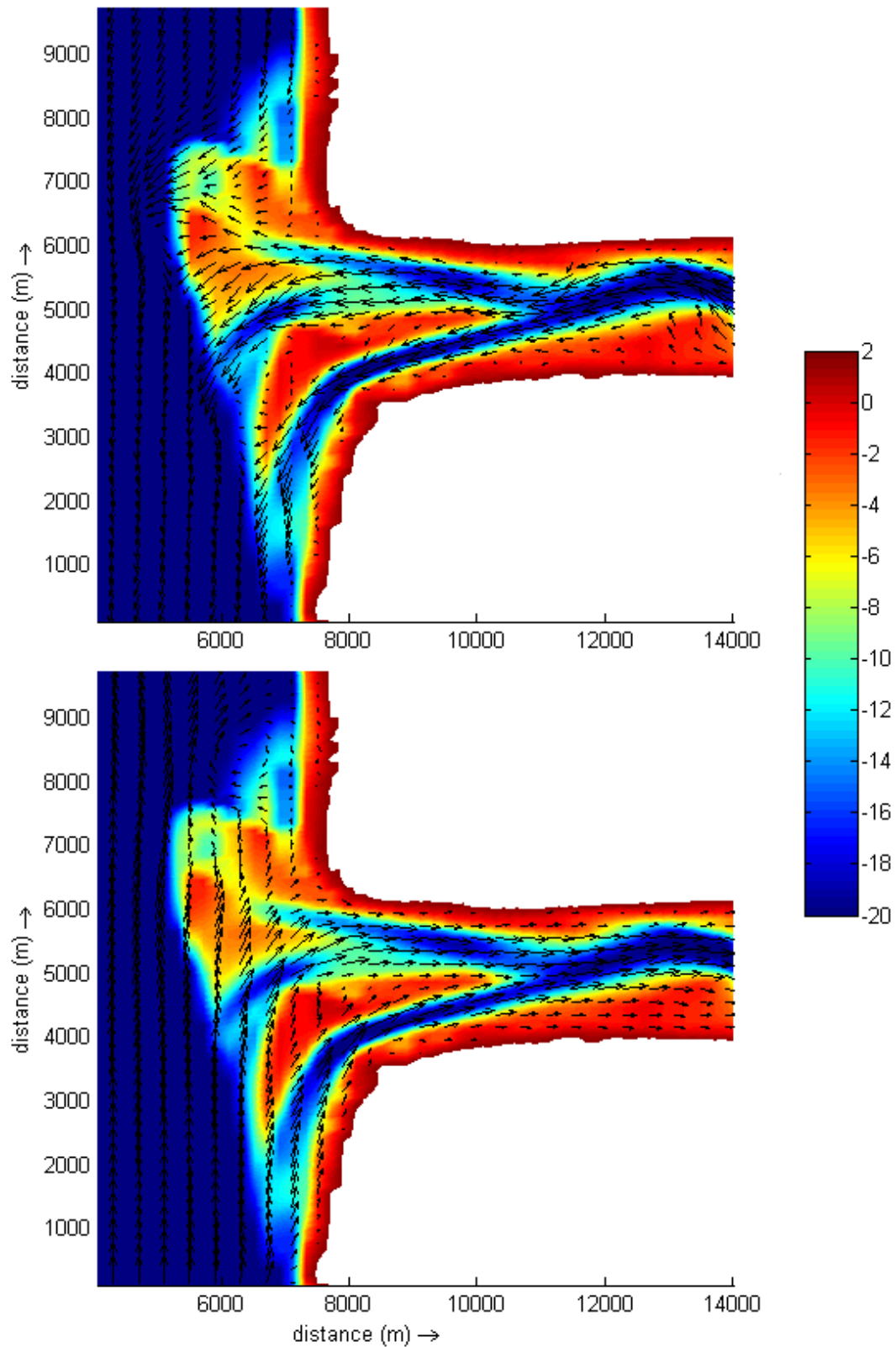
Figure 4.17 below shows the shoal pattern and velocity of Texel inlet in The Netherlands located at 53° north and

Figure 4.18 shows the the shoal pattern and velocity after 200 years modelling. We found that the model result resembled this inlet. It is noted that the banks near “Den Helder” are heavily protectd against erosion.



**Figure 4.17** Tidal current roses for a tidal cycle in the ebb-tidal delta of Texel inlet

So, as the result show, we recommend using the tide propagating parallel to the coast.



**Figure 4.18** Current pattern at mid-ebb (above) and mid-flood (below) after 200 years model. Tidal propagation is parallel to the coast

---

### 4.3. Effect of grain size diameter

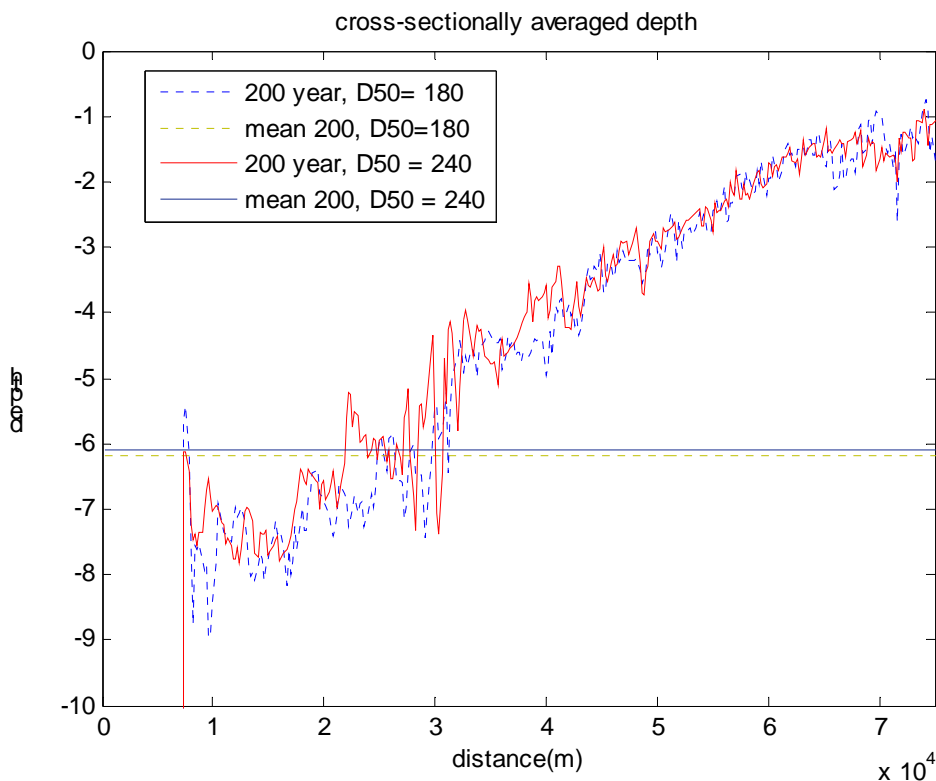
The model was run with grain sizes of  $D_{50} = 180\mu\text{m}$  and  $D_{50} = 240$ . The model was setup with tide propagating perpendicular to the coast.

Figure 4.19 and Figure 4.20 show the results of the model with difference in grain size in terms of longitudinal profile and width of embayment. There is no obvious difference between the longitudinal profiles as well as the widths of the embayment. The only small difference occurs is that with a smaller grain size the mean of longitudinal profile is lower than for bigger grain sizes. It means that the basin exports more sand to the sea.

Figure 4.19 shows the shoal pattern of the two kinds of grain size. With small grain size the length of sand bar in the basin seems shorter and also the channel is more bended. At the mouth with smaller grain size the shoal pattern develops to the transverse direction and the channel is more aligned to the left bank.

#### Discussion

The effect of the grain size to the model is not apparent in basin width development and evolution of the longitudinal profile.



**Figure 4.19** Longitudinal profile of the width-averaged depth for difference in grain size

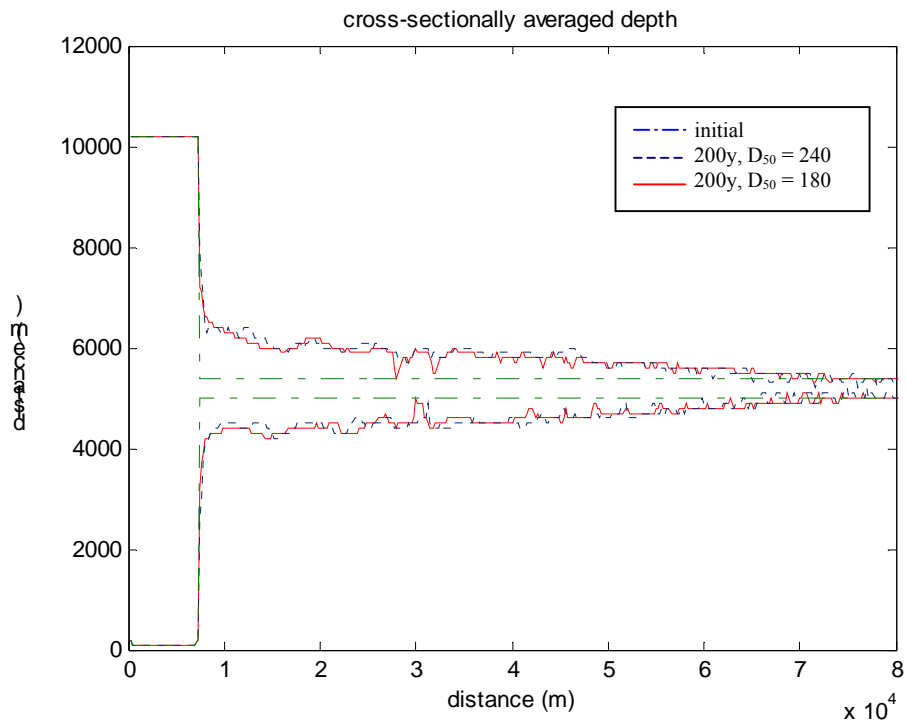


**Figure 4.20** Width of embayment with for difference in grain size

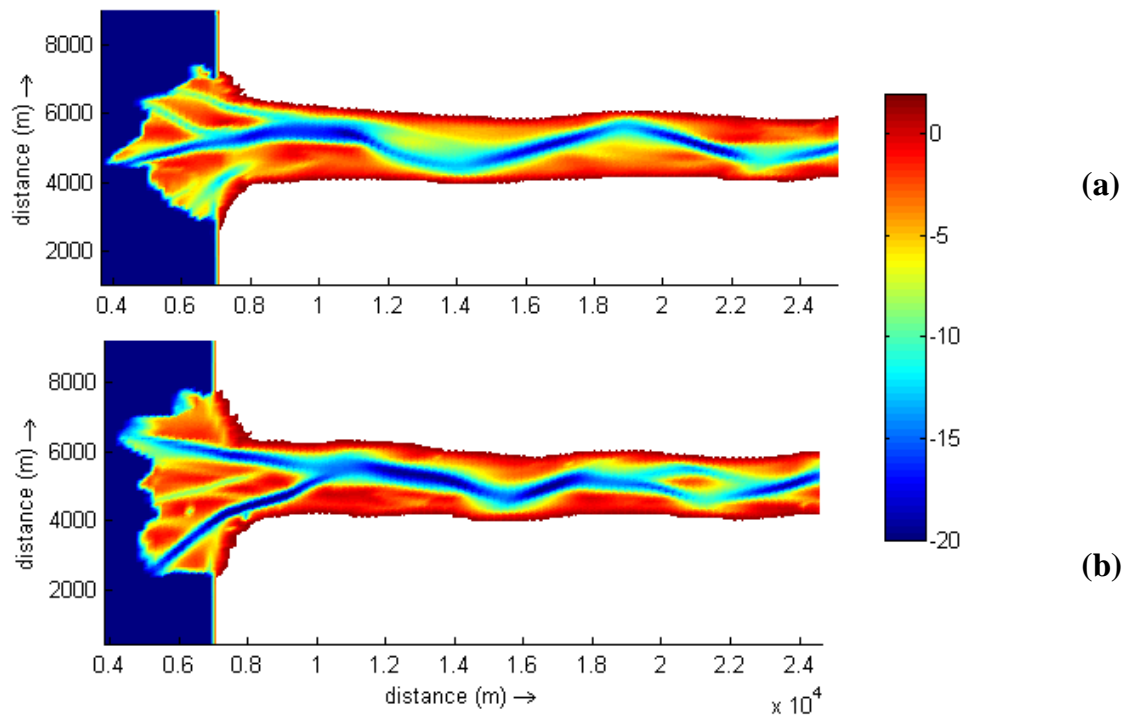


**Figure 4.21** Shoal pattern of estuary for different grain size; (a) D<sub>50</sub> = 240 μm, (b) D<sub>50</sub> = 180 μm, perpendicular tide



---

## 5. Result from long term model running

In order to investigate the conditions for a (possible) morphodynamic equilibrium state of the specific model configuration, long-term calculations (up to 4 years of hydrodynamic calculations with an equivalent of 800 years of morphodynamic development) were carry out. The model configuration is the same as the case of the parallel tidal propagation.

In the following sections the model results are analysed. Central question is whether the morphodynamic behaviour develops towards (dynamic) equilibrium conditions. Links are made to measurements (when available) to validate the model results.

### 5.1. Shoal pattern

Figure 5.1 shows the shoal pattern of the basin (80km long and 400m wide,  $\alpha_{bn} = 5$ ,  $D_{50} = 240\mu\text{m}$ , parallel tide), initially, after 200, 400, 600, and 800 morphological years. The initial bed consists of perturbations with randomly distributed values with maxima of +/- 5% of the water depth and linear from -20m at the mouth to 0m at the close end.

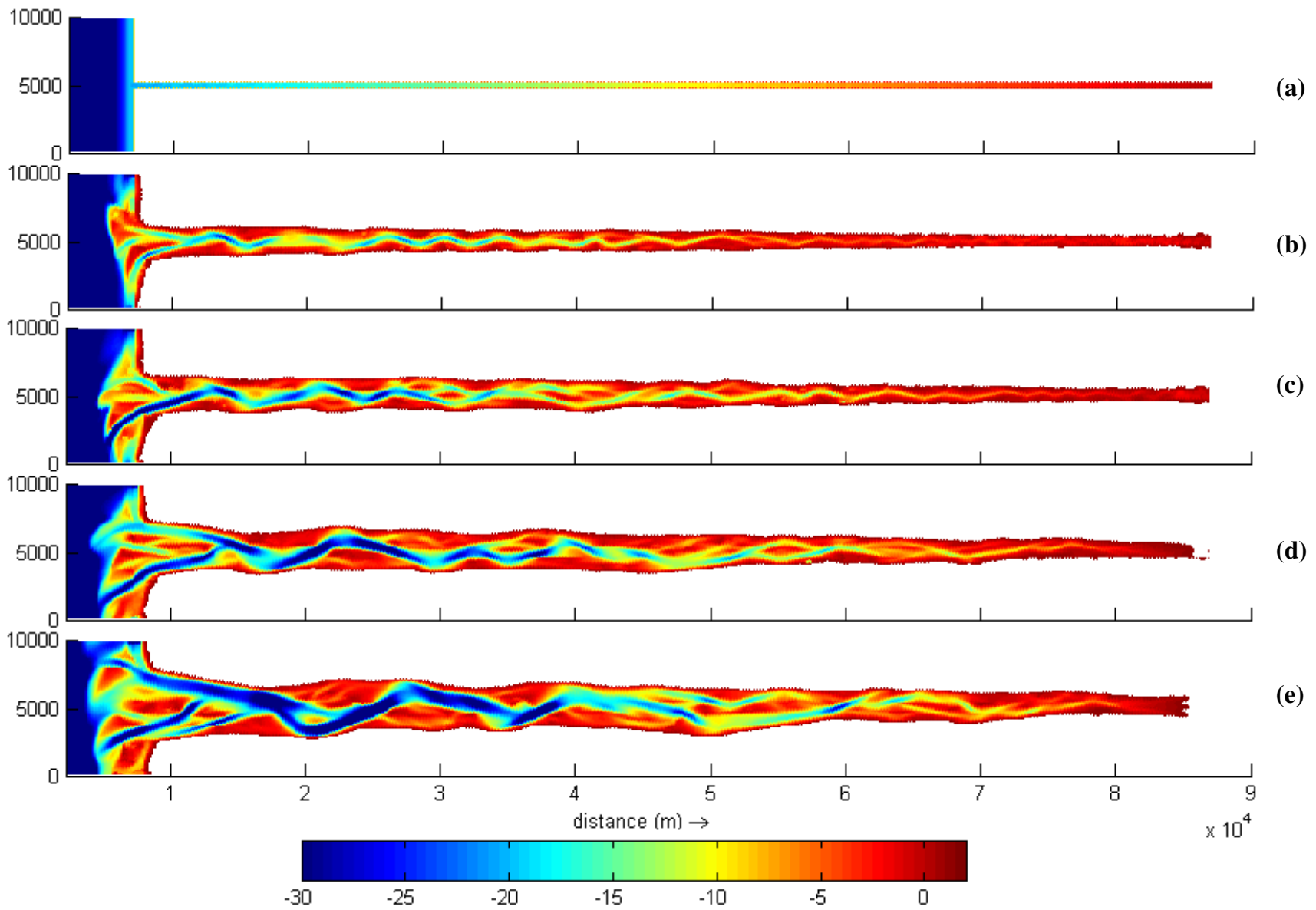
After 200 years the basin has already developed in the shape of meandering channel which is separated by shoals. After 400, 600, and 800 years the basin keeps the same shape as with 200 year but with a difference in geometry. The channel is wider and deeper and the morphological wavelength is longer. After 200 years the wavelength at the mouth is about 6km (longitudinally), after 400 years this is 10km, 600 years this is 12km and after 800 years, this is about 20km. The wavelengths also decrease in landward direction. Near the mouth the wavelength is longer. The width of the embayment is increasing as well. The initial width at the mouth is 400m. After 600 years, the width at the mouth is about 3.5km and after 800 years is about 5km.

Hibma (2004) developed a model with 80km long and 2.5 km width, and with a fixed lateral boundary (the dry-cell cannot be eroded). After 120 morphological model years, she concludes that the wavelength has increased to 12 km and there is no migration. Hibma (2004) does not include dry cell erosion and used a different morphological update scheme.

A more detailed view on the development of the channels and shoals is presented in Fig. 5.2, showing the first 20km of the estuary. From the initial condition to 10 years

---

the embayment only develops in lateral direction and develops merely at the mouth. This is due to of the effect of  $\alpha_{bn}$  to the lateral dry-cells and also highest of sediment transport and velocity at the mouth (see 4.1). At the landward side the first channel becomes visible after 10; 15 years (second and third panels). The wavelength of this channel is 4 km in longitudinal and 1.5 km in transverse direction. As time goes by, the channels become deeper and there is a slow development in transverse direction. Bank erosion merely takes place where channel bends 'touch' the banks. At the mouth of estuary, the channel develops to the south and sediment deposits in the north. This is due to the tide propagating parallel to the coast (see 4.2). By time, more sedimentation deposits at the mouth and the shoals reach to mean sea level or higher and dry at low water.



---

**Figure 5.1** Shoal pattern; (a) initial, (b) after 200 years, (c) after 400 years, (d) after 600 years, (e) after 800 years

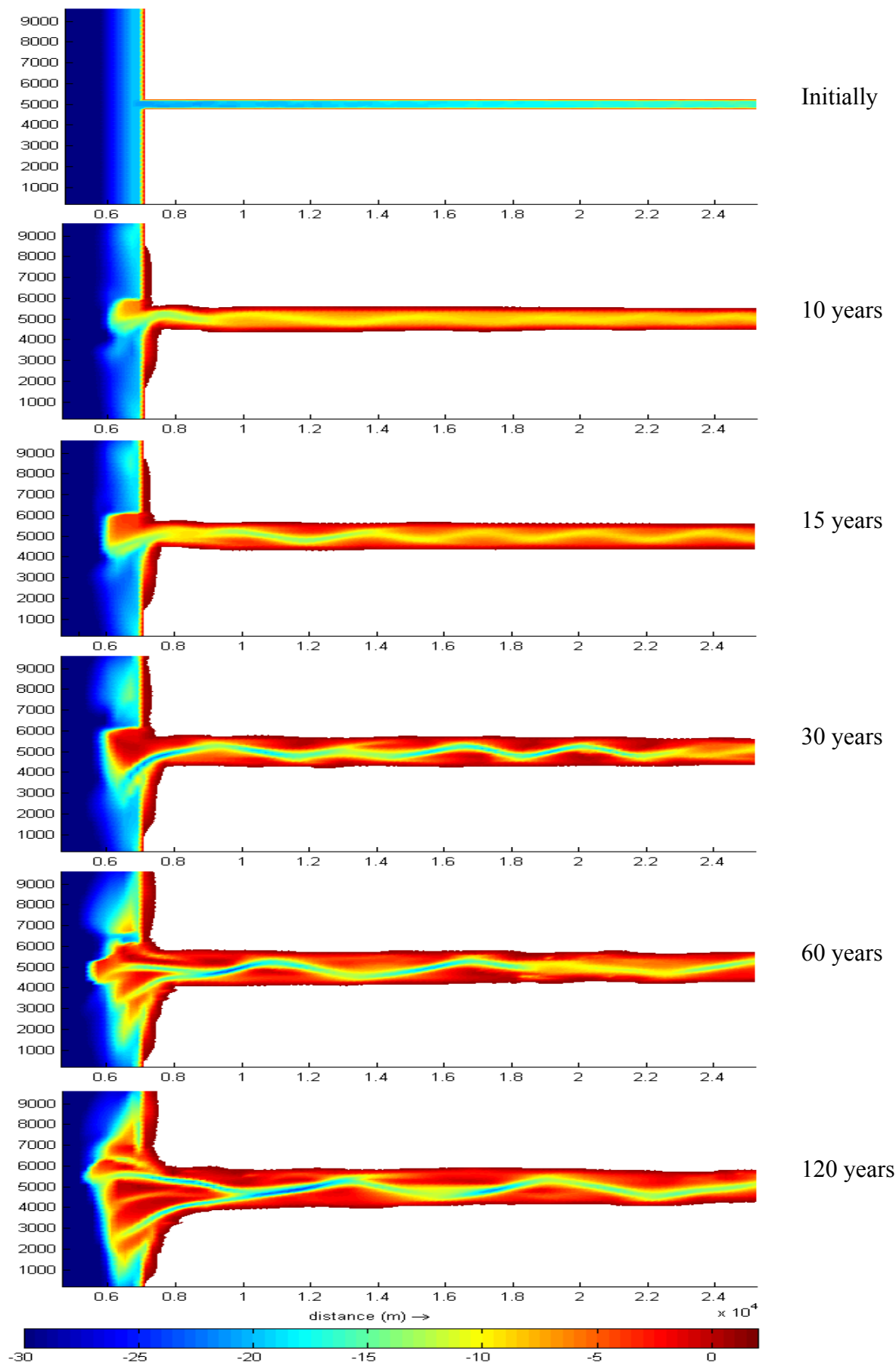


**Figure 5.2** Formation of channel and shoals at the first part of estuary

The model is validated against field observations by Van Veen (1950) and Ahnert (1960). Ahnert studied the estuaries around the Chesapeake Bay, Maryland, USA. The main interest of Van Veen is the Western Scheldt estuary in The Netherlands. This 160 km long funnel-shaped estuary, with an entrance width of 6 km, exhibits a well-developed system of channels and shoals. In his characterisation of channel patterns in estuaries, Van Veen categorised channels as ebb- and flood-dominated. His cartoon of an idealised channel system is presented in Figure 5.3(b). It shows a single meandering ebb-dominated channel separated by shoals from the flood-dominated side channels. The pattern resembles the one in the model estuary presented in Figure 5.3

The similarity is confirmed by the tidally-averaged flow pattern of the model simulation. Figure 5.3(a) shows a continuous ebb-dominated meandering flow, with flood dominance found in interrupted channels. This pattern results in a water and sediment circulation pattern like the one observed by Van Veen (Figure 5.3(c)).

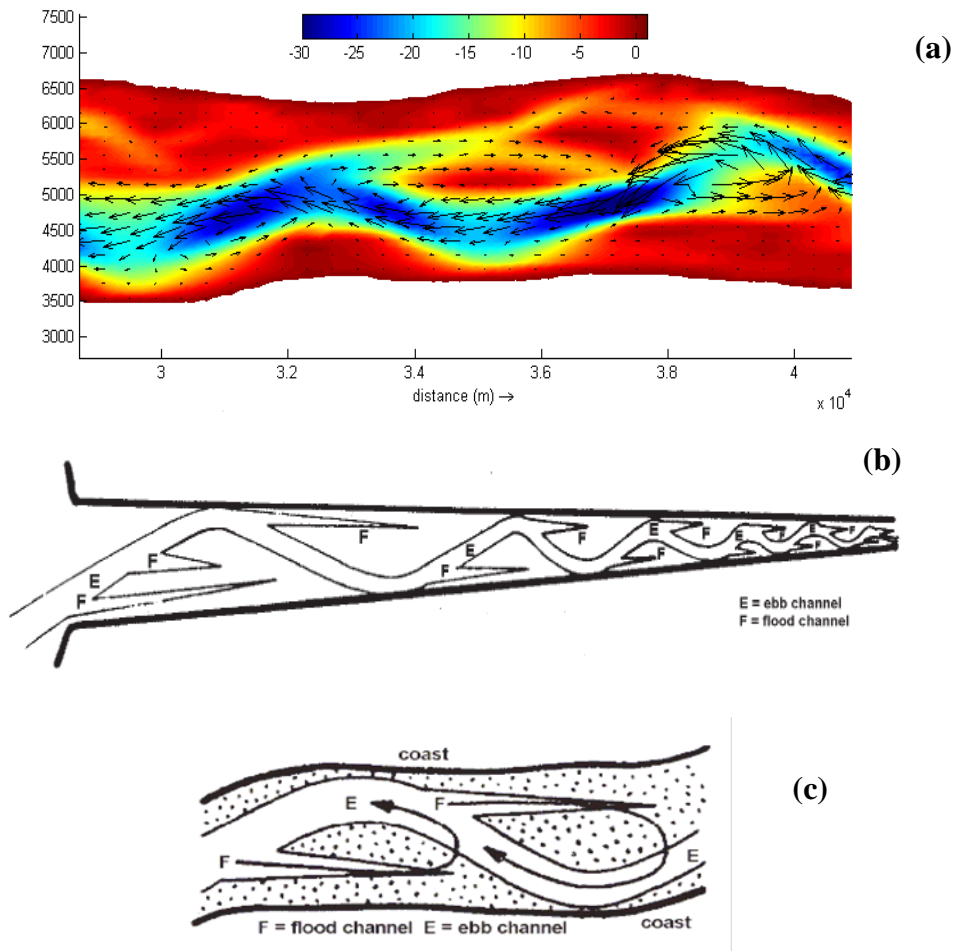


**Figure 5.3** (a) The result from model at 35km from mouth after 600 years, the arrows show the residual sediment transport direction ; (b) Sketch of ebb (E) and flood (F) channel system by Van Veen (1936-1950). (c) Sketch of "circulating sand currents" by Van Veen (1950).

---

In the landward part of the model estuary, the pattern is different: the flood-dominated channels do not end in a shoal in a similar way as the ebb-dominated channels (Figure 5.4a). This yields a pattern that can be characterised as a sequence of braided ebb- and flood-meanders with shoals in between. The wavelength is about 10 km.

Such a pattern can also be observed in the Western Scheldt estuary. A section of this estuary, 40 km landward of the mouth, is presented in Figure 5.4b. The direction of the residual current in the channels is indicated in the figure. The length of the two cells is 25 km, which is 2.5 times the wavelength of the pattern in the simulation. This probably due to the width of model simulation is smaller than the width in reality.

Field observations of this feature on a smaller scale are reported by Ahnert (1960), for the estuaries around the Chesapeake Bay area. He described the pattern in the Patuxent River estuary as a succession of oblong pools, connected by narrow channels at the bend. Underwater sandbars separate the channels in the pool. On this scale the wavelength amounts to 9 km. His cartoon of the meandering channel system is presented in Figure 5.4c and shows a striking resemblance to the model results. That this braided meandering is not found at the entrance of the estuary is also observed by Ahnert: "In the estuaries around the Chesapeake Bay estuarine meanders follow a strikingly regular pattern of occurrence. They extend neither landward all the way to the head of the tide nor seaward to the mouth, but occupy a stretch in the middle part of the estuary". The explanation was found in the modification of the tidal wave. The tide enters an estuary with the characteristic properties of a progressive wave, when the maximum flood current occurs at high tide and the maximum ebb current at low tide. As the tidal wave proceeds up the basin, the maximum water level lags behind the maximum current. This time difference increases until the maximum ebb and flood current occur at approximately mean water level. Thus the maximum strength of both currents is comparable and therefore causes comparable lateral erosion. At the entrance of the model estuary the time lag between extreme tide and maximum currents is already around two hours. This time difference increases further landwards, causing a decrease of water level difference at maximum currents.

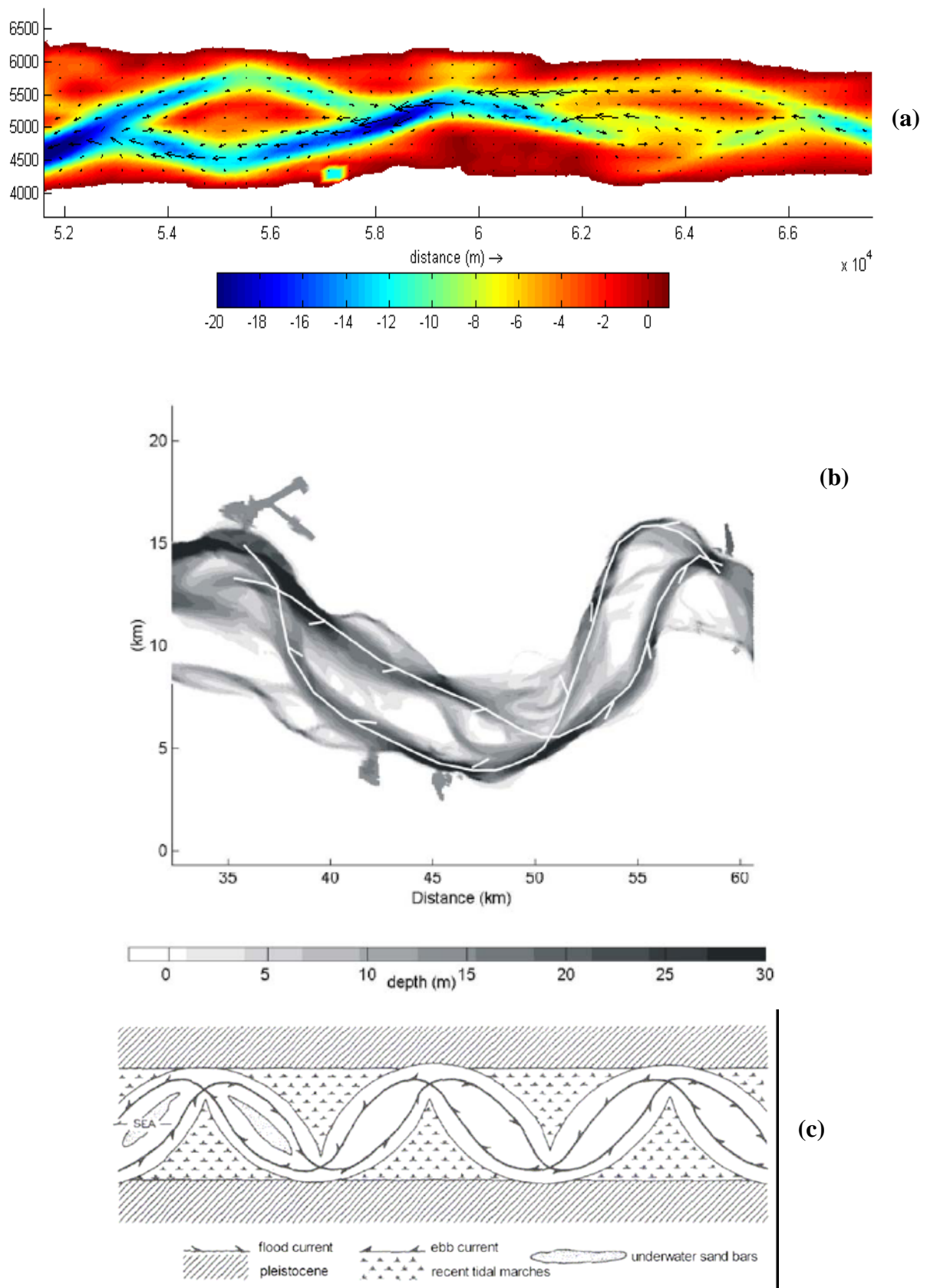


**Figure 5.4** The result of model at 50km from mouth after 600 years; the arrows show the residual sediment transport direction. (b) Section of the Western Scheldt estuary, the Netherlands, 1996. The trajectories indicate the direction of the residual velocity. (c) Sketch of meandering tidal channel system by Ahnert (1960).

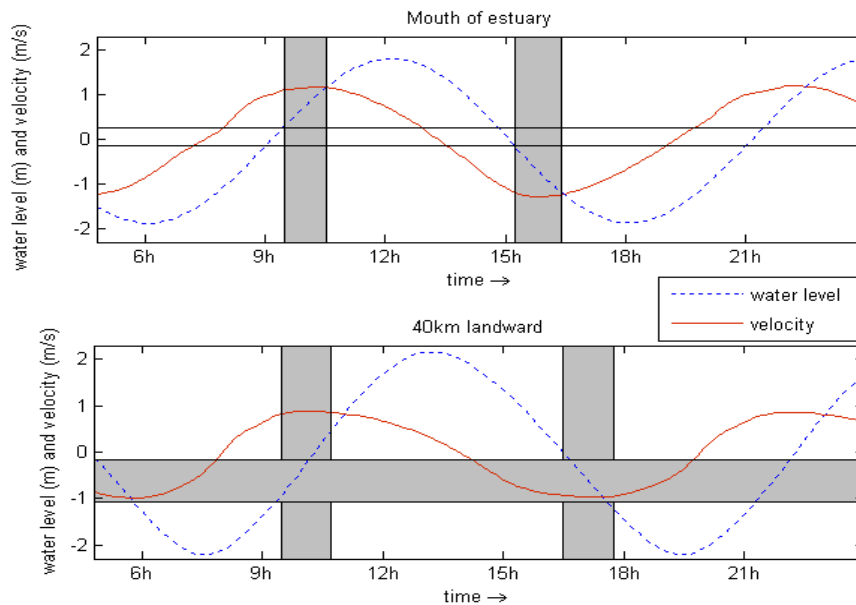


**Figure 5.5** Water level (dashed) and velocity (line) at the mouth of the estuary (left panel) and halfway up the estuary (right panel). Ebb velocities have a negative sign, flood velocities are positive

In Figure 5.5 the water level and currents during one tidal period at the entrance and halfway up the basin of Ahnert are presented. The vertical grey columns mark the time period during which the current velocity is more than 90% of the maximum. The horizontal lines indicate the maximum water level during this high ebb current and the minimum water level during high flood currents. Halfway up the estuary (below panel), where the previously described features form, a range of water levels exist at which both ebb and flood currents flow with more than 90% of maximum velocity, indicated by the grey horizontal bar. At the mouth (above panel), this overlap in water levels is not present. Despite the changes in the hydrodynamics due to the formation of channels and shoals and the development of the longitudinal profile, the overlap in water levels present at high ebb and flood currents persist halfway the estuary but do not occur at the mouth. In addition to this hydrodynamic cause for differences in patterns, the width-to-depth ratio of the estuary is also found to be important. Further landwards, the depth decreases and so does the wavelength of the channel.

Field observations in various estuaries imply that as the width-to-depth ratio increases, more multiple rows or braided bars are produced (Dalrymple and Rhodes, 1995). For a width-to-depth ratio less than approximately 100, alternate bars are produced. This can be associated with a meandering flow in a straight channel, as in their context, bars are part of the channel. The length of the alternate bar pattern is found to be six times the channel width, i.e. 12 km for a 2 km wide estuary, in good

agreement with our model result.(Figure 5.1 shows that the length of sand bar is about 12km and the width at that location is about 2.2km and the average depth is about 10m. The width-to-depth ratio at the that location is however, is 220, This is considerably larger than 100. At the mouth the ratio of width to depth is about 5100m to 11m this equal to 463. With this width to depth ratio we found that exist the multiply channel system in accordance with (Dalrymple and Rhodes, 1995).

## 5.2. Longitudinal profile

You have to update this figure for the total level instead of the level below MSL... Figure 5.6 shows longitudinal profiles of the width averaged bed level and the bed level averaged over width and over length for different points in time. It is clear that the basin exports sediment all the time. Apparently, the banks initially offer a surplus of sediment that needs to be transported seaward. After 200 years, the longitudinal profile more concave near the seaward part and convex at landward part. However, after 400, 600 and 800 years the longitudinal profile becomes linear. In addition, we see that the sill exist at the mouth of estuary.

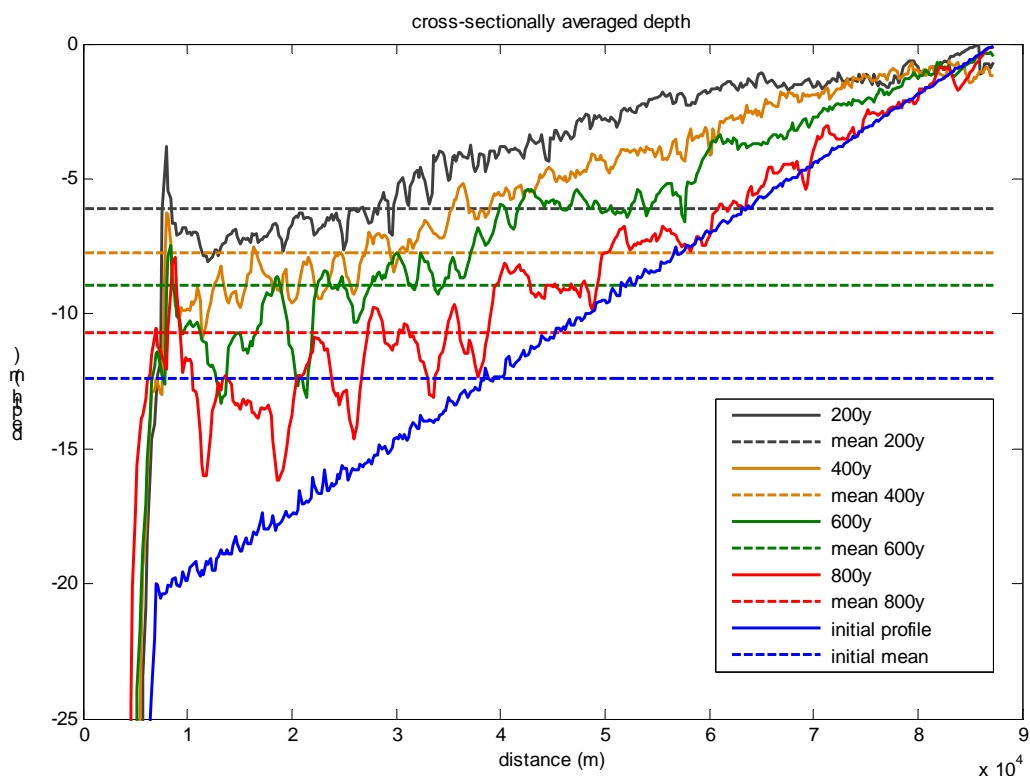


**Figure 5.6** Longitudinal profile for different points in time

### 5.3. Cross-section

Figure 5.7 shows the widths of the embayment in longitudinal direction of the model after years. These widths were determined at mean water level. The initial width of channel is 400m. After 800 years, the width of the mouth is about 5km. Obviously, the widths of the embayment open with time

Figure 5.8 and Figure 5.9 shows the widths of embayment fitted with an exponential function and linear function. The results show that the widths of embayment is a better fit with linear function (the R-square values of linear function is higher)

According to Savenije (1992) the width of embayment can be described as an exponential function:

$$B = B_o \exp\left(-\frac{x}{b}\right)$$

Where:

$B_o$ : the width at the mouth of estuary

$b$ : Convergence length at MSL

After years the widths of embayment can be described in an exponential function is:

	200 years	400 years	600 years	800 years
$B_o$ (m)	2264	3306	4301	5136
$b$ (m)	50	50	50	50

We can notice that the convergence lengths of the embayment by time are the same.

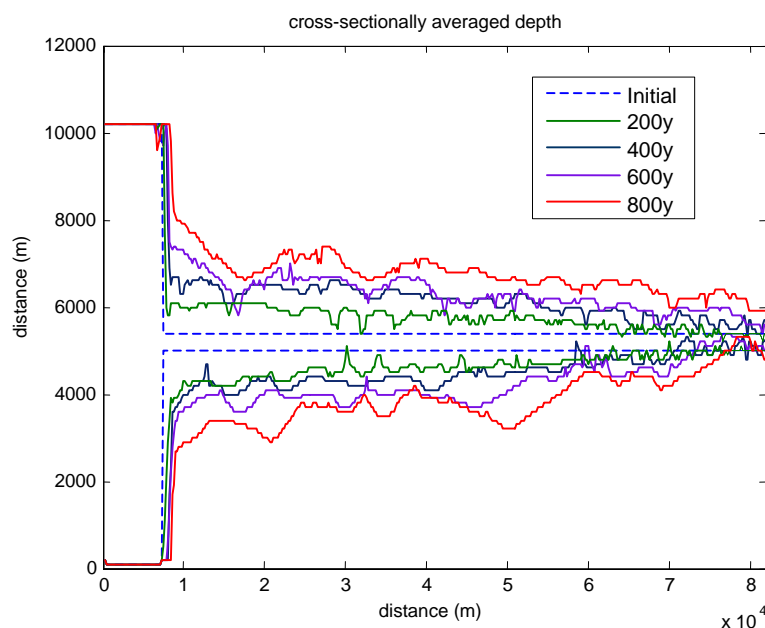


**Figure 5.7** Width of embayment after 200, 400, 600 and 800 years

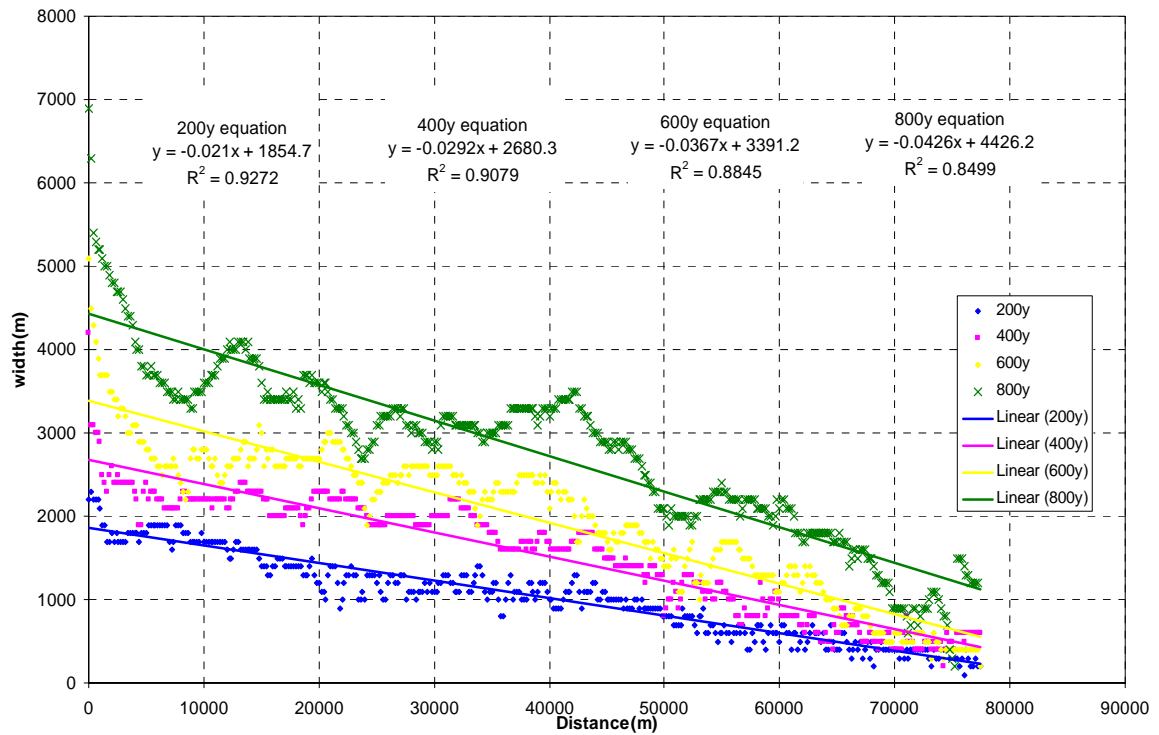


**Figure 5.8** Fitting the length of the cross-section with a linear function

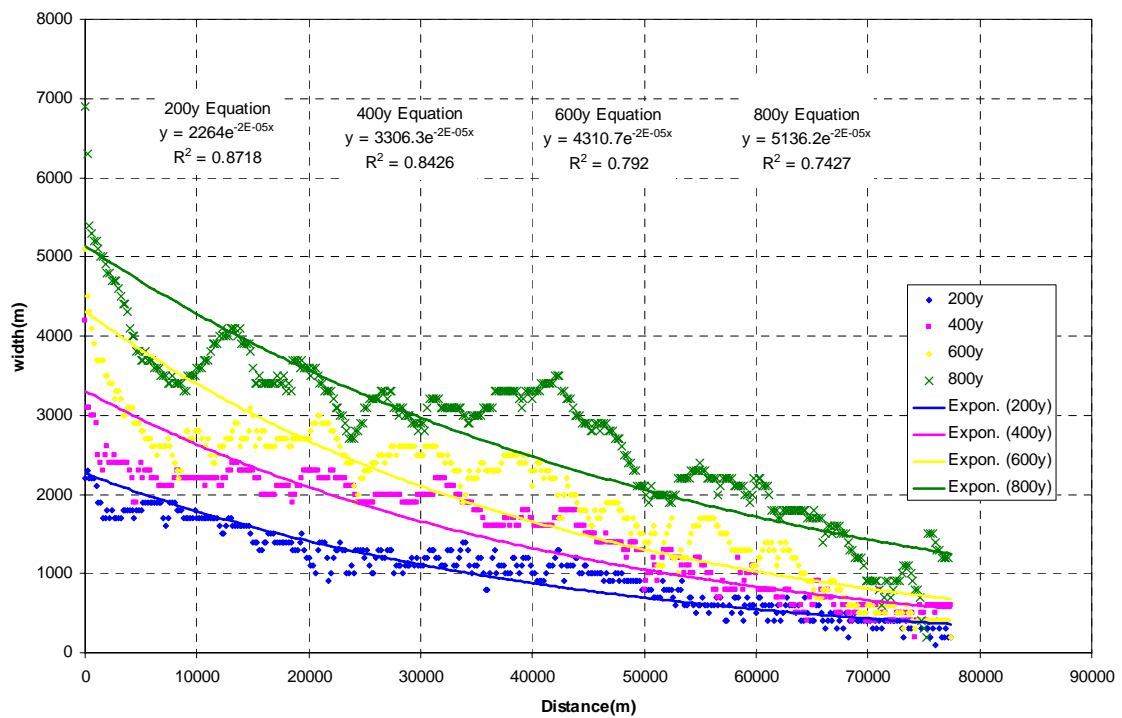


**Figure 5.9** Fitting the length of the cross-section with an exponential function

## 5.4. Cross-section and prism relationship

Jarret (1976) suggests a relation between cross-section and prism based on a review of 108 inlets on the US Gulf coast, the US Pacific coast and the US Atlantic coast. Comparison of the model results and the relationship by Jarret derived for basins in Atlantic coast and had no jetties or single jetty at the mouth (for the prevention of siltation) is presented in Figure 5.10. It shows that cross-section and prism relationship from the beginning to 800 morphological years evolves towards the Jarret relation.

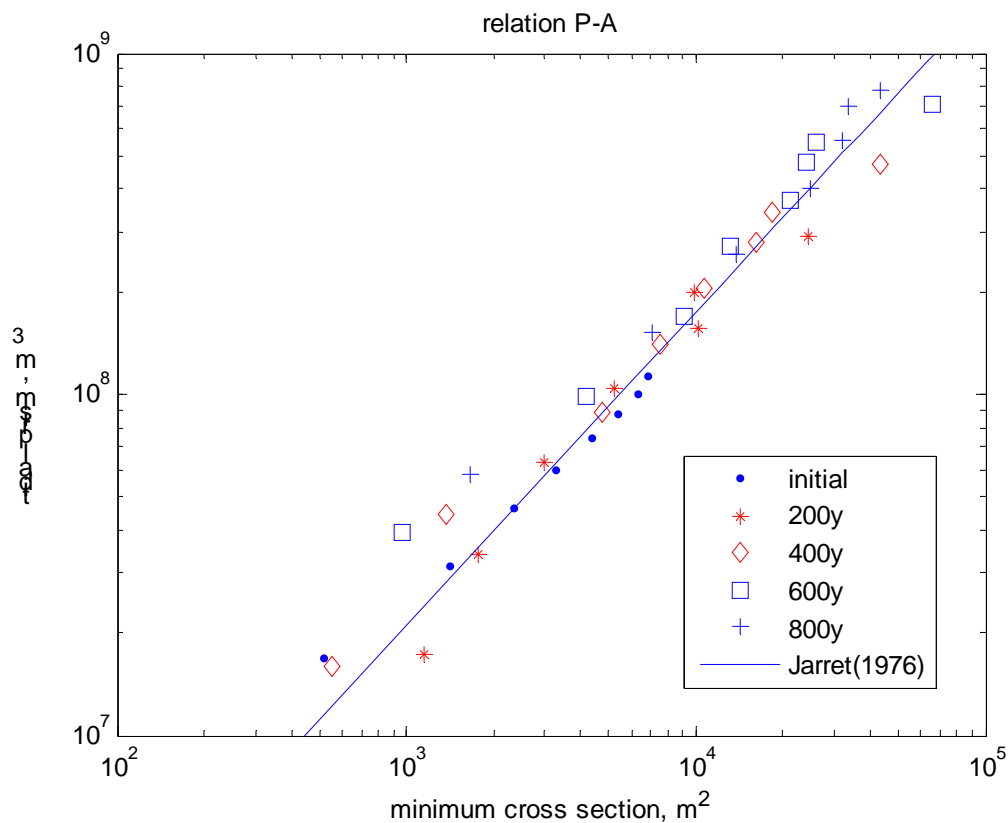


**Figure 5.10** Relation between tidal prism ( $\text{m}^3$ ) and the cross-section below MSL ( $\text{m}^2$ ) for different points in time plotted on a logarithmic scale. The line represents the relation by Jarret (1976) for a basin with no jetty or single jetty.

Eysink (1990) suggests a relation between a characteristic tidal volume and the volume that the channels hold as follows:

$$V_c = c_c V^\beta$$

where

- $V_c$  channel volume below MSL
- $c_c$  empirical coefficient
- $\beta$  exponent with default value

For different basins in the Netherlands, Eysink calibrated the coefficient  $c_c$  to value ranging from  $65 \cdot 10^{-6}$  in Waddensea, to  $80 \cdot 10^{-6}$  in Eastern Scheldt, and  $\beta$  was kept constant at 1.5.

Figure 5.11 shows a comparison of model results with the suggest value of Eysink. The figure shows that at initial the model very different but by time the result of the model show the good resemble. It because of that, at initial the width of the channel has not opened yet. After 200 year the width is more open and the result nearly fit the line. After 400, 600 and 800 years the result almost fit with the line.

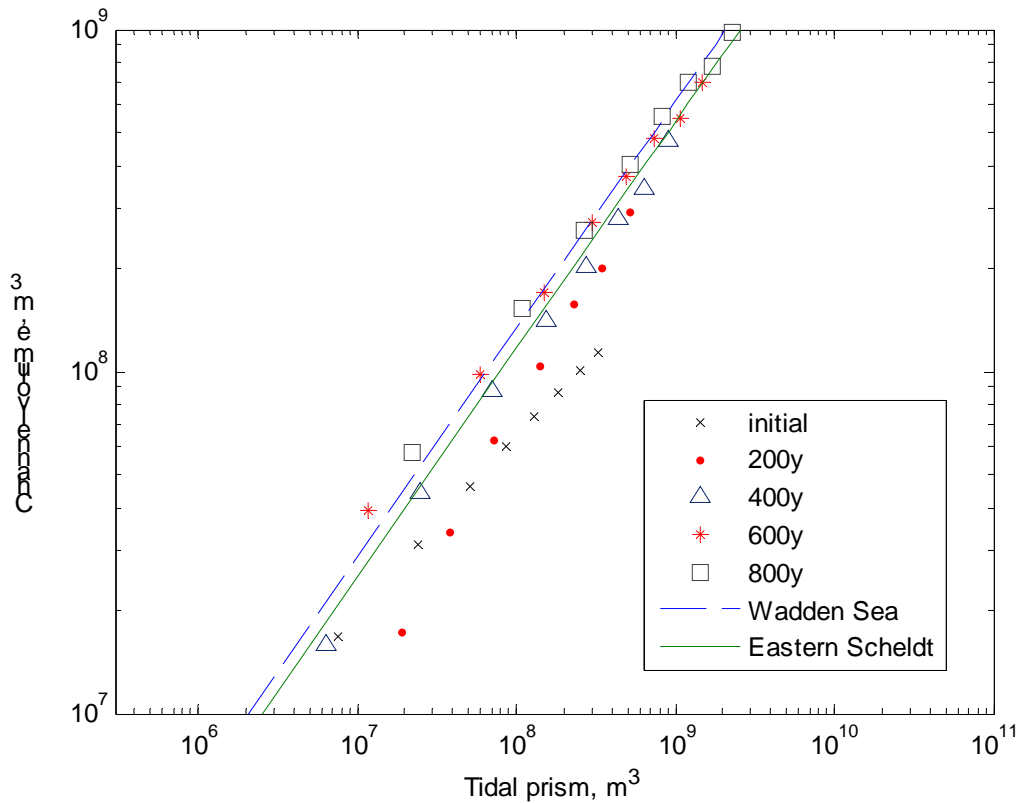


**Figure 5.11** Relation between Channel volume below MSL and tidal prism. In relationship with Eysink equation.

### 5.5. Hydrodynamic equilibrium

Using the hypothesis that morphological equilibrium equates to a uniform tide, Dronkers derived an asymmetry ratio based on certain estuary form parameters (Dronkers, 1998):

$$\left( \frac{h+a}{h-a} \right) = \sqrt{\frac{S_{hw}}{S_{lw}}}$$

Where

$h$  : the mean hydraulic depth of the estuary

- a: the tidal amplitude,
- $S_{lw}$  : the surface area at low water,
- $S_{hw}$ : the surface area at high water,

A value of  $\gamma$  equal to one suggests a uniform tide, with values greater than one indicating flood dominance and less than one indicating ebb dominance.

The Figure 5.12 shows the result of the model. It shows that the basin fall in flood dominance.

Comparing the result with Dutch tidal water (Figure 5.13) is shows that the model has the same result area with Texel inlet, Western Scheldt, Eastern Scheldt, Vlie inlet. This means that the basin is flood dominant according to Dronker, 1998

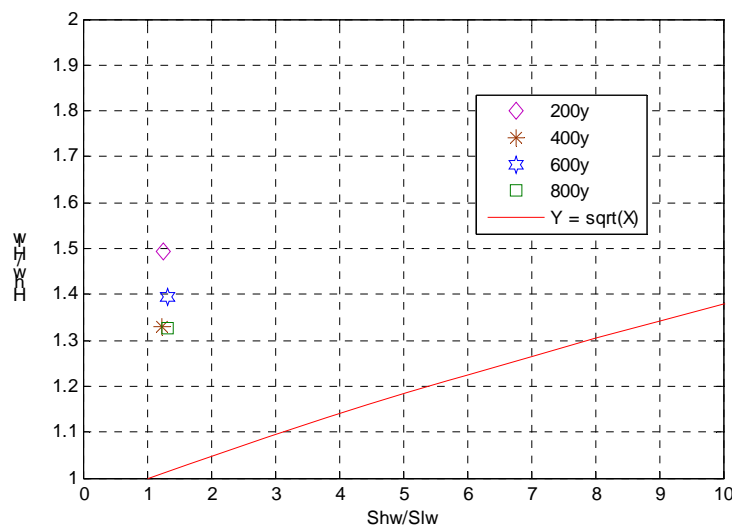


**Figure 5.12**  $H_{hw}/H_{lw}$  versus  $S_{hw}/S_{lw}$  including relation of Dronkers (1998)

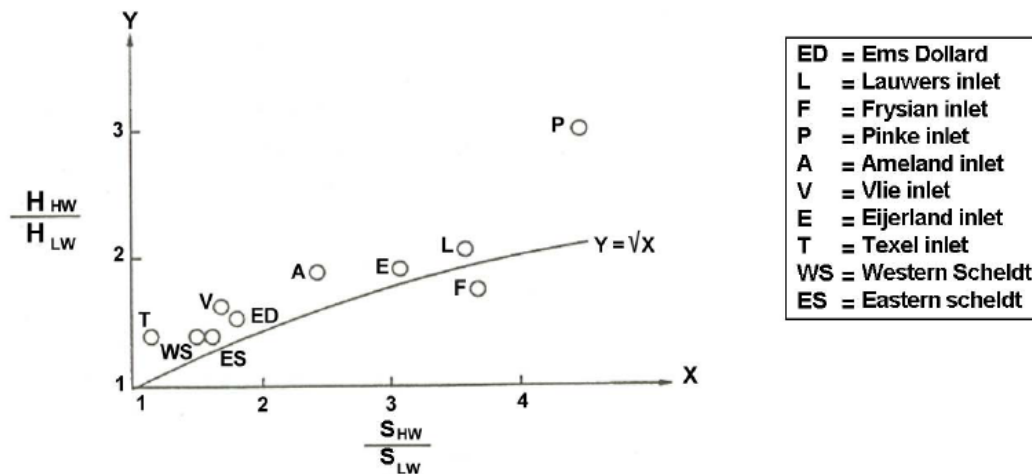


**Figure 5.13** Ratio of channel depth at High Water (Hhw) and Low Water (Hlw) and the ratio of wet surface at these water levels (Shw and Slw) for all Dutch tidal waters. The curve represents the condition for approximately equal ebb and flood duration and indicates a morphological equilibrium (from Dronkers, 1998).

Figure 5.14 show the suggested values for ebb or flood dominant by Friedrichs and Aubrey (1988). Figure 5.15 plots the model results of the current research on the same axes as. This shows that, according to Friedrichs and Aubrey, the basin falls in the flood dominant domain.

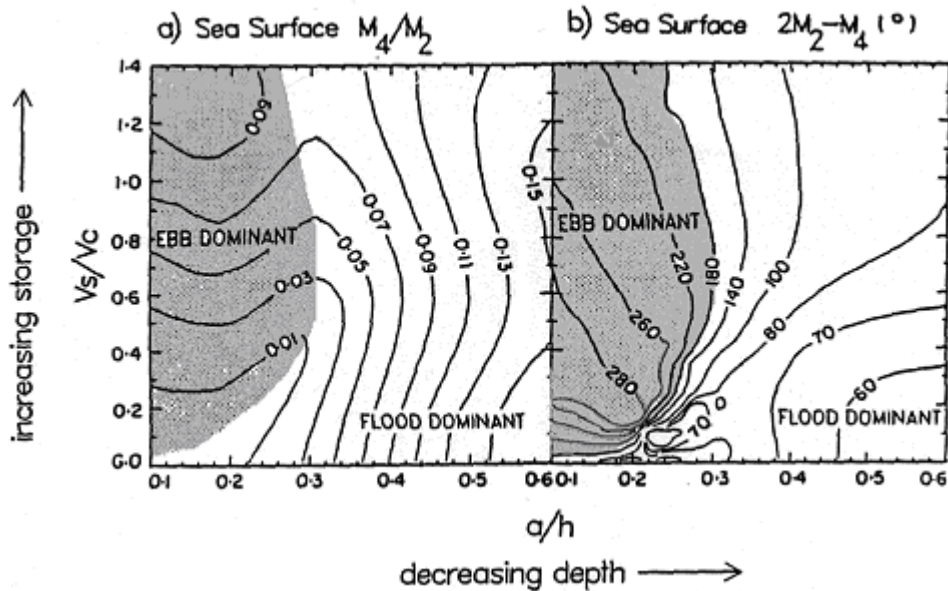


**Figure 5.14** Diagram of Friedrichs and Aubrey (1988).  $V_s$  = Volume of intertidal storage,  $V_c$  = Channel volume,  $a$  = tidal amplitude at mouth,  $h$  is average waterdepth at MSL. Shaded area represents ebb dominant model configurations and clear area flood dominant conditions.

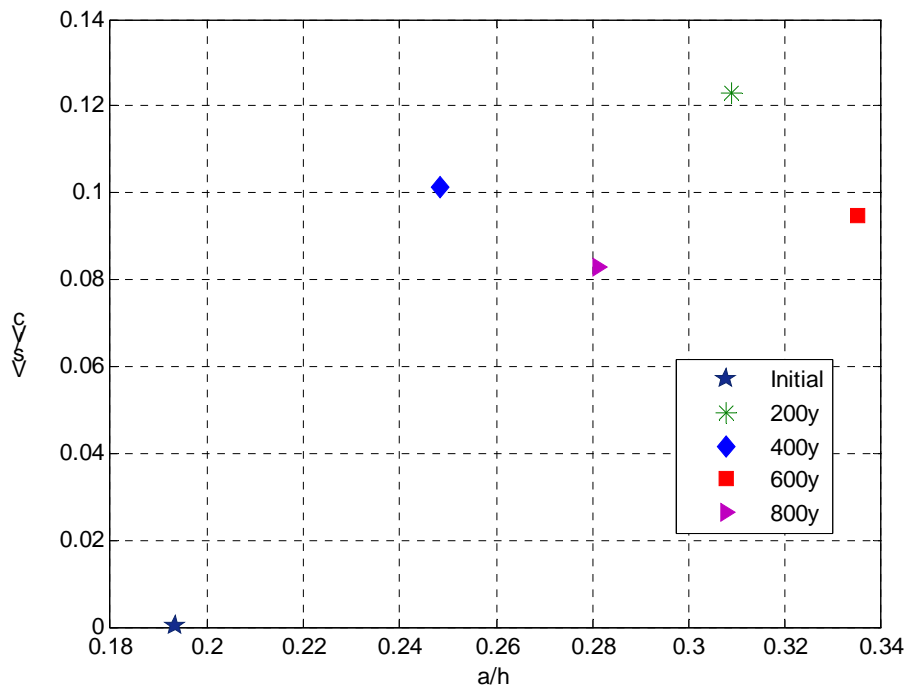


**Figure 5.15**  $V_s/V_c$  versus  $A/h$  of the model

According to Dronker (1998) , Friedrichs and Aubrey (1988) the embayment falls in the flood dominant domain. However, the longitudinal profile shows that the embayment is exporting sediment all the time. The explanation for this was given by Duijts (2002) He found that despite the shorter flood duration, which implies that the discharge during flood per unit time should be larger than during ebb, the maximum flood velocity appears to be smaller than the maximum ebb velocity. This is mainly due to the effect that the water level is higher during flood than during ebb, so a higher discharge during flood does not cause larger flow velocity. By assuming that the sediment transport rate is proportional to a power of the flow velocity it is shown that a residual sediment export occurs.(Figure 5.16). Also, the non-uniform distribution of the velocity and the associated sediment transport over the width might play an important role.

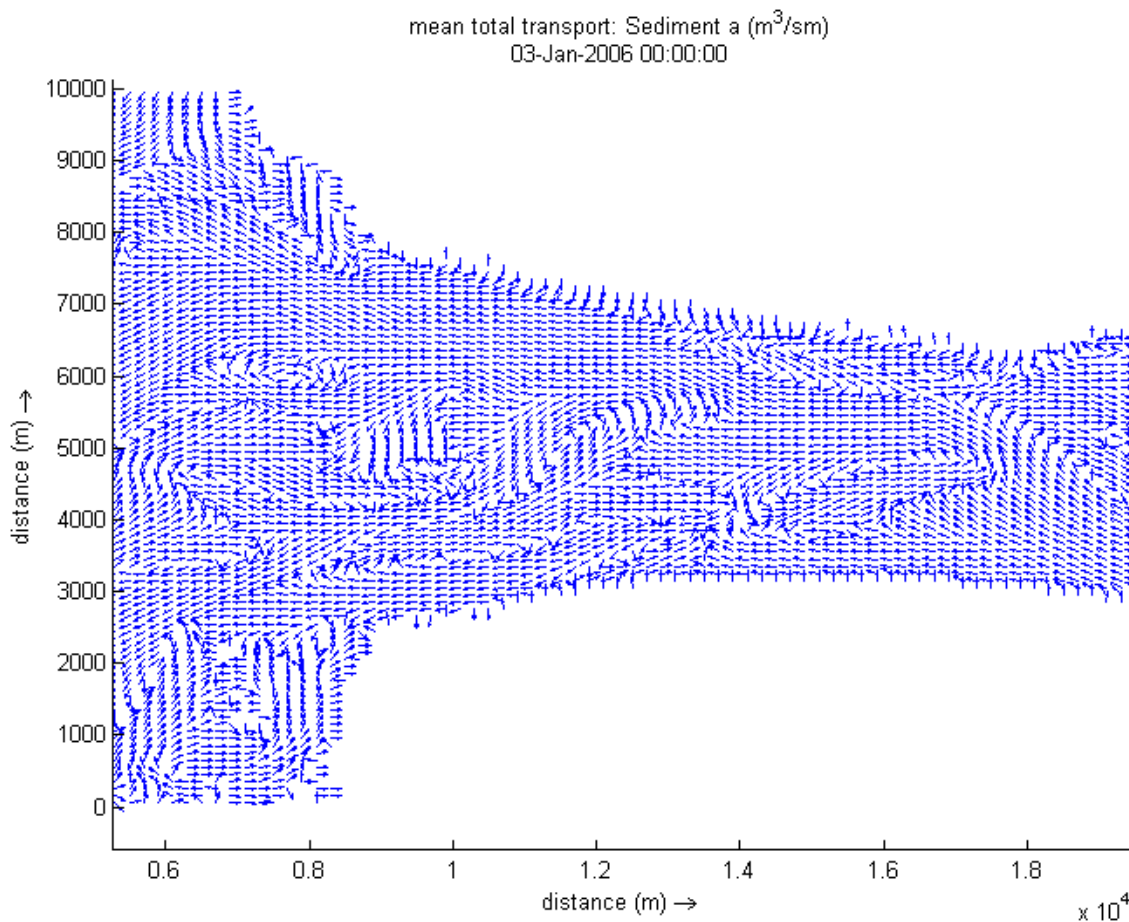


**Figure 5.16** Mean total sediment transport at the mouth after 800 year model.

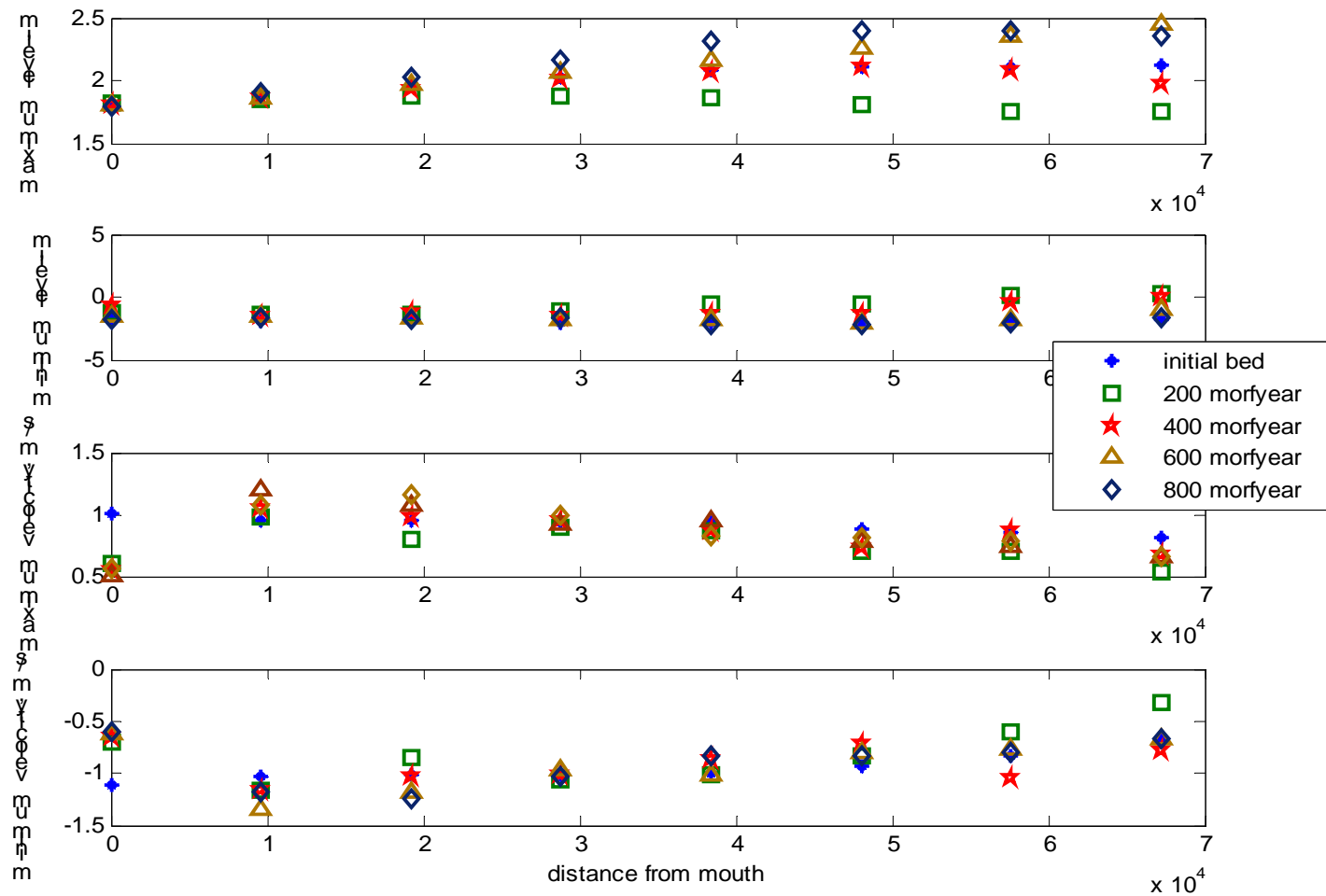


Figure 5.17 Overview in water level and velocity

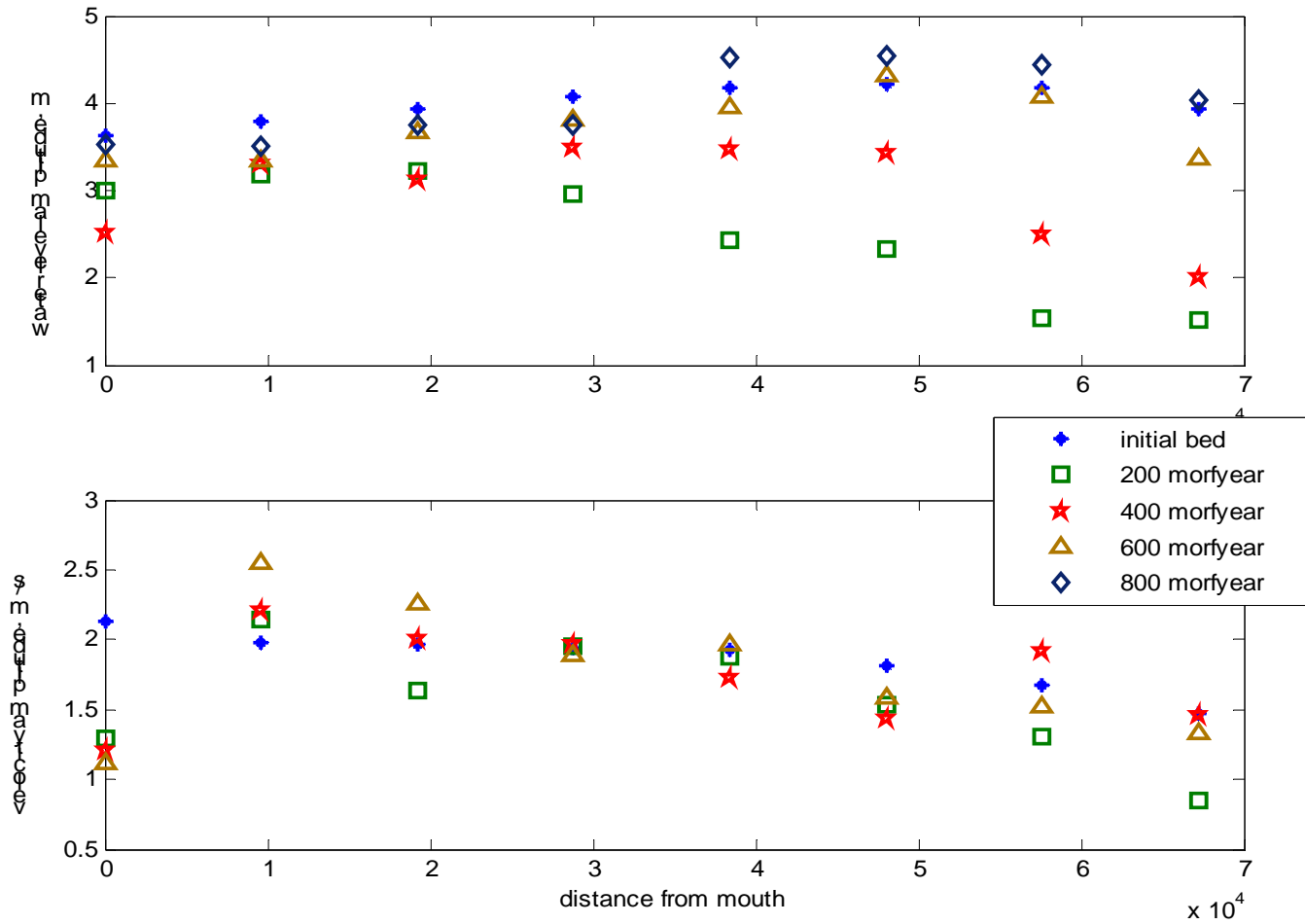
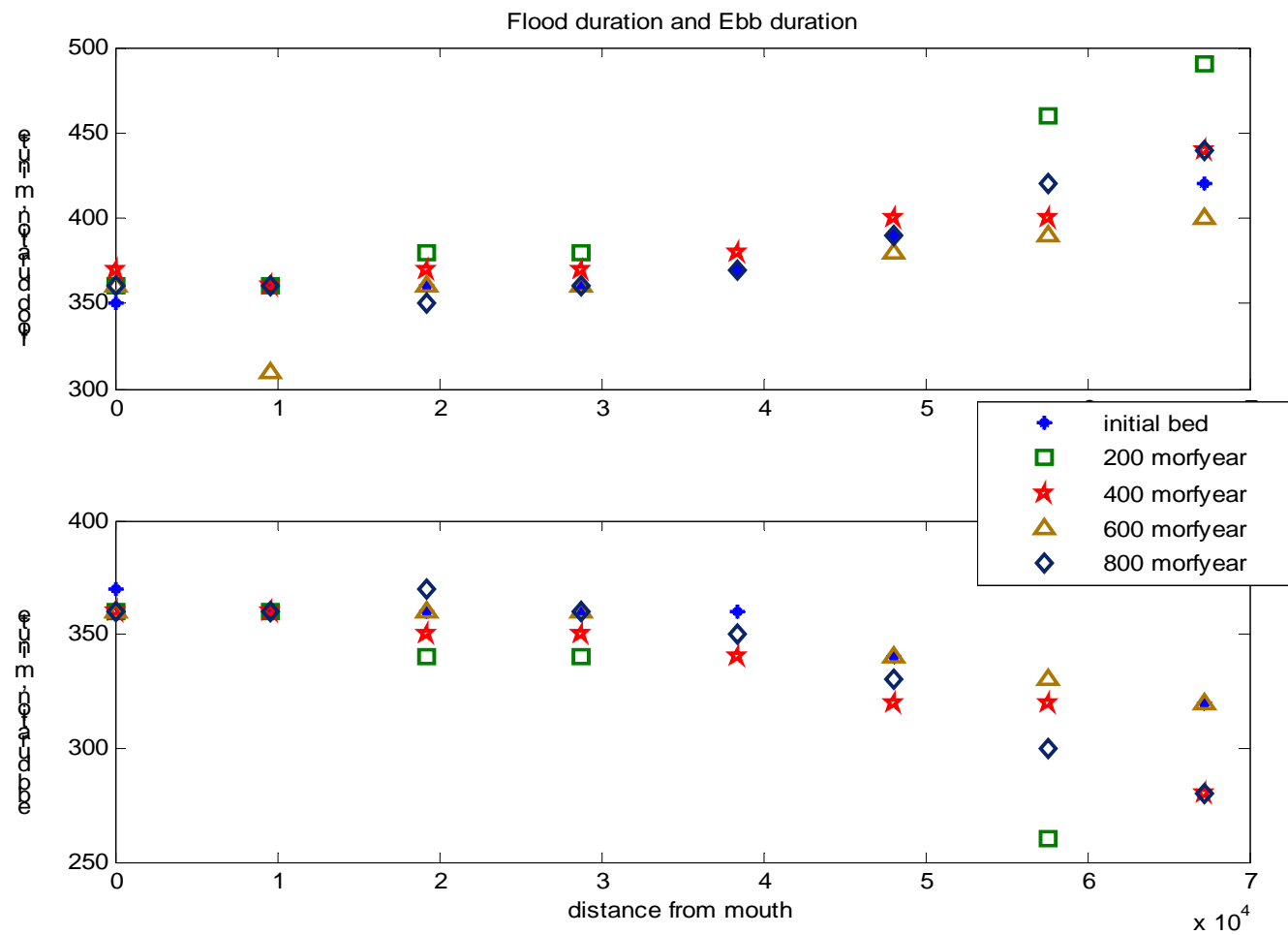


Figure 5.18 Overview in water amplitude and velocity amplitude



**Figure 5.19** Overview in flood duration and ebb duration

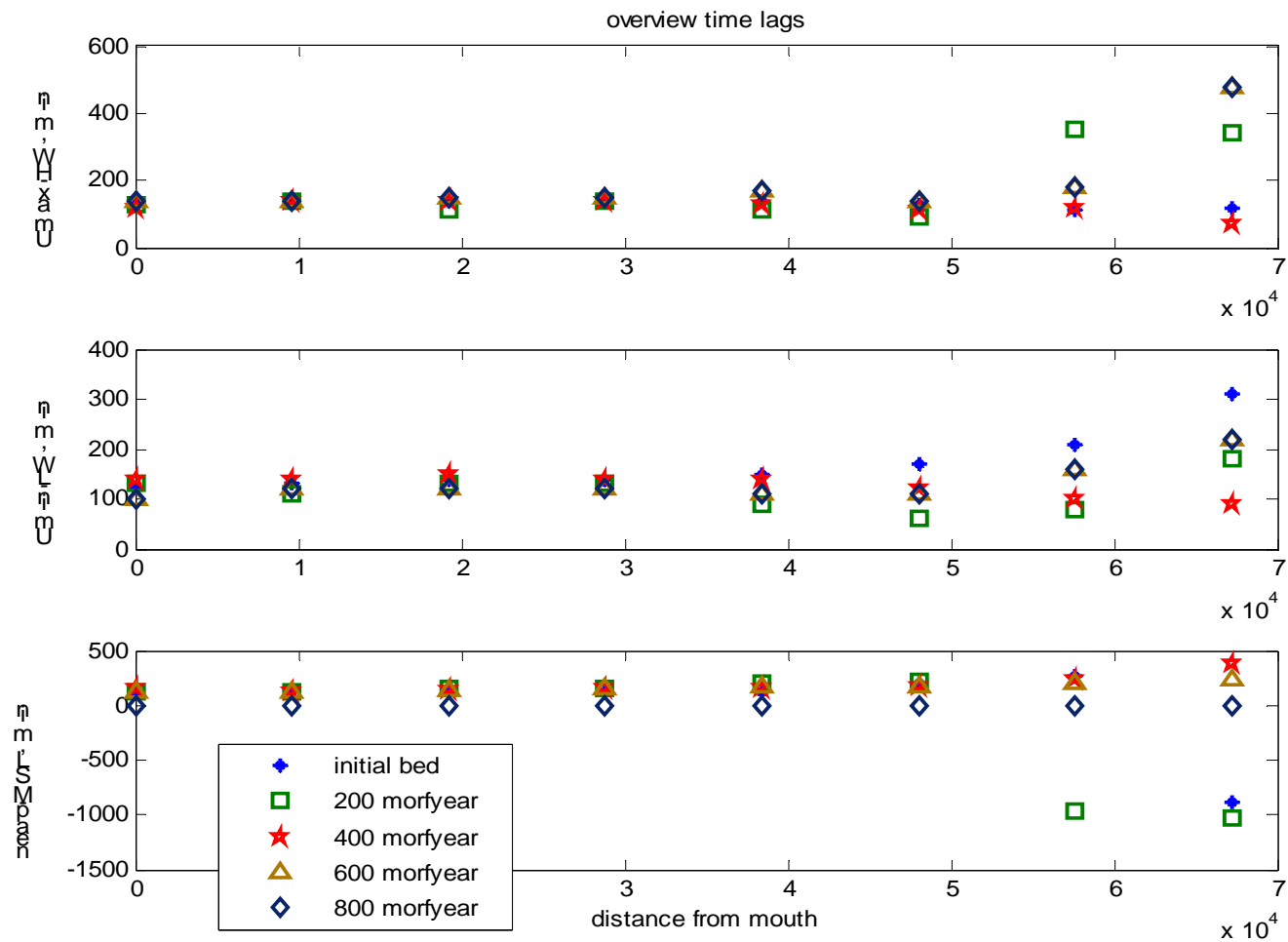


Figure 5.20 over view in time lags



---

## 6. Conclusion and recommendation

### 6.1. Conclusion

The objective of this research is to investigate the morphodynamic equilibrium of an alluvial estuary with special emphasis on bank erosion effects by using a process-based model (D3D). The model run uses the online approach for the morphodynamic update scheme and allows erosion of dry –cells

The model configuration initially consisted of a rectangular embayment of 500 m wide and 80 km long, with a bed linearly sloping from -15 MSL to 0 at the landward end. Results show that the first 10's of years the banks of the embayment erode rapidly resulting in a filling of the embayment. Additionally, pattern formation takes place at the bed. On a larger timescale the width averaged longitudinal profile develops from linear towards a more concave profile.

Furthermore, the current model result shows that the estuary still exports sediments and therefore the longitudinal profile is still developing (Figure 5.6). Also from the results it appears that the estuary has not reached equilibrium in terms of the shoal pattern (the morphological wavelength continues developing (Figure 5.1) and in the width of embayment (the width increasing with time Figure 5.7)

From a hydrodynamic point of view, there is no tidal damping or amplification in an ideal estuary, and amplitudes of water level and velocity are constant (Savenije 1998). However, the model shows that the amplitude and velocity is not constant (Figure 5.18). This seems obvious, because the estuary has not reached equilibrium in morphodynamic sense.

Although the model has not reached morphodynamic equilibrium, but it shows a good resemblance in terms of shoal patterns compared to shoal patterns of the Western Scheldt and Texel (Figure 4.18, Figure 5.4.). Channel volume and tidal prism relationships from the model give good resemblance with Eyssink and Jarret (Figure 5.11). The hydrodynamic results give good results compared to some Dutch tidal water (Figure 5.12).

---

From the sensitivity analysis results that the model is sensitive to the effect of the bed slope which is given by value  $\alpha_{bn}$ . The default value of  $\alpha_{bn}$  gives unrealistic results especially for a high morphological factor. In this study only 2 values of  $\alpha_{bn}$  were analyzed due to time limits, and the value of  $\alpha_{bn}$  equal to 5 was chosen. More analysis is needed to determine the best value for  $\alpha_{bn}$ .

The boundary condition seems to be defined in a good way. However, the open sea area should be bigger to avoid influence of the shoal pattern at the mouth. The effect of the grain size to the model is not apparent in basin width development and evolution of the longitudinal profile.

Appreciating the need for further validation and analysis, it can be concluded that this model provides a tool, complementary to fieldwork, theoretical behaviour analyses and laboratory experiments, for the analysis of the large-scale morphological behaviour of estuaries and tide dominated coastal lagoons.

## **6.2. Recommendations**

Due to the lack of time, the model was only run for 800 morphological years. The morphological factor is 200, the time step is 1 minute. Therefore, the total time in model is 4 years. For 1 year, the model costs me about 10 days to run in computer with Pentium 4 2Gz processor. After 800 years, the model did not reach morphological equilibrium. However, the results are very promising. Therefore, I suggest that the model should be run in longer time (8 or 10 years model (1600 or 2000 morphological years))

The embayment length is 80km and it seems rather short and maybe causes resonance of tide. Therefore, sensitivity analysis to embayment length is needed.

The mechanism of dry-cell erosion in Delft3D needs to be redefined. When a cell becomes wet in the model, it cannot be eroded, although this cell is still higher the maximum water level and a very steep scour-hole exist next to it.

The influence of the bank slope ( $\alpha_{bn}$ ) to sediment transport needs more sensitivity analysis and more clarification in order to obtain correct values to be used in the model.

The model use Engelund and Hansen (1967) formula. Therefore, only total bed-load sediment transport is calculated and it maybe influence the result. So the recommendation is that suspended sediment transport is added to the model.

---



---

## 7. References

Ahnert, F., 1960. Estuarine meanders in the Chesapeake Bay area. *Geographical Review* 50, 390-401.

De Vriend, H.J., 1996. Mathematical modelling of meso-tidal barrier island coasts. Part I: Empirical and semi-empirical models. In: Liu, P.L.F. (Ed.), *Advances in coastal and ocean engineering*. World Scientific, Singapore.

Delft3D-Flow. Simulation of multi dimensional hydrodynamic flows and transport phenomena, including sediments. User manual 2003

Dronkers, J., 1998. Morphodynamics of the Dutch Delta. In: Dronkers, J., Scheffers, M. (Eds.), *Physics of estuaries and coastal seas*. Balkema, Rotterdam.

Eysink, W.D., 1990. Morphologic response of tidal basins to changes. IN: ASCE Proceedings of Coastal engineering Conference, Vol 2. 1948-1961 Delft

Friedrichs, C.T. and Aubrey, D.G., 1994. Tidal propagation in strongly convergent channels. *Journal of Geophysical Research*, Vol. 99, No. C2, 3321-3336

Hibma, A., 2004. Morphodynamic modeling of estuarine channel-shoal systems. Ph.D. thesis, Technical University Delft, The Netherlands

Lanzoni, S., Seminara, G., 2002. Long-term evolution and morphodynamic equilibrium of tidal channels. *Journal of Geophysical Research* 107, C, 1-13.

Roelvink J.A , Overview of coastal morphodynamic evolution techniques, *Journal of coastal engineering*, private communication

Roelvink. J.A and Walstra. D.J R \* Keeping it simple by using complex models. *Advances in hydro-science and engineering*, volume VI

Savenije, H.H.G, 1998. Analytical expression for tidal damping in alluvial estuaries. *Journal of Hydraulic Engineering*, ASCE, 124 (6), 615-618

Savenije, H.H.G., 2001. A simple analytical expression to describe tidal damping or amplification. *Journal of Hydrology*, 243, 205-215.

Sha, L.P., 1989. Sand transport patterns in the ebb-tidal Delta off Texel inlet, wadden sea, The Netherlands

Tidal asymmetry analysis

(<http://www.estuaryuide.net/toolbox/pages/Tidal%20asymmetry%20analysis.htm>)

Van Rijn, L.C., 1993. Principles of sediment transport in rivers, estuaries and coastal seas. AQUA Publications, the Netherlands

Van Veen, J., 1950. Ebb and flood channel systems in the Netherlands tidal waters (in Dutch, English summary). *Journal of the Royal Dutch Geographical Society (KNAG)*

---

67, 303–325, Republished, translated and annotated by Delft University of Technology, 2001. (<http://www.waterbouw.tudelft.nl/research/specialPublications/VanVeen.pdf>).

Wegen. M.V.D ,2005 Long-term morphodynamic equilibrium in alluvial estuaries. PhD proposal thesis, UNESCO-IHE, Delft, The Netherlands.

---

# APPENDIX

---

## \*.mdf file

```
Ident = #Delft3D-FLOW .03.02 3.39.12.01#
Runid = #a8 #
Commnt=
Runtxt= #continue 2d after 600 year #
Filcco= #bs.grd#
Fmtcco= #FR#
Anglat= 5.1000000e+001
Grdang= 0.0000000e+000
Filgrd= #bs.enc#
Fmtgrd= #FR#
MNKmax= 437 102 1
Thick = 1.0000000e+002
Fildep= #600_2_5dn.dep#
Fmtdep= #FR#
Commnt=
Fildry= ##
Fmtdry= #FR#
Filtid = ##
Fmttd = #FR#
Nambar= # #
MNbar = [ ] [ ] # #
MNwlos= [ ] [ ]
Commnt=
Itdate= #2006-01-01#
Tunit = #M#
Tstart= 0.0000000e+000
Tstop = 5.2560000e+005
Dt = 1.0000000e+000
Tzone = 0
Commnt=
Sub1 = # #
Sub2 = # C #
Namc1 = #Sediment a #
Namc2 = # #
Namc3 = # #
Namc4 = # #
Namc5 = # #
Wnsvwp= #N#
Filwnd= ##
Fmtwnd= #FR#
Wdint= #Y#
Commnt=
Filic = ##
Fmtic = #FR#
Zeta0 = 1.7500000e+000
U0 = [.]
V0 = [.]
S0 = [.]
```

---

```

T0 = [.]
C01 = 0.0000000e+000
I0 = [.]
Restid= ##
Commnt=
Filbnd= #base.bnd#
Fmtbnd= #FR#
FilbcH= #base.bch#
FmtbcH= #FR#
FilbcT= ##
FmtbcT= #FR#
FilbcQ= ##
FmtbcQ= #FR#
Filana= ##
Filcor= ##
FilbcC= #base.bcc#
FmtbcC= #FR#
Rettis= 0.0000000e+000
        0.0000000e+000
        0.0000000e+000
Rettib= 0.0000000e+000
        0.0000000e+000
        0.0000000e+000
Commnt=
Ag = 9.8100004e+000
Rhow = 1.0250000e+003
Alph0 = [.]
Tempw = 1.5000000e+001
Salw = 3.1000000e+001
Rouwav= # #
Wstres= 6.3000002e-004 0.0000000e+000 7.2300001e-003 1.0000000e+002
Rhoa = 1.0000000e+000
Betac = 5.0000000e-001
Equili= #N#
Tkemod= # #
Ktemp = 0
Fclou = 0.0000000e+000
Sarea = 0.0000000e+000
Filtmp= ##
Fmttmp= #FR#
Temint= #Y#
Tstmp = [.] [.]
Commnt=
Roumet= #M#
Filrgh= ##
Fmtrgh= #FR#
Ccofu = 2.6000001e-002
Ccofv = 2.6000001e-002
Xlo = 0.0000000e+000
Htur2d= #N#
Filedy= ##

```

---

```

Fmtedy= #FR#
Vicouv= 1.0000000e+000
Dicouv= 1.0000000e-001
Vicoww= [.]
Dicoww= [.]
Irov = 0
Z0v = [.]
Cmu = [.]
Cpran = [.]
Filsed= #base.sed#
Filmor= #base.mor#
Commnt=
Iter = 2
Dryflp= #YES#
Dpsopt= #MAX#
Dpuopt= #MOR#
Dryflc= 1.0000000e-001
Dco = 9.9900000e+002
Tlfsmo= 6.0000000e+001
ThetQH= 0.0000000e+000
Forfuv= #Y#
Forfw= #N#
Sigcor= #N#
Trasol= #Cyclic-method#
Momsol= #Cyclic#
Commnt=
Filsrc= ##
Fmtrc= #FR#
Fildis= ##
Fmtdis= #FR#
Commnt= no. observation points: 3
Filsta= #base.obs#
Fmtsta= #FR#
Filpar= ##
Fmtpar= #FR#
Commnt=
Eps = [.]
Commnt=
Commnt= no. cross-sections: 0
Filers= ##
Fmtrc= #FR#
Commnt=
SMhydr= #NNNNN#
SMderv= #YYYYYY#
SMproc= #NNNNNNNNNN#
PMhydr= #NNNNNN#
PMderv= #NNN#
PMproc= #NNNNNNNNNN#
SHhydr= #NNNN#
SHderv= #NNNN#
SHproc= #NNNNNNNNNN#

```

---

SHflux= #NNNN#  
PHhydr= #NNNNNN#  
PHderv= #NNN#  
PHproc= #NNNNNNNNNN#  
PHflux= #NNNN#  
Commnt= attribute file fourier analyzed  
Filfou= ##  
Online= #N#  
Prmap = [.]  
Prhis = [.] [.] [.]  
Flmap = 0.000000e+000 2.880000e+003 5.256000e+005  
Flhis = 0.000000e+000 0.000000e+000 5.256000e+005  
Flpp = 0.000000e+000 0.000000e+000 0.000000e+000  
Flrst = 1.440000e+009  
Commnt=  
Cstbnd= #yes#  
TraFrm= #md-tran.tr1#  
Bndneu= #yes#  
Commnt=

---

## \*.mor file

2.0000000e+002 [-] :MORFAC, morphological scale factor  
7.2000000e+002 [min] :MORSTT, spin-up interval before morphological changes  
5.0000001e-002 [m] :THRESH, threshold sediment thickness  
.true. :MORUPD, update bathymetry during FLOW simulation  
.true. :EQMBC, equilibrium sediment concentration profile at open boundary  
.false. :DENSIN, include effect of sediment on water density  
1.0000000e+000 [-] :AKSFAC, van Rijn's reference height factor  
2.0000000e+000 [-] :RWAVE, estimated ripple height factor  
.false. :ROUSE, set equilibrium sediment conc. to Rouse profiles  
1.0000000e+000 [-] :ALFABS, long. bed gradient factor for bed load transport  
5.0000000e+000 [-] :ALFABN, tran. bed gradient factor for bed load transport  
1.0000000e+000 [-] :SUS, current-related reference concentration factor  
1.0000000e+000 [-] :BED, current-related transport vector magnitude factor  
1.0000000e+000 [-] :SUSW, wave-related suspended transport factor  
1.0000000e+000 [-] :BEDW, wave-related bed-load transport factor  
1.0000000e-001 [m] :SEDTHR, minimum depth for sediment calculation  
1.0000000e+000 [-] :THETSD, global / maximum dry cell erosion factor  
9.9999998e-003 [m] :HMAXTH, maximum depth for variable THETSD  
1.0000000e+000 [-] :FWFAC, tuning parameter for wave streaming

---

## \*.sed file

1 1.6000000e+003 [kg/m3] :LSED, no. of sediment; CSOIL, reference density for hindered settling  
sand :SED TYP, type of sediment (sand or mud)  
2.6500000e+003 [kg/m3] :RHOSOL, specific density  
2.3999999e-004 [m] :SEDDIA, mean sediment diameter (D50)  
0.0 [ppt] :SALMAX, salinity saline water  
0.0 [m/s] :WS0, settling velocity fresh water  
0.0 [m/s] :WSM, settling velocity saline water  
0.0 [N/m2] :TCDUNI, critical bed shear stress for sedimentation  
0.0 [N/m2] :TCEUNI, critical bed shear stress for erosion  
0.0 [kg/m2/s] :EROUNI, sediment erosion rate  
1.6000000e+003 [kg/m3] :CDRYB, dry bed density  
8.0000000e+004 [kg/m2] :SDBUNI, initial sediment mass at bed per unit area

---

## \*.bcc file

```
table-name      'Boundary Section : 1'
contents        'Uniform '
location        '(1,2)..(1,101) '
time-function   'non-equidistant'
reference-time  20060101
time-unit       'minutes'
interpolation   'linear'
parameter       'time          ' unit '[min]'
parameter       'Sediment a      end A uniform' unit '[kg/m3]'
parameter       'Sediment a      end B uniform' unit '[kg/m3]'
records-in-table 2
0.0000000e+000 0.0000000e+000 0.0000000e+000
5.2560000e+005 0.0000000e+000 0.0000000e+000
table-name      'Boundary Section : 2'
contents        'Uniform '
location        '(2,1)..(35,1) '
time-function   'non-equidistant'
reference-time  20060101
time-unit       'minutes'
interpolation   'linear'
parameter       'time          ' unit '[min]'
parameter       'Sediment a      end A uniform' unit '[kg/m3]'
parameter       'Sediment a      end B uniform' unit '[kg/m3]'
records-in-table 2
0.0000000e+000 0.0000000e+000 0.0000000e+000
5.2560000e+005 0.0000000e+000 0.0000000e+000
table-name      'Boundary Section : 3'
contents        'Uniform '
location        '(2,102)..(35,102) '
time-function   'non-equidistant'
reference-time  20060101
time-unit       'minutes'
interpolation   'linear'
parameter       'time          ' unit '[min]'
parameter       'Sediment a      end A uniform' unit '[kg/m3]'
parameter       'Sediment a      end B uniform' unit '[kg/m3]'
records-in-table 2
0.0000000e+000 0.0000000e+000 0.0000000e+000
5.2560000e+005 0.0000000e+000 0.0000000e+000
```

---

### \*.bch file

0.0000000e+000 3.0000000e+001

0.0000000e+000 1.7500000e+000  
0.0000000e+000 1.2870000e-005  
0.0000000e+000 1.2870000e-005  
0.0000000e+000 1.7500000e+000  
0.0000000e+000 1.2870000e-005  
0.0000000e+000 1.2870000e-005

0.0000000e+000  
9.0000000e+001  
9.4214996e+001  
4.2150002e+000  
9.0000000e+001  
9.4214996e+001

### \*.bnd file

(1,2)..(1,101) Z H 1 2 1 101 0.0000000e+000  
(2,1)..(35,1) R H 2 1 35 1 0.0000000e+000 Uniform  
(2,102)..(35,102) R H 2 102 35 102 0.0000000e+000 Uniform

### md-tran1.tr1 file

1		IFORM
#1	Engelund Hansen	
1.0	-47.1.1-	ACAL
.06	-47.1.2-	RK